

Phase Locking of a Quantum Cascade Laser Using a THz Schottky Diode Harmonic Mixer

A Dissertation

Presented to

the Faculty of the School of Engineering and Applied Science



In Partial Fulfillment

of the Requirements for the Degree of
Doctor of Philosophy of Electrical Engineering

by

Berhanu Tafesse Bulcha

November 2015

Abstract

Terahertz-frequency quantum-cascade lasers (THz QCLs) are compact electrically-driven sources of narrowband, coherent radiation in the 1–5 THz band. Although peak output powers in excess of 1 W have been demonstrated, most potential applications of THz QCLs as a local oscillator (LO) in THz astronomy and atmospheric spectroscopy require both frequency stability better than 1 ppm and narrow linewidth, with low phase noise sidebands [1]. However, temperature and current bias fluctuations in the gain media of the QCL can cause the refractive index to change with time, which affects the lasing frequency.

Phase locking improves the stability by using a negative-feedback system that combines a current-controlled QCL with a phase comparator and a stable reference so that the QCL maintains a constant phase angle relative to a reference signal. Since it is challenging to find a stable THz-frequency source to use as a reference, a THz mixer is needed to down-convert the signal to a lower frequency where frequency and phase comparisons are possible. A number of groups have accomplished QCL phase locking using a Hot Electron Bolometer (HEB) or Semiconductor Superlattice nonlinear device (SSL) as mixers [2]. However, these mixers require an additional cryo-cooler, which increases the size and the complexity of the phase locking system. Furthermore, room temperature SSL devices exhibit conversion loss of 80 dB or more,

which makes phase locking difficult [3]. Therefore, a room-temperature, solid-state mixer with lower conversion loss is desirable to produce more compact phase-locked THz sources.

This thesis describes the phase locking of free running 2.518 THz and a 2.6906 THz QCLs, which have achieved a spectral resolution of $\frac{f}{\Delta f} \simeq 10^{10}$. To phase lock THz QCLs, a room temperature Schottky diode based WM-86 (WR0.34) harmonic mixer is developed. The mixer consists of quartz-based Local Oscillator (LO) and Intermediate-Frequency (IF) circuits and a GaAs based beam-lead THz circuit with an integrated diode. Measurements of the mixer are performed using a 2 THz solid state source and 2.6906 THz QCL, and a conversion loss of 27 dB for the 3rd harmonic mixing is achieved. This is the first time the development of a WM-86 (WR0.34) harmonic mixer with a beam-lead THz circuit for frequencies above 2.5 THz is demonstrated and the result represents the best Schottky-based mixer in this frequency range. Similarly, this thesis also prescribes the phase locking of QCLs at 2.518 THz and at 2.6906 THz using Schottky diode for the first time after a 2.32 THz QCL phase locking was reported by a group at University of Massachusetts [4]. A phase locked QCL can be used to build a heterodyne interferometer in the far-infrared range and high-resolution heterodyne tunable spectroscopy for different applications such as radio astronomy, molecular spectroscopy, and plasma diagnostics [5].

Acknowledgments

I would like to acknowledge the people who made this project possible. First, I would like to express my sincere gratitude to my advisors Scott Barker and Jeffry Hesler. I would like to thank Scott Barker for his guidance, being a tremendous mentor and the valuable discussions over the years. I would like to thank him for encouraging my research, reviewing my thesis and for allowing me to grow as a research scientist. In addition, I also would like to thank Jeffrey Hessler for offering me an interesting project that made my years productive, for advising me on every step of this project, for providing resources and for infecting me with his curiosity. Without his kind support and knowledge on Schottky Mixers, this project would not be successful. I also would like to thank Bobby Weikle, my committee chair and co-director of Far Infrared (FIR) laboratory, for his insights and for coordinating resources when I was using the FIR laboratory. Additionally, I would like to thank the members of my committee, Richard Bradley and Andreas Beling, for their valuable assistance.

I would like to thank Matthew Bauwens, Bascom Deaver and Acar Isin for their help at the FIR lab. I was very fortunate to have had the opportunity to work at Virginia Diodes Inc. (VDI) and learn designing and testing THz and sub-millimeter wave devices and systems. I am grateful for having access the use of VDI's cleanroom and testing equipment to accomplish several parts

of this project. Furthermore, I would like to thank Jeffery Hassler, Thom Crowe and Stephen Jones for creating an enjoyable atmosphere at VDI while I was pursuing graduate school and their generosity and willingness to supporting the PhD fellowship. I would also like to thank members of VDI, such as David Kurtz for his support and valuable discussions, Mike Algeri, the “magic hand”, for assembling the THz circuits and Daniel Koller for his willingness to proofread this thesis and give me productive comments.

I also would like to thank members from numerous institutes who have contributed to this project such as Jan Stake and Vladimir Drakinskiy from Chalmers University who fabricated the THz circuit, and Alexander Valavanis and his team from University of Leeds who provided the 2.5 THz and 2.7 THz Quantum Cascade Lasers. I also would like to thank David Burghoff from Massachusetts Institute of Technology (MIT) for valuable discussions, a lab tour and providing 2.9 THz QCL. I would like to thank Jean-François Lampin from Lille University of Science and Technology for allowing me to work in his lab to test the THz harmonic mixer.

Finally, I would like to thank my family who has always been at my side and encouraging me to follow my dreams. Words cannot express how grateful I am to my brother Jote Tafesse who has challenged me since I was young. I would also like to thank all of my friends who supported me in writing this, and motivated me to strive towards my goal. In the end, I would like to express my appreciation to my mom, Yeshihareg Abate, who raised me with unconditional love, support, and continuous prayer, and I would like to dedicate this work to her.

Contents

Abstract	i
Acknowledgments	iii
List of Figures	vii
List of Tables	xvii
1 Introduction	1
1.1 THz Sources	2
1.2 Stabilizing Quantum Cascade Laser	5
1.3 Thesis Overview	7
2 Background	11
2.1 Quantum Cascade Laser	11
2.1.1 Chirped Active Layer Design	14
2.1.2 Bound-to-Continuum Active Layer Design	15
2.2 Phase Locking a THz Source	18
2.3 LO and RF Driver Chains	22
2.4 Amplitude Noise (AM) Measurement	24

3	THz Schottky Diode-based Harmonic Mixer	29
3.1	Harmonic Mixer LO and IF circuit designs	34
3.2	Harmonic Mixer THz Circuit Design	39
3.2.1	Circuit Position Sensitivity	43
3.3	Diagonal Horn Design	45
3.4	Fabrication of THz Circuits and Integrated Diode	47
3.5	Block Machining and Assembly	50
3.6	Harmonic Mixer Test and Measured Performance	52
3.6.1	Video Response and Responsivity	54
3.6.2	Harmonic Mixing	61
3.6.3	Mixer Noise Temperature and Conversion Loss using Y-Factor Technique	68
3.7	Comparison of Test and Simulation Results	74
3.8	Room Temperature Schottky based Receiver	78
4	Characterizing and Phase Locking of Quantum Cascade Lasers	81
4.1	Characterizing Quantum Cascade Laser	82
4.1.1	THz Beam Characterization	88
4.1.2	QCL Output Power Measurement	102
4.1.3	Real-Time Spectrum	107
4.2	Phase Locking of 2.518 THz and 2.6905 THz QCL	109
4.3	Phase Locking System	114
4.3.1	Frequency Tuning of the THz QCL	118
4.4	Phase Noise and Long Term Frequency Drift	119
4.4.1	Frequency Drift	123

5	Conclusion and Future Work	127
5.1	Conclusion on THz Harmonic Mixer	127
5.2	Harmonic Mixer Future Work	129
5.2.1	WR-52 (WR0.22) Harmonic Design	129
5.2.2	Double Balance Design	130
5.2.3	Schottky based THz Receiver	131
5.3	Conclusion on Phase Locking a THz QCL	133
5.4	Phase Locking a THz QCL Future Work	134
5.4.1	Phase Locking of a 4.7 THz QCL	134
5.4.2	Integrating QCL within a Mixer Block	135
A	Schottky Diode	137
A.1	Diode Parasitic Elements	138
B	WM-102 (WR0.4) Harmonic Mixer Performance	141
B.1	Block Design	142
B.2	LO Return Loss and Video Response	143
B.3	Conversion Loss	145
C	WM-86 (WR0.34) Harmonic Mixer Block Design	147
D	QCL Mount Design	151

List of Figures

1.1figure	submillimeter-wave satellites and telescopes.	2
1.2figure	Microwave and optical THz sources and their output power: The image is taken from Dr. Aik Tang [6]	4
2.1figure	a) QCL structure, b) QCL's lasing principle of operation	12
2.2figure	Chaiped active layer design with periodic structures of the injector and active regions, the image is taken from [7].	15
2.3figure	Bound-to-Continuum active layer design with mingap, the image is taken from [7].	16
2.4figure	Schematic of (a) simi-insulating surface plasmon waveguide and (b) metal-metal waveguide, this image is taken from [8].	17
2.5figure	Phase locking of a free running YIG based 2.01 GHz RF source with a stable microwave source	19
2.6figure	Phase locked IF signal from the second stage down conversion	21
2.7figure	LO chian for 500-750 GHz operation.	23
2.8figure	23
2.9figure	Experimental AM noise test setup	26

2.10figure	AM noise performance of a WM-2540 (WR10) system with different references	27
2.11figure	WM-380 (WR1.5) system AM noise performance (AM noise vs. output IF frequency) for different input power.	28
3.1figure	Summary of VDI's Schottky based mixers a) Conversion Loss vs. RF Frequency, b) Noise Temperature vs. RF Frequency	30
3.2figure	WM-102 (WR0.4) harmonic mixer THz circuit	32
3.3figure	WM86 (WR 0.34) Harmonic mixer internal circuitry	33
3.4figure	35
3.5figure	S_{11} simulation of the 500-750 GHz LO termination provided by the beam lead right after the RF probe	36
3.6figure	WM-380 (WR1.5) LO input waveguide with LO probe connected to IF circuit using 1 mil gold bond wire	37
3.7figure	38
3.8figure	1.9-3.2 THz harmonic mixer internal design.	39
3.9figure	RF filter with five sections of HI_Z and Low_Z transmission lines.	40
3.10figure	RF filter performance	40
3.11figure	41
3.12figure	THz circuit performance (return loss and transmission vs. output frequency)	42
3.13figure	43
3.14figure	44
3.15figure	Schematic of diagonal feedhorn	45
3.16figure	WM-86 (WR0.34) harmonic mixer block	46

3.17figure	The simulated antenna pattern of the WR0.34 diagonal feedhorn for an angle theta of -90-90 degrees and an angle phi of 180 degree. . . .	47
3.18figure	1.9-3.2 THz circuit with beam lead, the SEM image is taken at the University of Chalmers	48
3.19figure	THz Schottky diode structure.	49
3.20figure	The WM-86 (WR0.34) harmonic mixer block and circuit channels.	51
3.21figure	THz diode model	52
3.22figure	I-V curve of the THz diode	53
3.23figure	LO return loss measurement using VNA extender calibrated using SOLT.	54
3.24figure	LO video response test setup	55
3.25figure	LO responsivity measurement for WM-86 (WR0.34HM) with WM-380 (WR1.5) LO input waveguide for different current biases is shown. Due to the calibrated waveguide connections and higher LO input power, the measurement uncertainty is neglected.	56
3.26figure	RF video response test setup	57
3.27figure	RF responsivity of the WM-86 (WR-0.34) harmonic mixer for different current biases, measurement uncertainty is shown in Table 3.3, adding the uncertainty would change the RF responsivity at 1965 GHz and for a current bias of $50 \mu\text{A}$ to $600 \pm 130 \text{ V/W}$	58
3.28figure	Video response test setup using 2.6906 THz QCL	60

3.29figure	Responsivity performance of the WR0.34 harmonic mixer tested using approximately 2.6906 THz QCL at different current biases, measurement uncertainty is shown in Table 3.3, adding the uncertainty would change the RF responsivity at 2691 GHz and for a current bias of 50 μ A to 1200 ± 400 V/W.	60
3.30figure	Harmonic mixing test setup.	62
3.31figure	Experimental setup for harmonic mixing at 2 THz using solid state sources.	62
3.32figure	WM-86 (WR0.34) harmonic mixer performance (measurement uncertainty is shown in Table 3.3), adding the uncertainty for the 300 μ W LO drive would change the conversion loss to 32.5-35.5 dB.	63
3.33figure	Mixer's performance (IF output vs. current bias) for 380 μ W LO power, measurement uncertainty is shown in Table 3.3, adding the uncertainty for the current bias of 150 μ A of the 2 nd mixer would change the conversion loss to 27.5-30.5 dB.	64
3.34figure	Optimized conversion loss vs. RF frequency, measurement uncertainty is shown in Table 3.3, adding the uncertainty will change the conversion loss by 0.5-2.5 dB across the band.	65
3.35figure	Conversion Loss of the WM-86 (WR0.34) harmonic mixer tested using 2690-2691.8 GHz QCL, measurement uncertainty is shown in Table 3.4, adding the uncertainty will change the conversion loss by 0.9-3.5 dB across the band.	66

3.36figure	Conversion Loss of a 40 GHz IF bandwidth is tested for a fixed RF: 2690 GHz and LO: 2690.5-2730 GHz, measurement uncertainty is shown in Table 3.4, adding the uncertainty will change the conversion loss by 0.9-3.5 dB.	66
3.37figure	The Y -factor method for measuring the system noise temperature.	69
3.38figure	Noise temperature of a cascaded system.	70
3.39figure	T_{sys} versus T_{IF}	71
3.40figure	Noise temperature measurement of the WR0.34 harmonic mixer	73
3.41figure	Comparison of the simulated and measured performance of the WM-86 (WR0.34) LO responsivity at a current bias of $30\mu A$	75
3.42figure	ADS simulation circuit model	76
3.43figure	(a) Comparison of the simulated and measured performance of the WM-86 (WR0.34) harmonic mixer for RF: 2 THz, IF: 1 GHz, and current bias of $150\mu A$, measurement uncertainty is shown in Table 3.3, adding the uncertainty will change the conversion loss by 0.5-2.5 dB, (b) Inductance vs. conversion loss.	77
4.1figure	83
4.2figure	84
4.3figure	85
4.4figure	THz focal plane array of the microbolometer-based camera setup with a beam splitter to image the QCL beam.	89
4.5figure	Image of the THz beam at different current biases is taken using IRV-T0831 THz camera.	90
4.6figure	92

4.7figure	A ~2.6906 THz normalized power versus 2D beam pattern at 0.85 A current bias.	93
4.8figure	The 2.6906 THz beam radii at different locations in the optical axis. .	94
4.9figure	Power coupling efficiency at different distance along the optical axis. .	96
4.10figure	98
4.11figure	Experimental setup to map the focused beam using X-Y stage. . . .	99
4.12figure	The 2.6906 THz focused beam radii at different locations in the optical axis.. . . .	100
4.13figure	A ~2.6906 THz QCL focused beam coupling efficiency at different position.	101
4.14figure	Output power of the 2.6906 THz QCL measured using Erickson power meter (2dB correction is added), measurement uncertainty is shown in Table 4.4, adding the uncertainty would change the output power by approximately 0.9-3.5 dB.	103
4.15figure	Usable THz power measurement setup using an Erickson power meter.	104
4.16figure	Usable THz power measured using an Erickson power meter, measurement uncertainty is shown in Table 4.4.	105
4.17figure	System test setup and output power in each stage.	106
4.18figure	Real time spectrum view of a 2.6906 THz QCL down converted signal is shown for a 85 MHz span and 300 ms acquisition time.	108
4.19figure	Schematic of the setup for phase locking a QCL.. . . .	109
4.20figure	Experimental setup to down convert the QCL; beam splitter and THz camera is used to monitor the QCL output.	110
4.21figure	QCL phase locking loop test setup.	111

4.22figure	112
4.23figure	113
4.24figure	Phase locking loop diagram	115
4.25figure	XL-Microwave phase locking module circuit	116
4.26figure	120
4.27figure	Phase locked 2.5182 THz QCL beat signal long term stability test using signal tracking.	125
4.28figure	Phase locked 2.6906 THz QCL beat signal long term stability test using signal tracking.	125
5.1figure	WM-52 (WR0.22) harmonic mixer design.	130
5.2figure	WM-52 (WR0.22) harmonic mixer block.	130
A.1figure	Schottky diode equivalent circuit.	138
A.2figure	Schottky diode equivalent circuit, image is taken from [6].	139
B.1figure	142
B.2figure	142
B.3figure	143
B.4figure	143
B.5figure	144
B.6figure	144
B.7figure	145
B.8figure	145
C.1figure	147
C.2figure	148

C.3figure 149

D.1figure 151

D.2figure 152

List of Tables

3.1table	WM-86 (WR0.34) harmonic mixer block channel and waveguide dimensions.	51
3.2table	Measured DC parameters of the THz diode	53
3.3table	Estimated measurement uncertainty.	59
3.4table	Estimated measurement uncertainty.	67
3.5table	Measured noise Temperature of the IF chain.	72
4.1table	Current bias and frequency versus 2.69 THz QCL mounting temperature	86
4.2table	Parameters used to calculate thermal time constant.	88
4.3table	Power correction factors for near field.	103
4.4table	Estimated measurement uncertainty.	103
4.5table	Measured available THz power and correction factors used, measurement uncertainty is shown in Table 4.4, adding the uncertainty would change the RF available THz power by approximately 0.9-3.5 dB.. . .	105

1. Introduction

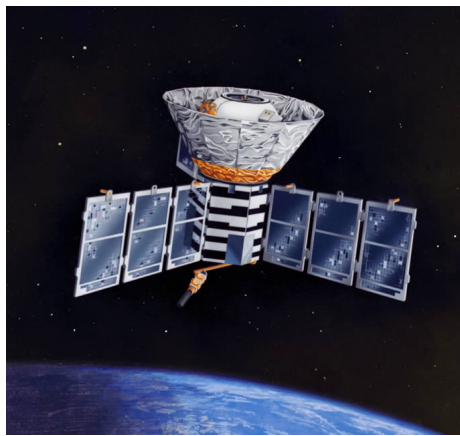
The frequencies above 1 THz are a relatively unexplored segment of the electromagnetic spectrum. Since a wealth of molecular and atomic transitions is in the THz frequency range, the transition provide vast amounts of information in different research areas such as radio astronomy, atmospheric science and spectroscopy. Atmospheric researchers investigate the ozone destruction cycles caused by OH radicals at 2.510 THz and 2.514 THz [9], [10]. Additionally, the molecular oxygen line at 2.502 THz and the astrophysically important neutral atomic oxygen line at 4.7448 THz, which facilitate the understanding of star formation processes, are within the THz spectrum. Currently, highly advanced submillimeter-wave satellites and telescopes shown in Figure 1.1, such as COBE, APEX, ALMA, SOFIA and Herschel Space Observatory, provide a wealth of information for the astronomy community for better understanding of the planetary atmospheres and the universe formation [11]. Most of these tools utilize spectroscopic techniques to investigate properties of distant stars and galaxies, such as their chemical composition, density and mass. Therefore, it is desirable to build compact and high output power THz sources to produce tunable spectrometers for those applications.



(a) ALMA



(b) SOFIA



(c) COBE

Figure 1.1.: submillimeter-wave satellites and telescopes

1.1. THz Sources

High output power vacuum-tube technology sources such as Klystrons and Gyrotrons provide 5-0.5 kW power for frequencies 1-1.3 THz [12]. However, these types of sources are too bulky for space based applications. Other high power THz source such as Far Infrared (FIR) lasers that use different gaseous organic molecules filled in (1-3 m) cavity are optically pumped and they are only line tunable [13].

Progressing upward in frequency from the microwave regime, Schottky-based frequency mul-

multipliers is widely used. The two leading groups in high power Schottky-based technology are Virginia Diodes Inc, (VDI) and the Jet Propulsion Laboratory (JPL). The high power Schottky technology is varactor-based (variable reactance) multipliers that use the nonlinear capacitance of the Schottky diode to produce harmonic of the input signal. Typically, high power varactor multipliers have an efficiency of 40-70 %, however their bandwidth is limited to less than 20 %. VDI provides frequency sources by cascading high power varactor doublers up to 1 mW output power at 790 GHz and by cascading varactor doublers and varistor (variable resistance) triplers extending the frequency up to 3 THz with a microwatt output power. In general, the output power from Schottky based microwave sources for frequencies greater than 2.5 THz is less than 100 μ W [14]. This is due to the poor conversion efficiency of the last stage multipliers used in the Amplifier Multiplier Chain (AMC).

Progressing downwards from the optical domain, the output power of the optical source are improving, however these sources are not stable enough for space based applications. The output power of different THz sources is shown in Figure 1.2. The lack of compact, high output power and stable sources in the THz region is known as the ‘THz gap’. Furthermore, due to high water absorption in the atmosphere between 2–5 THz, it is challenging to do astronomical studies using ground based telescopes. For airborne and space-based spectroscopy measurement, receivers need to have high sensitivity and sharp spectral resolution $\frac{f}{\Delta f}$ at least of $\sim 10^6$ [15]. Therefore, it is desirable to have high output power, stable and compact Local Oscillators (LO) to implement THz receivers that can be used in space-based or suborbital observatories.

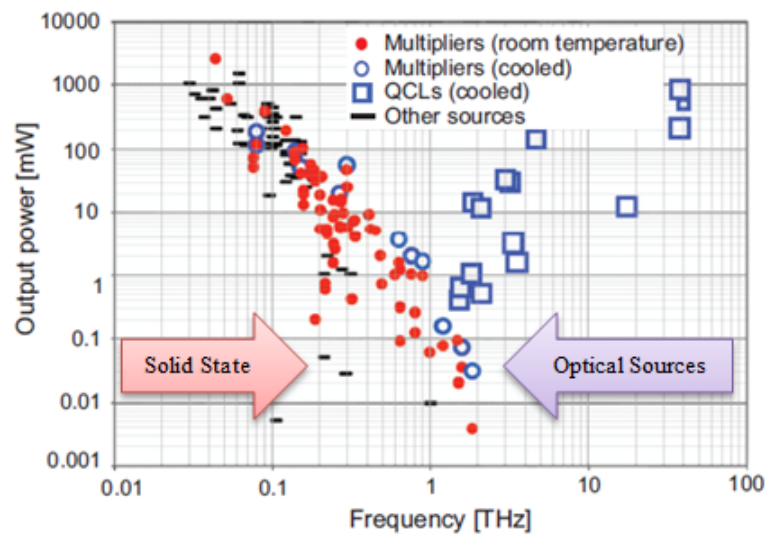


Figure 1.2.: Microwave and optical THz sources and their output power: The image is taken from Dr. Aik Tang [6]

THz Quantum Cascade Laser (QCL) is a promising solid state THz source with applications ranging from security imaging, chemistry and astronomy. The principle of operation of a QCL is different from interband bipolar lasers; the radiative transitions involve electron-hole recombination. In this approach, the lasing frequency is determined by the band gap of the material used. Due to the lack of semiconductor materials with band gap energy less than 40 meV, producing lasers in the far-infrared region becomes impractical. Hence, it is important to tailor a semiconductor material and produce an electronic state with the desired band gap. QCLs are engineered to operate using the intraband radiative transitions within two dimensional quantum-wells. Intraband transitions are a uniplor process that only involves electrons in the valance band. By cascading many superlattice hetrostructures, it is possible to produce larger number of photons.

1.2. Stabilizing Quantum Cascade Laser

QCL source has a great potential in the THz region for certain applications, however, temperature and current bias fluctuations in the gain media of the QCLs cause the refractive index to change with time, which affects the lasing frequency. For a practical solution to use a THz QCL as an LO for radio astronomy beyond 2 THz, the laser must be phase locked. A phase locking system improves the stability by using a negative-feedback system that combines a current-controlled QCL with a phase comparator so that the QCL maintains a constant phase angle relative to a reference signal. Phase locking to a reference transfers the spectral line profile of the reference to the QCL output; this controls the phase and frequency precisely in sub-megahertz accuracy [2].

Stabilizing a QCL using a stable reference was first demonstrated by Betz in 2005 [1]. Since then, a locked QCL using different techniques has been utilized as an LO in a receiver system [16]. Betz frequency locking technique stabilizes the QCL to a stable FIR gas laser by down converting the QCL's output to 48 GHz using a Schottky-diode mixer in a corner reflector mount. The down converted signal is fed to the IF port of the mixer and mixes with the second harmonic of a 24.6 GHz microwave source driven by a phase locked YIG oscillator and produces a 1.2 MHz output signal. The 1.2 MHz signal is fed to a programmable locking module and the output DC current due to the error signal biases the QCL and stabilizes the QCL. This technique frequency locked the QCL, nevertheless, the locking system involves FIR laser that uses transitions of methanol gas. Hence, the system is bulky and expensive to run.

Another phase locking approach is demonstrated by down converting the QCL's output using a super-lattice device as a harmonic mixer operating at room temperature and 10 K [3][17]. The mixer is pumped with a lower LO frequency and a higher harmonic factor ($N=18$) to mix with the QCL output and down convert to lower frequency beat note. This approach worked quite

well when the super lattice device was operated at 10 K which improves the signal-to-noise ratio to phase lock the system. However, a cryogenic system is required to operate the super-lattice device at this temperature, which increases the size of the phase locking system. Similarly, different groups have demonstrated phase locking using a superconducting NbN HEB as a mixer. The mixer is pumped using a superlattice multiplier at the 15th harmonic to extend the frequency to ~2.7 THz. The down converted signal is fed to the phase locking module and the DC output locks the QCL [18]. This experiment is able to concentrate less than half of the THz power in the narrow band of the reference. This approach also requires an additional cryocooler to operate the superconducting HEB mixer. Another technique implemented to stabilize a QCL is by phase locking using a photomixer-based frequency comb generated by a mode locked femtosecond fiber laser. Even though this approach requires additional laser to the phase lock the QCL, the THz power spectrum is phase locked [19] [20].

The Stratospheric Observatory for Infrared Astronomy (SOFIA) heterodyne spectroscopy project has three receivers at 1.4 THz, 1.9 THz and 4.7 THz. The first two receivers use a stable LO source using solid state based technology. However, due to the lack of stable LO source at the 4.7 THz range, the third receiver uses QCL source [21]. Since higher spectral resolution is required in this project, the QCL is relatively stabilized using a Stirling cooler, dedicated heat sink and a low-noise current source. As a result this technique is costly and the stability approximately 1 ppm.

Therefore, It is desirable to produce a more compact phase locking method using room temperature solid state devices for different applications. This thesis demonstrates phase locking of a free running QCL at 2.518 THz and 2.6906 THz to a stable quartz based reference using room temperature Schottky diode based 1.8-3.2 THz WM86 (WR0.34) harmonic mixers. The mixers use the harmonics of the LO to mix with the QCL's radiation and down convert into a lower

frequency beat signal to compare its phase with highly stable 100 MHz microwave reference signal. The digital phase detector captures the IF signal from the mixer and compares its phase with the reference. The DC voltage produced due to the phase difference feeds back into the QCL to complete the phase locked loop and stabilize the QCL within sub-kilohertz accuracy.

1.3. Thesis Overview

The achievements of this research can be grouped into three parts. The first step involves designing, fabrication, assembly and characterization of the 1.8-3.2 THz mixer. The Harmonic mixer circuitry is designed and analyzed using a three dimensional finite-element analysis program called High Frequency Structural Simulator (HFSS). This program is also used to analyze the circuit position sensitivity and its effect on the mixer's performance. Furthermore, Advanced Design Systems (ADS) based Harmonic Balance (HB) technique is used to assess the theoretical limit and at the end comparison is performed with the measured result. The mixer's housing is also designed and machined using a Computer Numerical Control (CNC) milling machine. The block is machined into two halves with the E-plane split between the two halves of the block. Once the circuitry are assembled on the block, the mixer is characterized using solid state WM-380 (WR1.5) LO source and 1.8-2 THz RF source and further characterization is performed using a 2.690 THz QCL.

The second step is mounting and setting up the QCL on a 4.2 K cryogenic stage dewar. Once the current bias to the QCLs is set up, the harmonic mixer is tested and RF video response is observed. The harmonic mixer is operated in the detector mode and the 2.6906 THz beam is characterized using an X-Y scanner. The beam waist radius of the THz beam at different positions in the optical axis is measured, the divergence angle and the beam quality factor are

determined.

The final step is to phase lock the 2.5 THz and 2.690 THz QCLs using harmonic mixer by down converting the QCL's radiation to 100 MHz. Phase locking involves a digital locking module that tracks the beat signal and feedback a DC voltage to the QCL to complete the locking loop.

Chapter 2 contains a basics of optical sources and the theory of different types of QCL designs, such as different active layers and waveguides to confine the THz mode. Furthermore, phase locking of a THz laser such as a free running YIG driven 2 THz solid state source with multiplication factor of $N=144$ is phase locked and the result is discussed. Moreover, phase locking of a QCL is introduced and discussed briefly. At the end of Chapter 2, performance of the LO and RF amplifier multiplier chains used to drive the harmonic mixer is presented and AM noise performance of the driving chain is studied to further improve the signal-to-noise ratio of the QCL's beat note and ease the phase locking process.

Chapter 3 is devoted to the WM-86 (WR0.34) harmonic mixer's structural and non-linear simulations, fabrication, assembly and presents testing results. The harmonic mixer is designed to cover 1.8-3.2 THz, the LO, IF and RF circuit designs and their design performance are presented. Techniques to characterize the harmonic mixers, such as video response, harmonic mixing test, Y-factor method, mixer's noise temperature and conversion loss are measured and briefly discussed. At the end of the chapter, some of the challenges and position sensitivity of the circuit during assembly is presented.

Chapter 4 is dedicated to the phase locking of the 2.518 THz and the 2.690 THz QCLs by implementing a system that contains a THz harmonic mixer, LO driving chain and phase locking circuit. In addition, a long term stability and phase noise of the beat signal after phase locking is presented.

Chapter 5 presents conclusions and ideas for future work such as the 3-5 THz harmonic mixer

1.3 Thesis Overview

design to phase lock a 4.7 THz QCL. The most direct audiences of the work presented in this thesis are academic institutions, companies and research labs that are working in THz detection, THz receivers and transmitters development.

2. Background

The first section of this chapter provide a broad discussion of the different types of QCL's, such as active layers and waveguide designs to confine the THz field. More discussion of the specific QCLs that are used in this research and the preparation to phase lock QCL using room temperature techniques is described. The second section describes the phase locking of a THz source, such as free running YIG driven 2 THz solid state source, THz QCL and the challenges associated with phase locking is also presented. Section three characterizes the LO and RF amplifier multiplier chains used to drive the harmonic mixers and to phase lock the THz QCLs. Finally, section four focuses on mitigating the AM noise performance of the LO chain that pumps the mixer to maximize signal-to-noise ratio, thus optimize phase locking process.

2.1. Quantum Cascade Laser

The technology of gas lasers in the Far-Infrared (FIR) and Mid-Infrared (MIR) frequencies have been developed for quite sometime and they are one of the few source that provide relatively stable and high power output above 1.5 THz. However, these frequency sources are bulky, line tunable and difficult to use for space based applications. On the other hand, semiconductor

lasers such as diode lasers are compact and produce significant output power (>1 mW) [22]. Diode laser transition occurs between the conduction band and valance band of the semiconductor; a single photon is emitted when an electron from the conduction band recombines with a hole at the valance band. The energy emitted in this process is proportional to the radiated frequency, $E = hf$; hence, there is a lack of natural semiconductor material with energy gap less than 40 meV to produce a CW mode for frequency less than 10 THz. To alleviate this challenge, Quantum Cascade Laser (QCL) was produced by Federico Capasso's group at Bell labs in 1994 [23]. QCL is a type of semiconductor laser which uses epitaxially grown quantum wells that contains electrons in the lasing state.

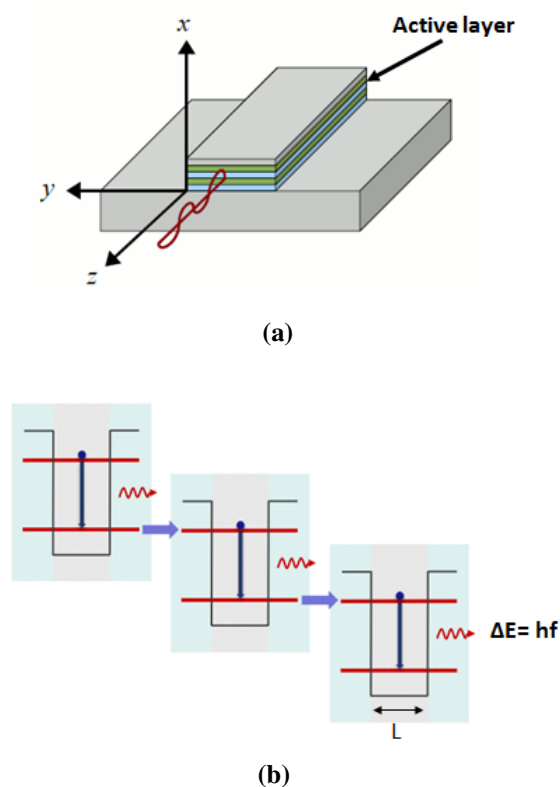


Figure 2.1.: a) QCL structure, b) QCL's lasing principle of operation

2.1 Quantum Cascade Laser

These heterostructure devices mostly use *GaAs/AlGaAs* material grown using molecular beam epitaxy (MBE). The *GaAs* is used as a quantum well and the *AlGaAs* is used as a barrier. The principle of operation of a QCL is different from other types of semiconductor lasers such as diode laser. In a QCL the transition occurs between states within a given quantum well. The conduction band energy difference ΔE_c between *GaAs* and *Al_xGa_{1-x}As* for different values of x is relatively small energy gap that is compatible to laser terahertz radiation. The lasing frequency is proportional to the heterostructure thickness L ; therefore, precise device fabrication is important to achieve the desire output frequency, (see Eqn. (2.2)).

For a simplified one dimensional quantum well, the bound state wave functions $\psi(z)$ can be found by solving the Schrödinger equation numerically.

$$\left[-\frac{\hbar^2}{2m_e^*} \frac{d^2\psi(z)}{dz^2} + V(z)\psi(z) \right] = E\psi(z) \quad (2.1)$$

For an electron that is confined between *AlGaAs* and *GaAs* is located in the middle, we can assume an infinite potential well ($V(z) = \infty$) and the energy eigenvalues for positive principal quantum number n is given as:

$$E_n = \left(\frac{\hbar^2}{8m^*L^2} \right) n^2 \quad (2.2)$$

The gain of a QCL occurs from the interband radiative transition between the quantum well. This process is a unipolar occurrence where only an electron in the conduction band is involved between quantized states. Once the electron is confined within the quantum well and emits photon by transitioning to lower energy level, the applied electric field due to the voltage bias forces the electron to transition in the active region and to emit more photons; thus, it is possible to create large number of photons by cascading many layers of *GaAs/AlGaAs* heterostructure

[24].

To achieve a gain via stimulated emission, population inversion between upper and lower bands is required. Once an electron is injected to the upper radiative state with injection efficiency η , it has a finite lifetime to either relax to a lower state or to scatter out to the device. It is important to have a longer lifetime at the upper energy state and a lower lifetime at the lower energy state to maintain population inversion.

Achieving population inversion in FIR is difficult due to various scattering mechanisms. This create challenges to selectively depopulate the lower radiative state when the energy separation between the upper and the lower state is too small (5-20 meV). Furthermore, in a QCL, there are manly two types of active layer designs that have shown good performance. Section 2.1.1 and Section 2.1.2 discuss the two types of active layer designs, such as Chirped and Bound-to-Continuum [25][26].

2.1.1. Chirped Active Layer Design

The first QCL is demonstrated using chirped superlattice design [27][28], where the neighboring injector regions form minibands spaced by the active region. The active regions is properly designed by choosing material compositions and quantum well thickness to create an Eigenfunction with continuum energy level with energy gap (subbands). The injector region is also formed using sequence of decreasing quantum wells (chirped) to form miniband. Electron relaxation occurs between the upper state 3 and the lower state 2 in the active region by emitting photons and goes to a fast scattering process to subband 1. Due to the electric field, the electrons are injected via resonant tunneling from the injector to the next active region to produce more photons.

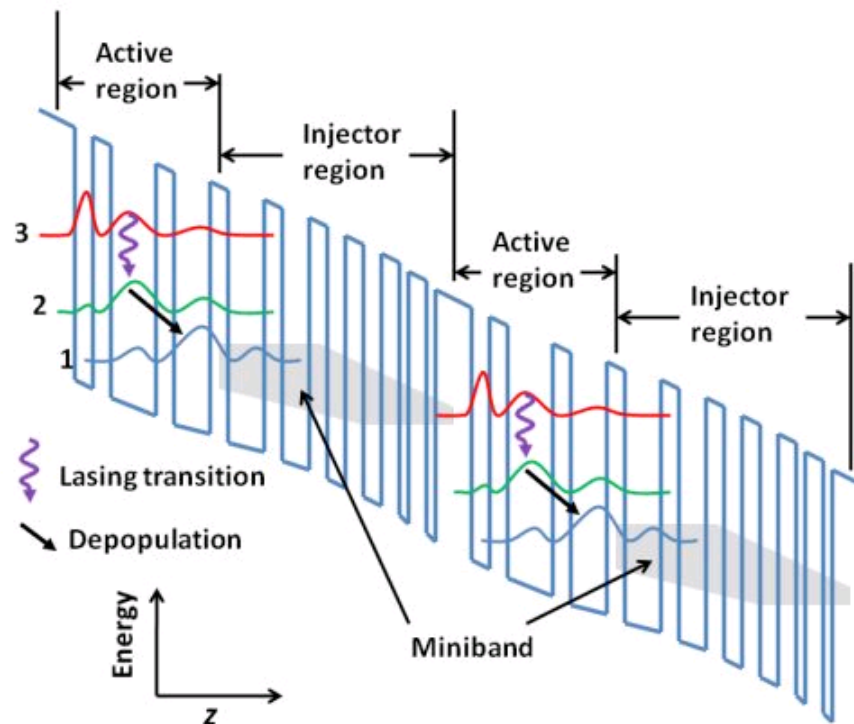


Figure 2.2.: Chaired active layer design with periodic structures of the injector and active regions, the image is taken from [7].

2.1.2. Bound-to-Continuum Active Layer Design

Bound-to-Continuum design is an improved version of the Chirped Superlattice that also utilizes minibands to depopulate the lower states [29]. This technique uses a bound upper state and lower state in the minigap to prevent electrons from escaping. The transition occurs between the upper state 1 and the lower state 2 and produces a photon. This process is followed by depopulation and resonant tunneling to the neighboring active region. At higher temperature, this approach helps to isolate non-radiative thermally agitated locally oscillating scattering from the upper state into the next miniband. As a result, this technique has shown improved temperature handling and power performance compared to chirped superlattice design. Furthermore, most

of the QCLs that function at lower frequency are based on this bound-to-continuum design [25][26].

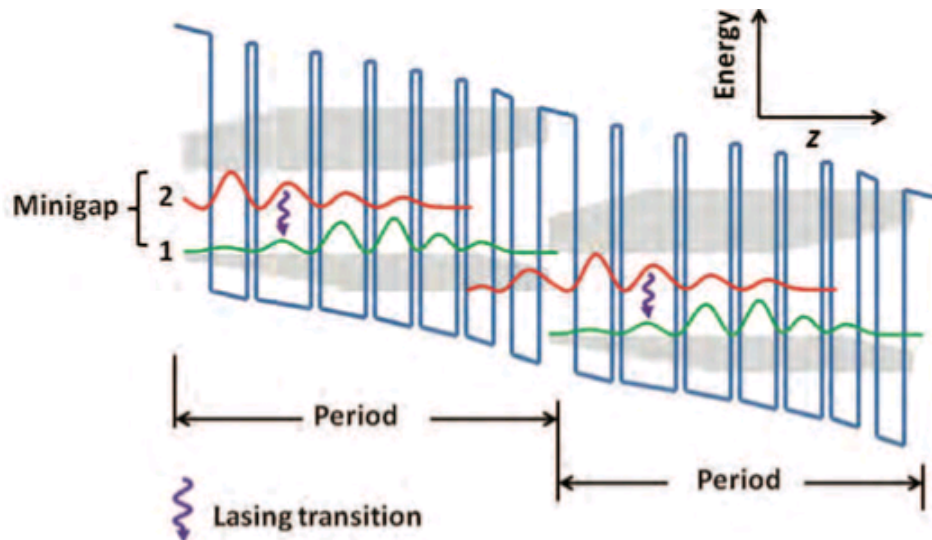


Figure 2.3.: Bound-to-Continuum active layer design with minigap, the image is taken from [7].

In *GaAs/AlGaAs* heterostructure QCL devices, *GaAs* has higher refractive index than *AlGaAs*. As a result the material cannot confine modes in the growth direction [8]. Therefore, highly doped materials, such as Semi Insulating Surface Plasmon waveguide (SISP) or Metal-Metal (MM) based waveguides can be used to confine the optical modes. The SISP waveguide uses metallic layer in the top of the active region and highly doped n^{++} material that is grown below the active region. Since the highly doped material is too thin, few modes leak into the substrate resulting in a smaller confinement factor that can be achieved in this type of waveguide. Metal-metal waveguide has shown a better confinement factor by replacing the highly doped material with metallic sheet. This also increases the heat removal process and it can be used to produce a QCL for higher temperature operation.

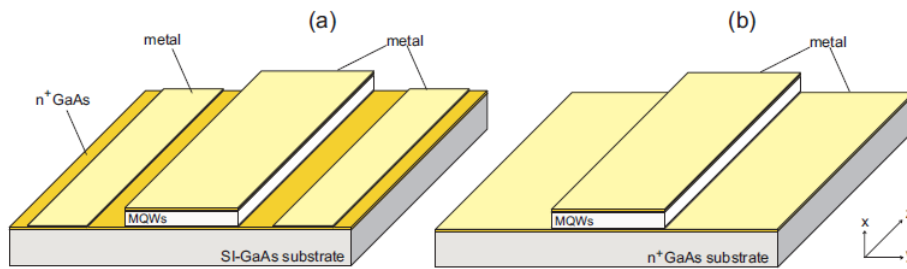


Figure 2.4.: Schematic of (a) semi-insulating surface plasmon waveguide and (b) metal-metal waveguide, this image is taken from [8].

For most applications in THz astronomy and atmospheric spectroscopy, the LO should have high frequency accuracy better than 1 ppm and narrow linewidth with low phase noise sideband [1]. However, temperature and current bias fluctuations in the gain media cause the index of refraction to change, in turn altering the optical path length of the cavity and the emission wavelength. The output frequency can be controlled by changing the bias current using a feedback mechanism [1]. Therefore, stabilizing a QCL using phase locking technique to a stable microwave reference is needed to control the frequency and linewidth to a submegahertz accuracy.

In general QCL with narrow linewidth is preferred for different applications however, the external noise factors such as mechanical vibration and temperature and bias fluctuations cause linewidth broadening [30]. Mostly, QCLs have a linewidth of few hundreds of megahertz down to a few KHz, and by removing the noise from the external factor using various techniques, the linewidth of the QCL can be reduced to few Hz. This can be attained by phase locking the QCL to a stable reference signal and removing the external drifts and vibrations, (experimental setup and phase locking of a QCL is briefly described in Chapter 4). Due to the fundamental quantum limitations, phase locking can not eliminate intrinsic noise sources such as carrier noise, blackbody radiation and spontaneous emission. This linewidth broadening due to the

intrinsic property of the QCL can be minimized by carefully designing and fabrication the heterostructure quantum wells [30][7][31].

In this project, two types of QCLs that operate at different frequency bands are used. The QCLs are fabricated at University of Leeds for single mode operations. The first QCL is designed to operate at 2.518 THz with a nominal current bias of 1.63 A and the second QCL is design to work at 2.6906 THz for approximately 2 GHz bandwidth with a current bias of 0.85 A. Both QCLs are based on GaAs/AlGaAs active region and the operation is based on bound-to-continuum design and it's a single plasmon ridge waveguide to confine the THz emission.

For phase locking applications, the QCL is driven in a continuous wave (CW) mode. Initially the output power of the QCL is measured at University of Leeds using helium-cooled Ge:Ga composite bolometer and the reading is scaled by the detector's responsivity. Similarly, the output power of the 2.69 THz QCL is measured using VDI's Erickson power meter and the output power for different current biases data is presented in Section 4.1.2. During operation the QCL dissipate approximately 3-8 W; thus, a closed cycle cooling system is used to dissipate the power produced from the QCL as well as to keep the QCL operation temperature to less than 40 K.

2.2. Phase Locking a THz Source

Phase locking of a THz source such as QCL and YIG driven solid state THz source uses a negative feedback system that combines a voltage controlled THz source with a phase comparator so that the THz source maintains a constant phase angle relative to a reference signal. Since it is challenging to find a stable reference in the THz frequencies to use as a reference, a THz mixer is needed to down convert the signal to a lower frequency where frequency and

2.2 Phase Locking a THz Source

phase comparisons are possible. A number of groups have accomplished QCL phase locking using a hot electron bolometer (HEB) or semiconductor superlattice nonlinear device as mixers [2]. These approaches require continuous cryogenic cooling during operation, which increases the size of the receiver. A room temperature phase locking method using solid-state devices is desirable to produce more compact LO sources.

Initially, we have demonstrated phase locking of a free running YIG based 2 THz AMC to a stable quartz based 100 MHz microwave reference. This phase locking system encompasses different components, such as a free running YIG driven 2.010 THz AMC as an RF source and phase locked synthesizer driven 667 GHz AMC as LO source. Figure 2.5 depicts the block diagram of the phase locking system.

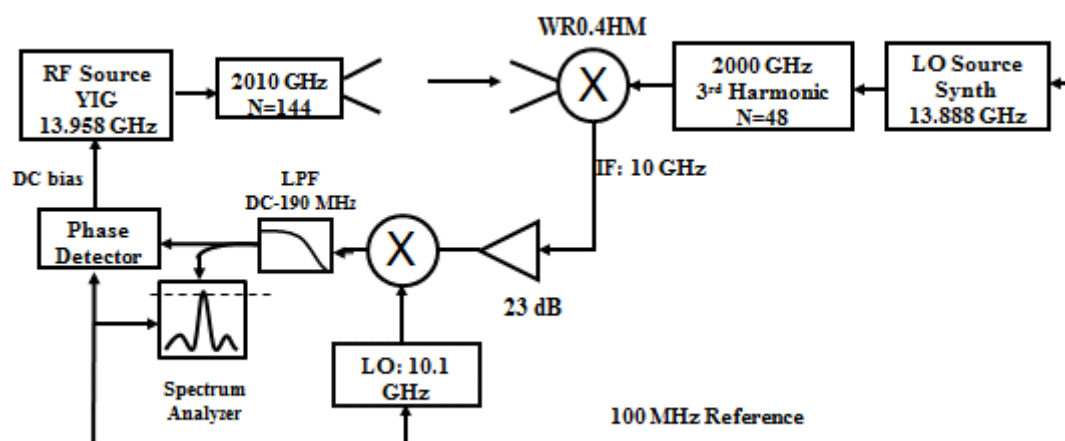


Figure 2.5.: Phase locking of a free running YIG based 2.01 GHz RF source with a stable microwave source

The WM-102 (WR0.4) harmonic mixer is used to down convert the RF signal into a lower frequency to compare its phase with a stable 100 MHz reference. The RF source consists of a free running YIG from Microlambda operating at 13.958 GHz that drives a solid state

AMC of multiplication factor of $N=144$, which gives an RF frequency of 2.01 THz. A phase locked microwave synthesizer is used as an LO source to drive an AMC to produce a 667 GHz signal with an output power of 1 dBm. When the LO source is pumping the WM-102 (WR0.4) harmonic mixer, it generates the 3rd harmonic at 2 THz and mixes with the 2.01 THz RF signal resulting in a 10 GHz IF signal.

Due to a significant AM noise from the LO source, the down converted signal-to-noise ratio is less than 8-10 dB/MHz and phase comparison with a synthesized reference signal at 100 MHz becomes challenging, thus a second stage down conversion is required. Since 10 GHz provides relatively better AM noise performance, the THz signal is down converted to 10 GHz. The 10 GHz IF signal from the first stage mixes with a stable microwave source at 10.1 GHz and produces a 100 MHz signal. The IF signal from the second stage mixer feeds into a low pass filter to clean unnecessary intermodulated signals. The digital phase detector compares the IF signal from the second mixer and the 100 MHz reference signal and produce a DC voltage. The DC voltage produced due to the phase difference feeds back to the YIG to complete the phase locked loop [16].

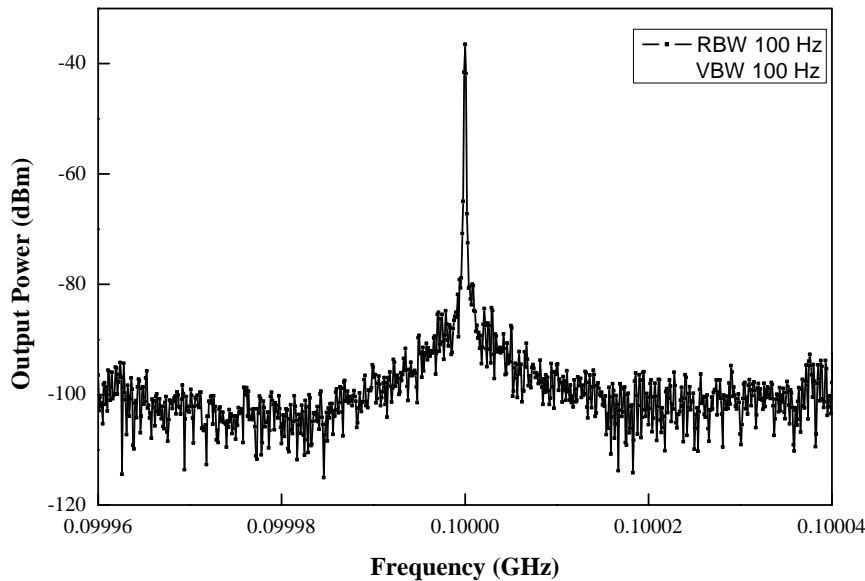


Figure 2.6.: Phase locked IF signal from the second stage down conversion

Once the YIG is phase locked to a stable microwave source, a coupler is used to sample the down converted 100 MHz IF signal from the second stage mixer and is observed on a spectrum analyzer; Figure 2.6 depicts the stabilized 100 MHz IF output. The the phase noise of the phase locked YIG is implemented by coupling the signal while it is phase locked and comparing its phase noise with a free running YIG. N9030A Agilent's spectrum analyzer is used to measure the phase noise performance. The phase noise of the phase locked YIG is ~ 95 dBc/ Hz at 1 KHz offset. Therefore, phase locking improved the phase noise by 50 dB, which is similar to a typical phase locked VDI's synthesizer.

In general, phase locking of a QCL is similar to phase locking a free running YIG driven 2 THz source. Phase locking of a 2.5 THz and 2.69 THz QCL also requires the harmonic mixer to down convert the signal to 100 MHz, and the down converted IF signal phase is compared with a reference signal. The voltage produced due to the phase difference between the two signals

biases the QCL and stabilizes it. During the phase locking of a YIG driven 2 THz source, two down conversion stages were required due to the AM noise performance of the LO chain, therefore, it is necessary to quantify the AM noise performance of a system and minimize its influence to the signal-to-noise ratio of the IF output. In the next section, the LO and RF driver chain output performance and investigation of AM noise of the LO chain is presented and the LO chain is optimized to drive harmonic mixer to phase lock a QCL using a single stage down conversion.

2.3. LO and RF Driver Chains

The WM-380 (WR1.5) high power LO source and the WM-130 (WR0.51) RF source are a cascade of amplifier multiplier chains based on solid state technology. All components in the multiplier chains are based on Schottky based multipliers with a final frequency multiplication factor of $N=48$. Since the LO requires more than -5 dBm input power to pump the harmonic mixer, a varactor based multipliers are needed. Although, a varactor based multiplier chain offer better output power, the fractional bandwidth is limited to less than 15 %. Therefore, to cover the entire WM-380 (WR1.5) LO frequency band (500-750 GHz), more than one chain is required to test the full WR0.34 harmonic mixer LO band. A phase locked VDI's synthesizer supplies a 10.4-15.6 GHz signal with a nominal output power of 18 dBm. The first stage of the amplifier multiplier chain contains a doubler and a power amplifier followed by three varactor based doublers with an output power of 19.5 dBm at approximately 225 GHz stage. The final stage of the multiplier chain contains a tripler that takes the WM-1092 (WR4.3) band to WM-380 (WR1.5) band and has an output power of approximately 1 dBm.

2.3 LO and RF Driver Chains

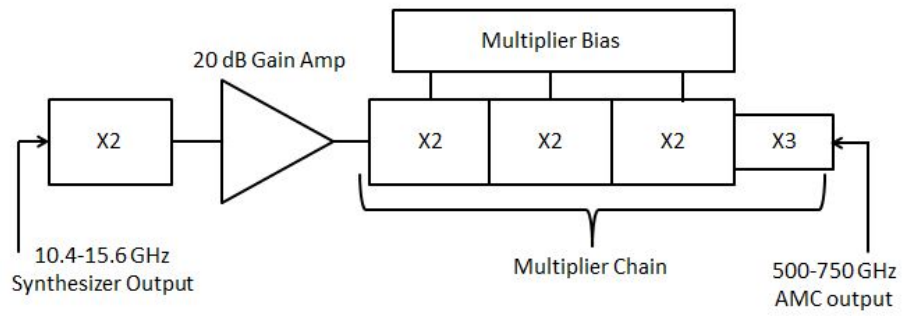
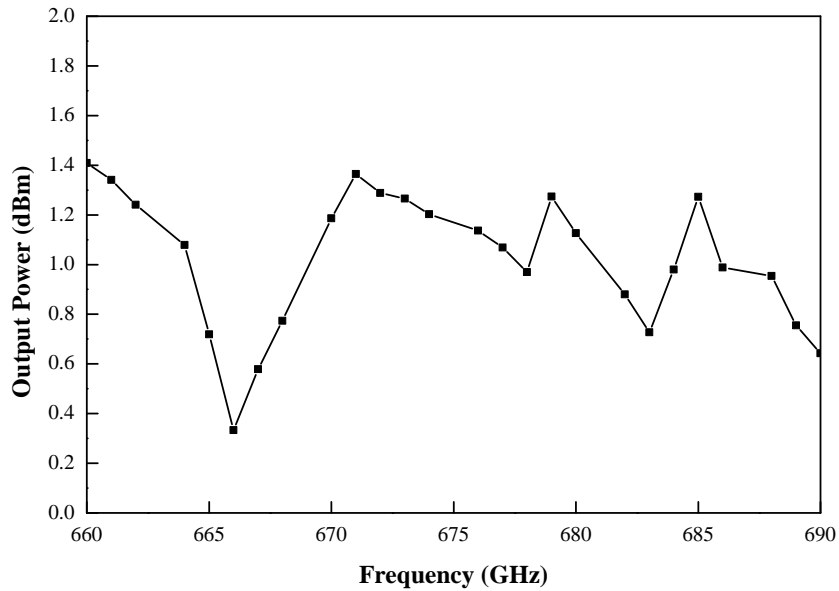
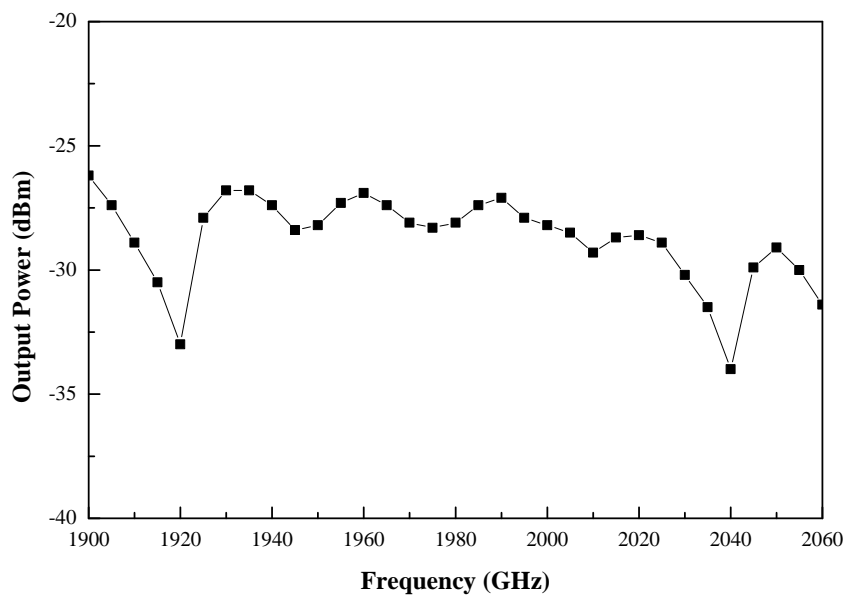


Figure 2.7.: LO chain for 500-750 GHz operation.



(a) Output power of the LO chain



The RF source has similar configuration as the LO multiplier chain with the addition of a WM-130 (WR0.51) tripler to extend the frequency from 633-700 GHz to 1.9-2.1 THz with a final multiplication factor of $N=144$. The last stage multiplier of the RF source has an integrated WM-130 (WR0.51) diagonal horn antenna that transmits approximately -29 dBm quasi-optically to the harmonic mixer for down conversion. The solid state based RF source is mainly used to characterize the lower band of the WM-86 (WR0.34) harmonic mixers developed to phase lock a QCL. Furthermore, initial phase locking of a THz source is also implemented by driving the RF chain using free running YIG source.

2.4. Amplitude Noise (AM) Measurement

The phase locking system requires an input of high signal-to-noise ratio of the down converted signal. One reason for poor signal to noise ratio of the THz harmonic mixer output is the contribution of noise from the driving multiplier chains, particularly noise from the LO chain, [32]. Therefore, it is important to measure the noise performance of the driver chain (WR1.5 AMC) in order to maximize the signal to noise ratio at the harmonic mixer IF output. Amplitude Modulation (AM) and Phase Modulation (PM) noises exist in receiver and transmitter systems and affect the quality of the IF signal. These noises are superposition of a random, non deterministic, time-dependent phase and amplitude fluctuations generated from thermal, shot and flicker noise sources. Noise superimposed on a carrier frequency results on both AM and PM of the tone. Furthermore, single sideband noise superimposed on a carrier frequency, expressed as AM and PM noises, produces upper and lower sidebands. The sidebands of the AM and PM noises differ only in the relative phase of the two sidebands. AM noise sidebands are in phase and phase noise sidebands are 180 degree out of phase. Due to the phase orientations of the sidebands, the phase noises of a single ended harmonic mixer cancel out, whereas, the AM

2.4 Amplitude Noise (AM) Measurement

noise sidebands of a single ended mixers are in phase and add up.

Since the harmonic mixers developed for this project are single ended mixers, they suffer from the AM noise generated from its driving multiplier chain. The goal of the AM noise test shown in Figure 2.9 is to determine the level of AM noise presented in the LO chain compared to a reference source. Testing the AM noise performance of a high carrier frequency LO chain is challenging due to the lack of noise free sources that can be used as references to compare the AM noise contribution from the Device Under Test (DUT). Gunn oscillators are relatively clean sources, but the frequency of operation of Gunn oscillators are limited to approximately 120 GHz. As a result, noise contribution of a WM-2540 (WR10) system relative to a 110 GHz InP Gunn oscillator and a $50\ \Omega$ reference is studied. The Gunn oscillator used in this research is from Carlstrom and has a nominal output power of 20 mW. To insure the mixer diode is pumped with similar LO power during the experiment, we use a bias tee to monitor the video response of a constant 100 mV. To isolate the noise contribution of the Radiometer from DUT, noise temperature of the Radiometer is measured using Y-factor technique and a noise temperature of 2760 K with SD of 35K is found.

For the AM noise test setup in Figure 2.9, the reference level is set by having an isolator between the coupler and the Gunn oscillator to create a matched load, so that it reduces the radiation power from the Gunn oscillator when it is not in use. Similarly, there is an isolator between the coupler and the DUT to create a matched load when the DUT is not under operation. The mixer is pumped alternatively between the Gunn oscillator (reference-1) and the DUT and their output noise power is measured.

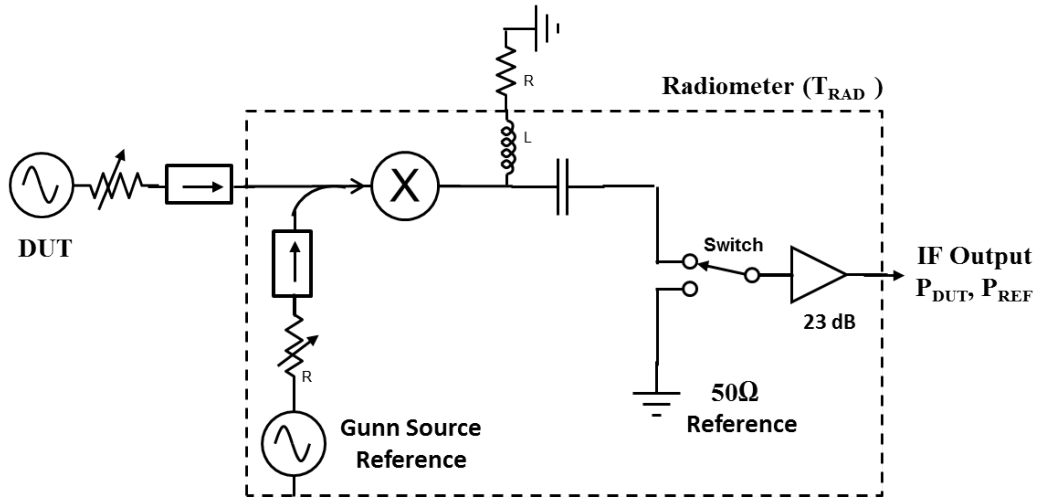


Figure 2.9.: Experimental AM noise test setup

Similarly, the 50Ω resistor (reference-2) is connected to the amplifier input and the output noise power is measured, and the AM noise contribution of the DUT is estimated using Y-factor method by taking the ratio of the output noise power from DUT and the references.

$$Y = \frac{P_{DUT}}{P_{REF}} \quad (2.3)$$

The excess temperature measured $T_{DUT}(excess)$ due to the DUT can be calculated using.

$$T_{DUT}(excess) = (T_{RAD} - T_{REF})(Y - 1) \quad (2.4)$$

Furthermore, taking the ratio of the excess temperature and input power of the carrier signal gives a noise-to-signal ratio.

$$NSR_{DUT} = \frac{T_{DUT}(excess)}{Input\ LO\ Power} \quad (2.5)$$

2.4 Amplitude Noise (AM) Measurement

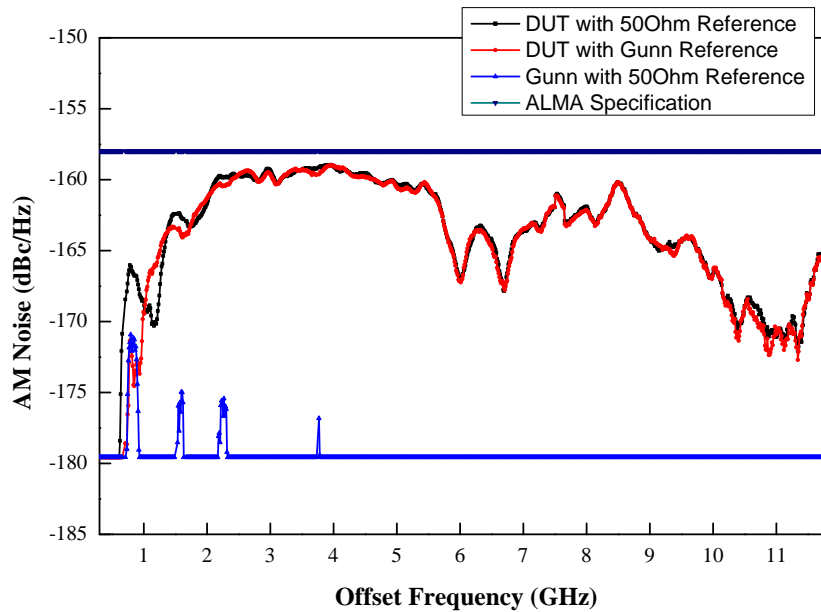


Figure 2.10.: AM noise performance of a WM-2540 (WR10) system with different references

Figure 2.10 depicts the AM noise performance of a WM-2540 (WR10) system is tested using different references. Since the Gunn oscillator and the $50\ \Omega$ reference produce relatively similar output noise power, the ratio between the Gunn oscillator reference and $50\ \Omega$ reference is close to unity. From the experimental data shown in Figure 2.10, the AM noise measurement of a $50\ \Omega$ reference against the Gunn oscillator pumping the mixer at 3.7 mW is similar and it is -179 dBc/Hz. Since $50\ \Omega$ reference is as good as a clean source such as Gunn oscillator, AM noise performance of the higher carrier frequency systems is tested using a $50\ \Omega$ load reference. AM noise performance of the LO chain (WR1.5) that is used to pump the THz harmonic mixer is investigated using $50\ \Omega$ as a reference. In this experiment, a WM-380 (WR1.5) single ended mixer is used to mitigate the AM noise performance. The mixer is pumped by the DUT (WR1.5 LO chain) with 3.4 mW and the noise power is measured.

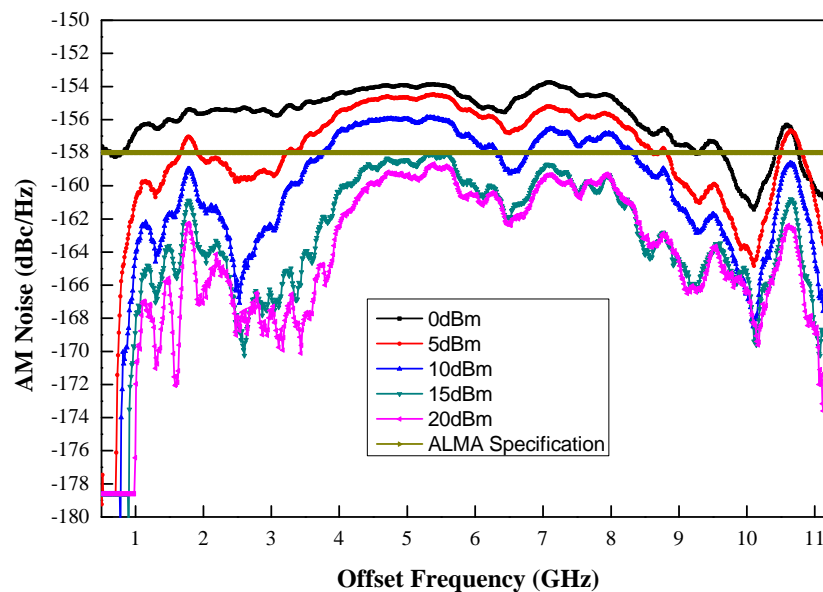
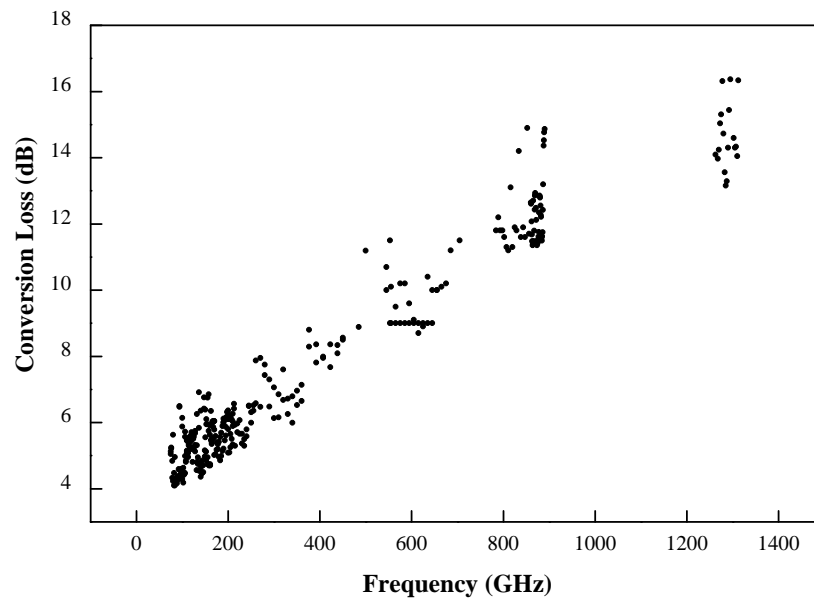


Figure 2.11.: WM-380 (WR1.5) system AM noise performance (AM noise vs. output IF frequency) for different input power.

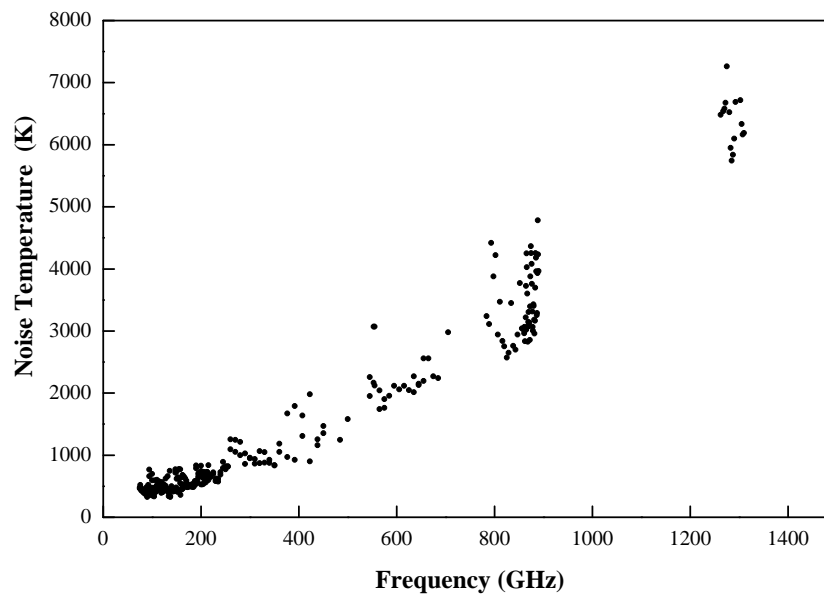
Figure 2.11 depicts the AM noise performance of a WM-380 (WR1.5) amplifier multiplier chain with a carrier frequency of 667 GHz. Increasing the input power to 20 dBm, the system AM noise reduces and the performance becomes better than ALMA AM noise specification, this result shows that by driving the pre-amplifier and each multipliers of the LO chain into saturation, the amplitude fluctuations will be reduced and the AM noise effect becomes negligible. For the consecutive experiments to phase lock QCLs, the LO chain is optimized and driven by approximately 10-15 dBm. Furthermore, driving the pre-amplifier into saturation to reduce the AM noise creates harmonics and inter-modulated products. However, since harmonics and inter-modulated products are predictable, it can be guided into unused frequency bands [33].

3. THz Schottky Diode-based Harmonic Mixer

Since the introduction of a Schottky barrier by a German physicist, Walter H. Schottky, the development of Schottky diode-based components have shown tremendous progress [34]. Schottky based mixers have advantages over other types of detection technologies, such as HEB or SIS. Schottky diode based mixers can operate at room temperature or cryogenic, and also have wide IF bandwidth and this allows fast modulation. In addition, Schottky based mixers use compact and planar technology, thus producing rugged components for space based applications; furthermore, these mixers can be operate in heterodyne or direct detection mode. Fundamental mixers and sub-harmonic mixers are currently used at lower frequency below 1.5 THz to down convert RF signals. VDI, one of the leaders in Schottky diode technology, has shown tremendous progress in the Schottky based mixer performance. Figure 3.1 shows the summary of VDI's mixers conversion loss and noise temperature performance for different frequencies.



(a)



(b)

Figure 3.1.: Summary of VDI's Schottky based mixers a) Conversion Loss vs. RF Frequency, b) Noise Temperature vs. RF Frequency

Due to the lack of an LO source with sufficient output power that can be used to pump at the fundamental frequency, it is difficult to develop Schottky based fundamental mixers above 2 THz. Similarly, sub-harmonic mixers that use antiparallel Schottky diode technology above 1.5 THz requires higher power to pump two diodes. Therefore, at higher frequencies it is important to develop harmonic mixers that can allow the use of LO harmonics to down convert the THz RF signals for different applications.

The main objective of this thesis is to phase lock THz QCL by down converting the signal to lower frequency. Since the mixer is central to the phase locking system, the development of mixers with low conversion loss and high signal to noise ratio is crucial to achieving phase locking at THz frequencies. Most of the components in the phase locking system discussed in Chapter 2 are commercially available, with the exception of the heterodyne based THz harmonic mixer. Therefore, Schottky based harmonic mixers are developed.

Initially, a VDI WM-102 (WR-0.4) fundamental mixer is modified to build WM-102 (WR-0.4) harmonic mixers by adding two different LO waveguide probe designs to couple LO signals for two different waveguide bands and allow harmonic mixing.

The first modified harmonic mixer incorporates a WM-1092 (WR4.3) LO waveguide and waveguide probe that is used to couple 170-260 GHz signals for the 9th and 10th harmonic mixing and the second harmonic mixer contains a WM-380 (WR-1.5) LO waveguide and waveguide probe that is designed to couple 500-750 GHz signals for the 3rd and 4th harmonic mixing.

Figure 3.2 shows the internal circuitry of the modified harmonic mixer which contains THz circuit, LO probe and IF circuit. The THz circuit incorporates an RF filter, RF probe, THz diode and IF filter. At the junction of the RF waveguide and THz circuit channel, the RF and LO signals are isolated by a low pass filter followed by a quarter wave long transmission line at the RF frequency, (seeFigure 3.2).

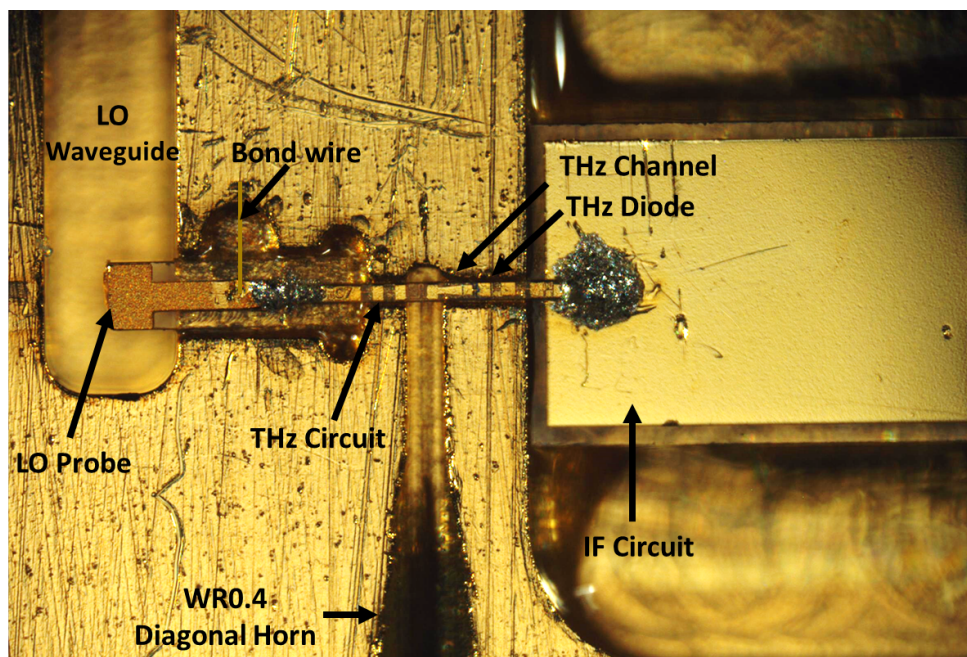


Figure 3.2.: WM-102 (WR0.4) harmonic mixer THz circuit

A microstrip High-Z, Low-Z low pass filter topology is used at the IF circuit to block the RF and LO while allowing IF and DC signals to pass. The THz circuit is placed in a $18\ \mu\text{m}$ by $36\ \mu\text{m}$ waveguide channel and connected with the LO and IF circuits using conductive epoxy. An IF/ DC ground is also formed in the LO channel using a 1 mil gold bond wire to the block. For the 9^{th} harmonic mixing, a conversion loss of 63 dB was measured using a 2 THz solid state source. The 3^{rd} harmonic mixer has poor LO coupling; however, it produces better conversion loss of 45 dB. Using the 3^{rd} harmonic mixer, a free running YIG driven 2 THz solid state based Amplifier Multiplier Chain (AMC) has been phase locked to a 100 MHz reference. The detailed measurements of these mixers are presented in Appendix B.

To further improve the performance of the phase locking system and to broaden the operational frequency, a WM-86 (WR-0.34) harmonic mixer is designed. This chapter is devoted to the WM-86 (WR-0.34) harmonic mixer designs that cover 1.9-3.2 THz. It contains a quartz based

LO waveguide probe, quartz based IF circuit and GaAs based THz circuit. The THz circuit also incorporates GaAs based diode in its epitaxial layer and is integrated onto a 3 μm thick GaAs substrate. The IF circuit and the LO circuits are connected using 1 mil gold bond wire, (see Figure 3.3).

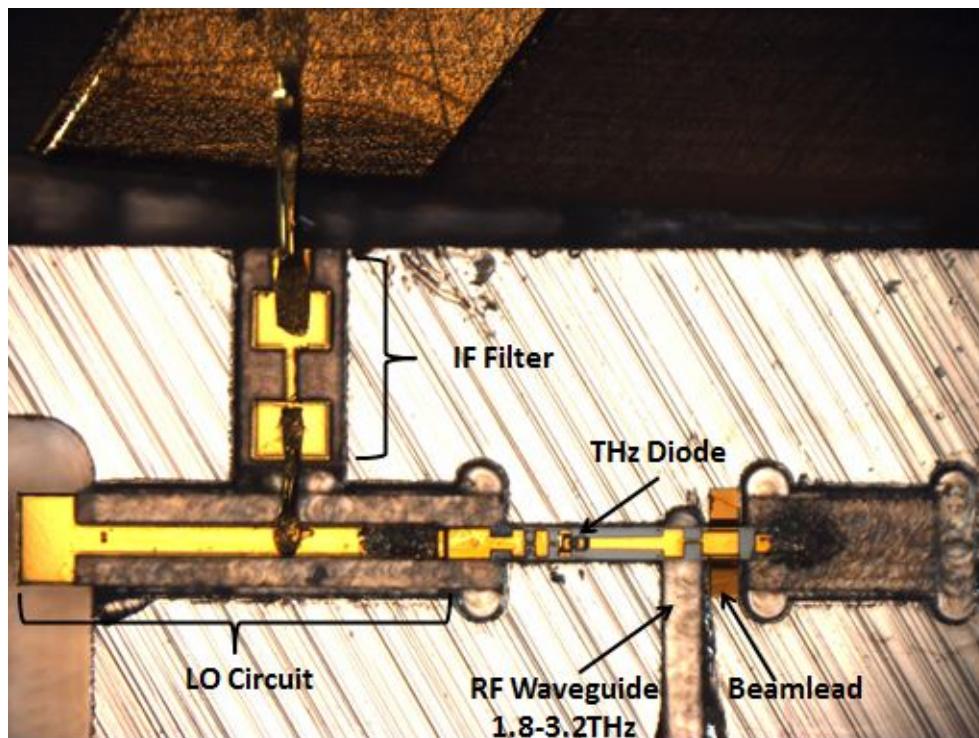


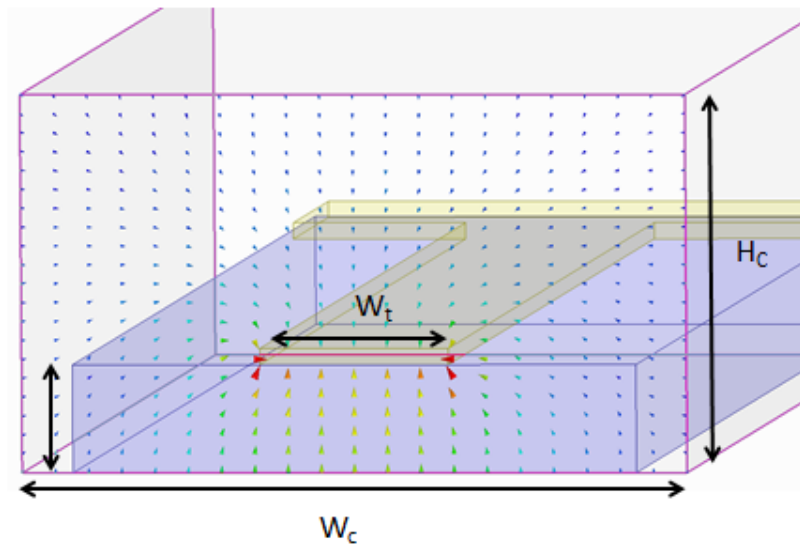
Figure 3.3.: WM86 (WR 0.34) Harmonic mixer internal circuitry

Section 3.1 focuses on the LO and IF circuit designs and their simulations for the WM-86 (WR-0.34) harmonic mixer. Section 3.2 presents the THz circuit and discusses the RF probe designs to cover 1.9-3.1 THz. Section 3.3 and section 3.4 present the diagonal horn design and THz circuit fabrication and section 3.6 focuses on the assembly of the harmonic mixers. At the end of this chapter, performance of the WM-86 (WR0.34) harmonic mixer and discussion about the design considerations of the harmonic mixers as well as some of the challenges and position sensitivity of the circuit during assembly are presented.

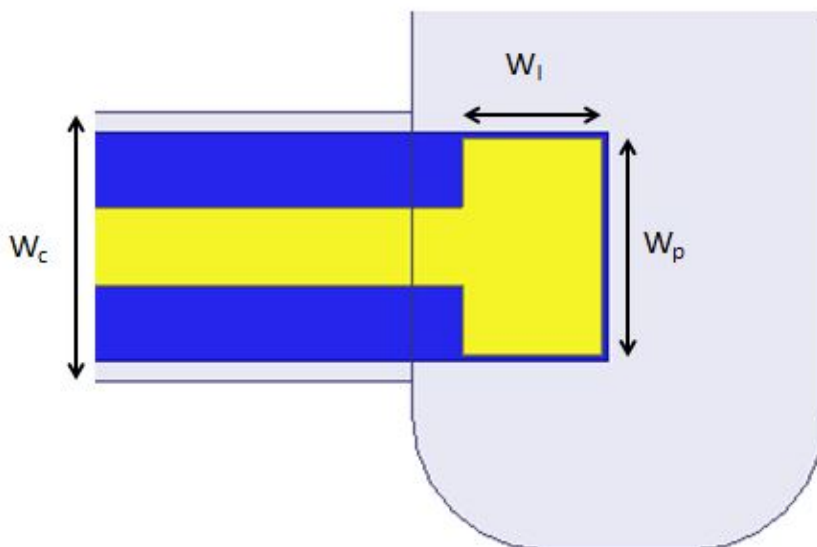
3.1. Harmonic Mixer LO and IF circuit designs

The initial design of the circuits are modeled and analyzed using Advanced Design System (ADS) and High Frequency Structural Simulator (HFSS). The WM-86 (WR-0.34) harmonic mixer design contains a WM-380 (WR-1.5) LO waveguide. The waveguide has a designed dimension of $190.5 \times 381 \mu\text{m}$ and this allows a 500–750 GHz signal to couple to the LO probe and terminate at the diode. The LO probe used a quartz substrate with $20 \mu\text{m}$ height and $100 \mu\text{m}$ width. A $2 \mu\text{m}$ thick gold conductor is electroplated on top of the quartz substrate to create probe structures. Fig 3.4b shows the LO probe dimensions are $W_p = 90 \mu\text{m}$ and $W_l = 60 \mu\text{m}$. Furthermore, the LO probe is placed on a waveguide channel with a channel width of $W_c = 125 \mu\text{m}$ and a channel height of $H_c = 62.5 \mu\text{m}$. The LO channel dimensions are determined based on the substrate dimensions for a single mode TE_{10} propagation by simulating using HFSS port solver and determining the starting frequency for all higher modes (see Fig 3.4a).

The LO power termination at the diode is provided by a short circuited beam lead located right after the RF probe which is clamped between the E-plane split of the block. To maintain the LO termination, the transmission line length is kept a half wavelength away from the diode to the short circuited beam lead. From the diode junction, the S_{11} is simulated for different LO frequencies to examine the transmission line length that provides short circuit to the LO frequencies. Figure 3.5 shows the simulated S_{11} result for a transmission line length of $145 \mu\text{m}$ from the diode to the short circuited beam lead for the LO frequencies, the simulation demonstrates a perfect short circuit to the LO center frequency (625 GHz) and nearly short circuit to the other frequencies.



(a) Cross section of LO microstrip channel and propagation mode



(b) WR1.5 LO probe structure

Figure 3.4.

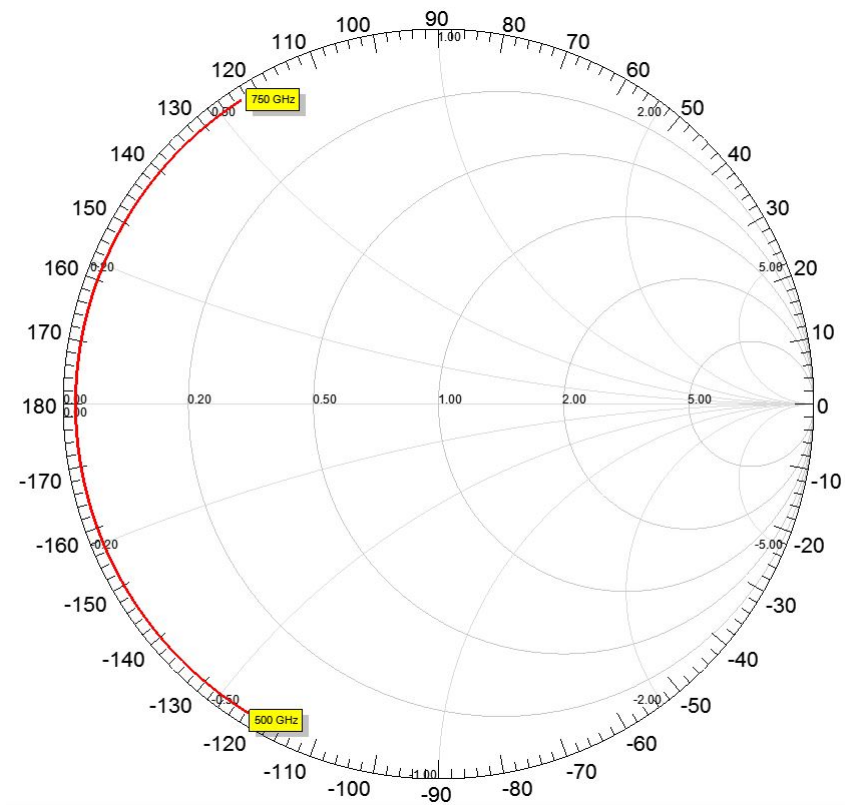


Figure 3.5.: S_{11} simulation of the 500-750 GHz LO termination provided by the beam lead right after the RF probe

When the mixer is pumped through the LO port, it is important to deliver maximum power by isolating the LO and IF channel; therefore, an IF circuit containing a Hi-Z and Low-Z based low pass filter is used to block the LO signal propagation into the IF channel. The IF filter incorporates a 20 μm thick quartz substrate and 2 μm thick gold conductor.

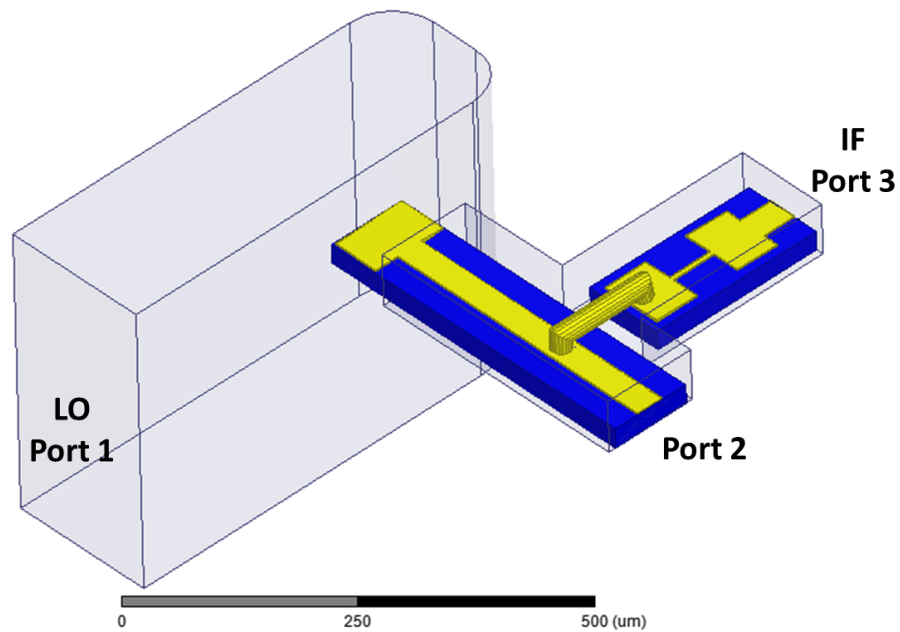
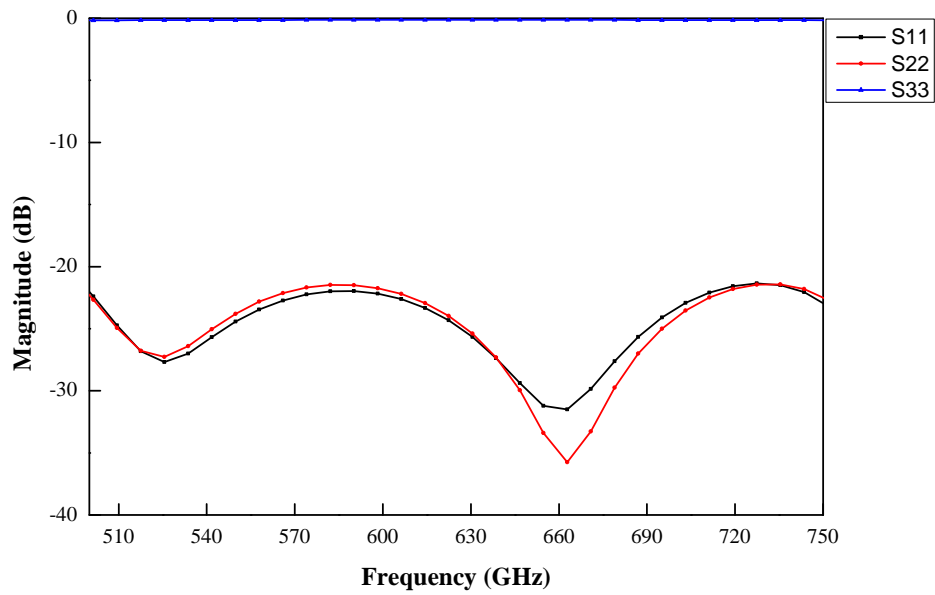
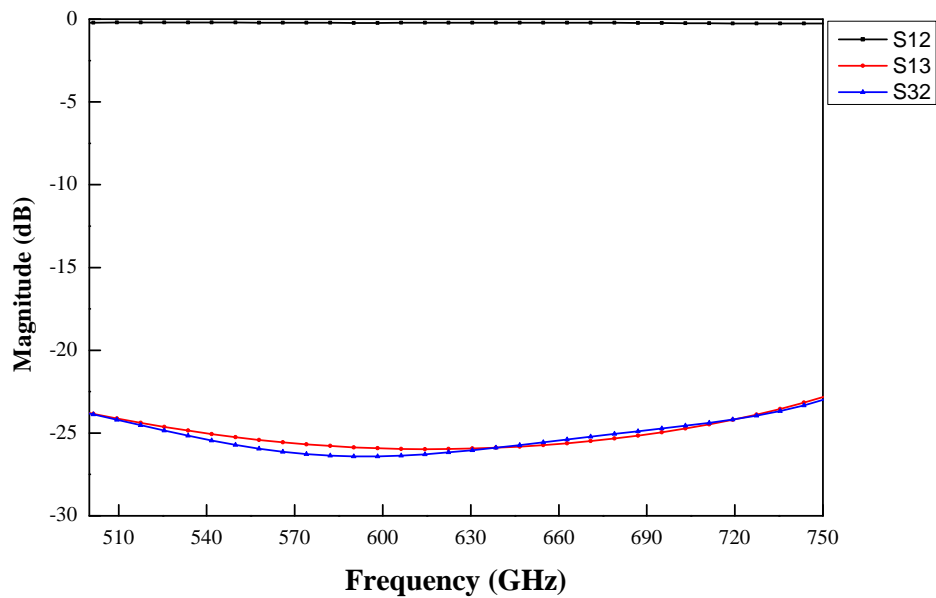


Figure 3.6.: WM-380 (WR1.5) LO input waveguide with LO probe connected to IF circuit using 1 mil gold bond wire

Based on the HFSS simulation result, the transmission and return loss performance of the IF and LO circuits are depicted in 3.7a and 3.7b. At port 1 and port 2, a return loss of 22 dB and an insertion loss of approximately 0.2 dB are obtained. This indicates that more than 95 percent of the power is coupled into port 1 and propagates to port 2. Similarly, better than 20 dB isolation between port 1 and port 3 is achieved for 500-750 GHz band.



(a) Simulated return loss of the LO and IF circuits



(b) Simulated insertion loss of the LO and IF circuits

Figure 3.7.

3.2. Harmonic Mixer THz Circuit Design

Due to the higher dielectric constant of the GaAs substrate $\epsilon = 12.9$, it is challenging to couple the RF signal as well as to create a lower impedance transmission line that can match with the LO circuit. Therefore, to reduce the effective dielectric constant of the GaAs-based circuit, the THz circuit is floated above the ground plane to average the dielectric with the air $\epsilon = 1$. Suspending the THz circuit $4 \mu\text{m}$ above the ground plane reduces the effective dielectric constant to $\epsilon = 2.8$, which is similar to the effective dielectric constant of the quartz-based LO circuits. The WM86 (WR0.34) THz circuit contains an RF probe, RF filter and single ended diode, (see Figure 3.8). A diagonal horn antenna with aperture radius of 0.21 mm feeds the RF signal into the RF waveguide and couples into the RF probe. The RF signal propagates through the tapered microstrip transmission line and couples to the diode.

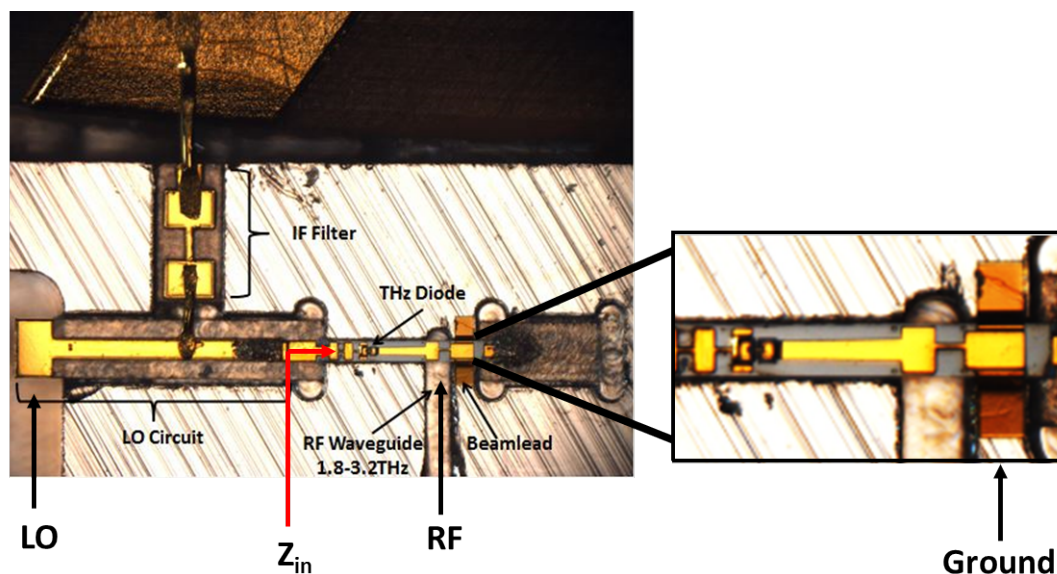


Figure 3.8.: 1.9-3.2 THz harmonic mixer internal design

The RF signal termination is provided by the low impedance section of the RF filter, which

serves as a short circuit to the RF signal. The RF filter contains five sections of high impedance and low impedance transmission lines, with low impedance dimensions of $W_l = 29 \mu m$ and $L_l = 13 \mu m$ and high impedance dimensions of $W_h = 2 \mu m$ and $L_h = 13 \mu m$, (see Figure 3.9).

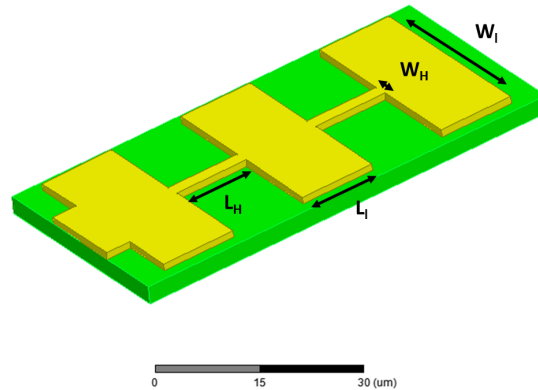


Figure 3.9.: RF filter with five sections of HI_Z and Low_Z transmission lines.

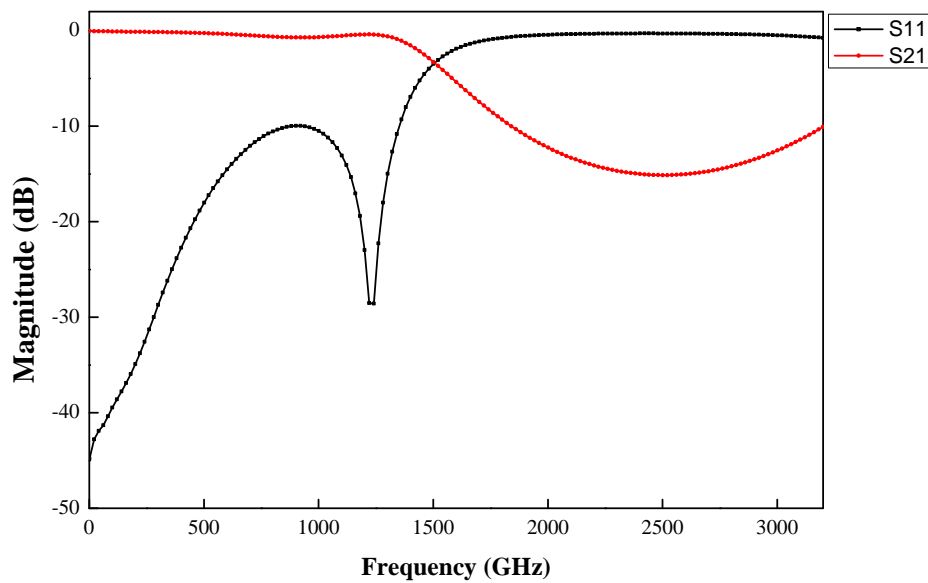
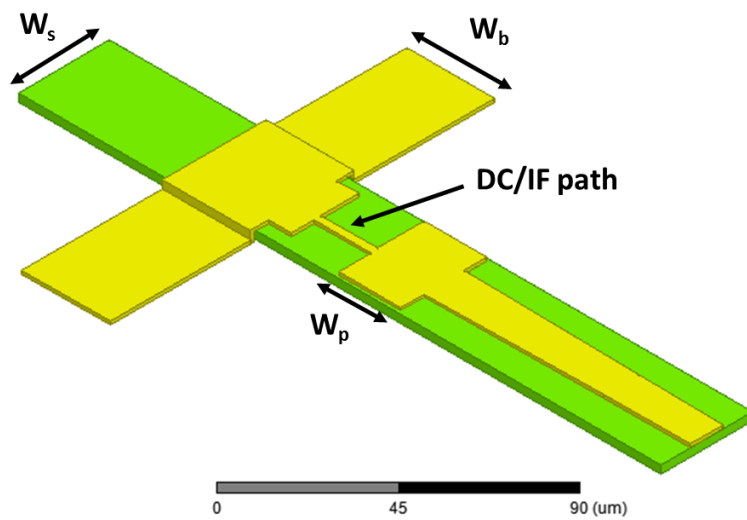


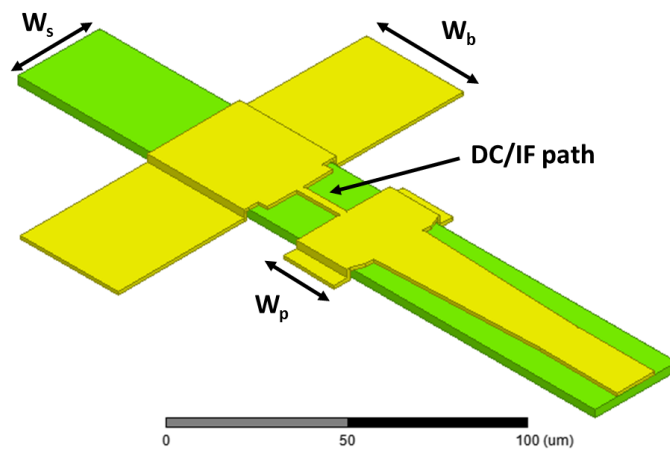
Figure 3.10.: RF filter performance

3.2 Harmonic Mixer THz Circuit Design

The simulated RF filter performance is shown in Figure 3.10, for the RF frequencies of 1.8-3.2 THz, the S_{11} is 0.2 dB and the S_{21} is better than -10 dB. Similarly for below 750 GHz, the S_{11} is less than -10 dB and the S_{21} is approximately 0.1dB. This shows the RF filter is blocking the signal for 1.8-3.2 THz frequencies while allowing the LO and the IF signals below 750 GHz.



(a) A WM-86 (WR0.34) harmonic mixer RF probe that covers 1.9-2.5 THz,



(b) A WM-86 (WR0.34) harmonic mixer RF probe that covers 2.3-3.2 THz

Figure 3.11.

Due to the DC/IF path to ground located between the RF probe and the short circuited beam lead, it is difficult to couple the full WM-102 (WR0.34) RF waveguide band. Therefore, there are two different RF probe designs to cover from 1.9 THz up to 3.2 THz, (see Figure 3.11). Both probes have similar substrate and probe width $W_s = 32 \mu m$ and $W_b = 18 \mu m$ respectively. However, due to power coupling at different frequency bands, the two probe structures are different. The lower frequency tuned RF probe gold structure is within the substrate, where as, the higher frequency tuned probe has a beam lead with floating gold structure of $5 \mu m$. The simulation performance of the lower band RF probe design that covers 1.9-2.5 THz and the higher band RF probe design that covers 2.3-3.2 THz are shown in Figure 3.12. The lower band and the higher band RF probes have nominal return loss of 15 dB.

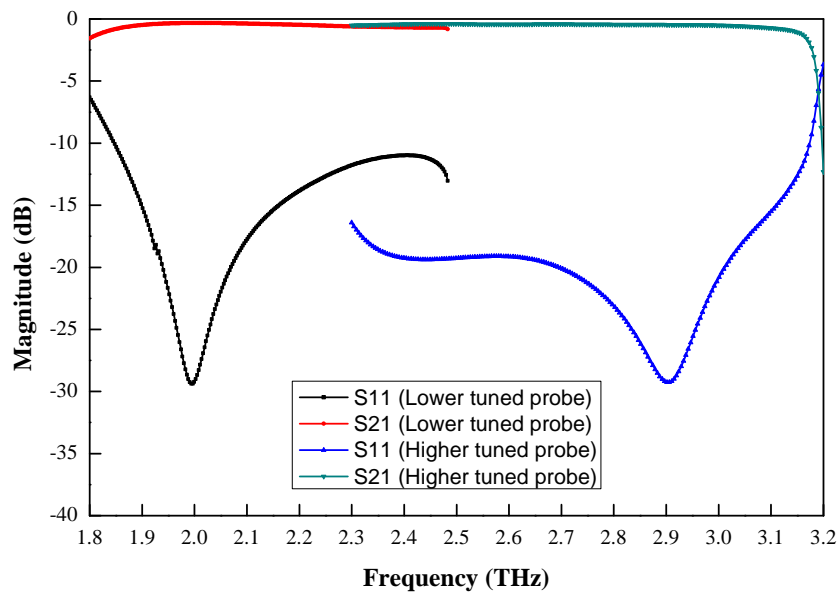


Figure 3.12.: THz circuit performance (return loss and transmission vs. output frequency)

3.2.1. Circuit Position Sensitivity

During assembly, it is challenging to set the bond wire that connects the IF and LO circuits to the designed length. Therefore, it is important to simulate by varying the bond wire length and determine the circuit performance, Figure 3.13a. The LO performance with different bond wire lengths ranging from 70 μm to 130 μm is simulated and the circuit performance is insensitive to the bond wire length.

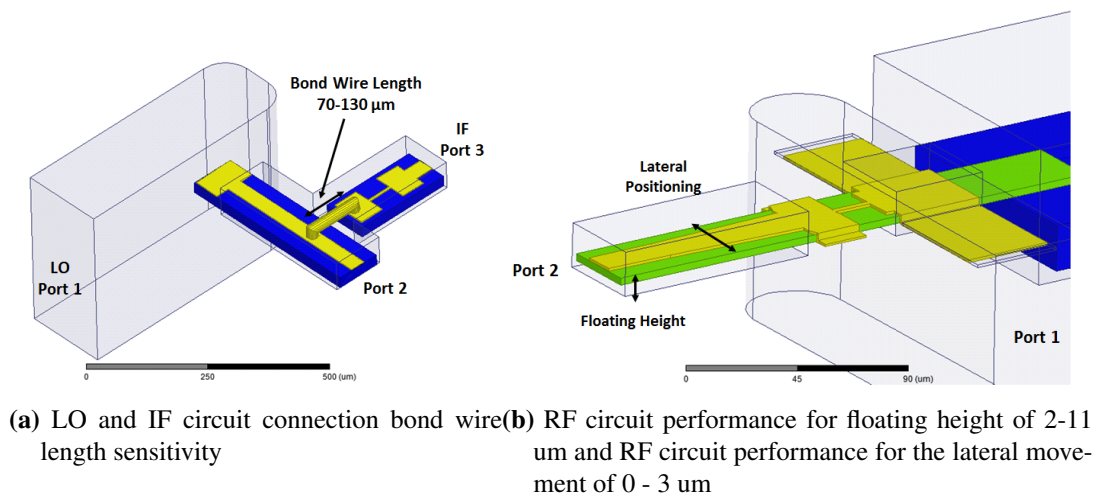
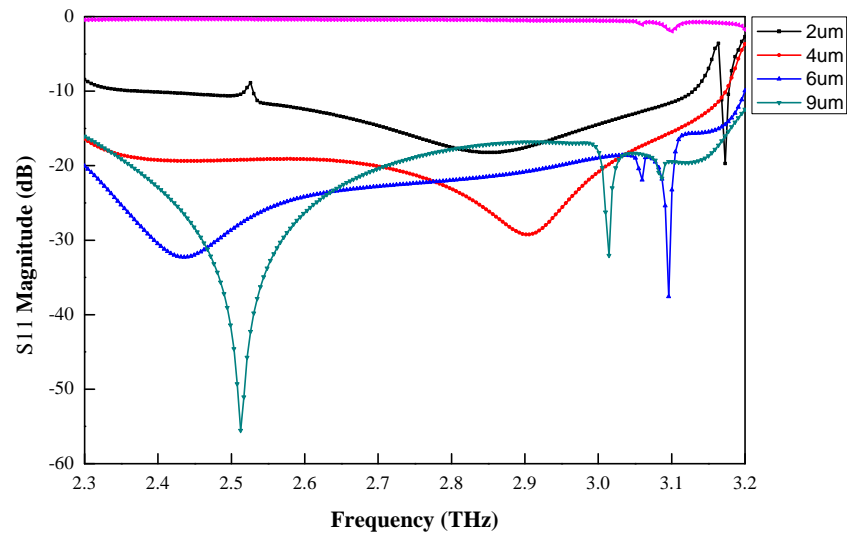


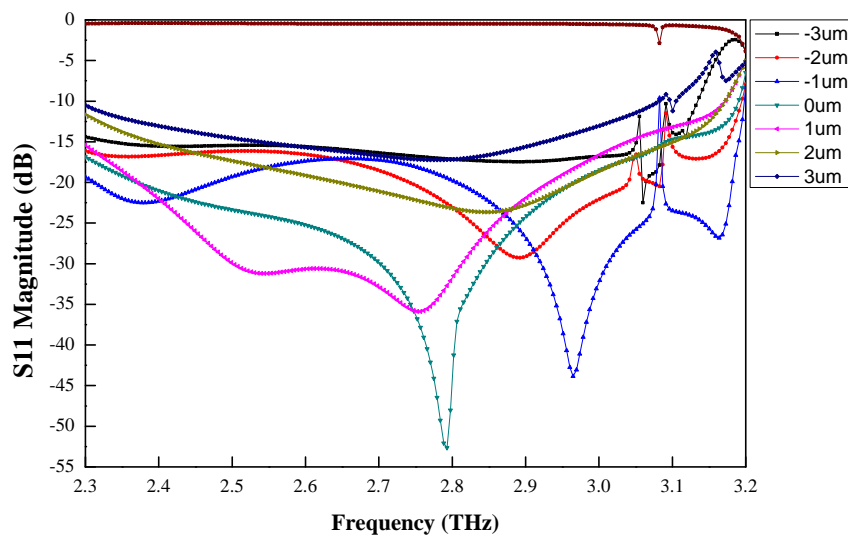
Figure 3.13.

It is also critical to analyze the position sensitivity of the THz circuit and its effect on the circuit performance. For the targeted design of a THz circuit floating height of 4 μm , assembly might be the hardest task to achieve. Surface roughness of the THz circuit waveguide channel could introduce 2-3 μm error which leads to 6-7 μm floating height. A simulation was set up for floating heights of 2-11 μm and 0-3 μm left and right lateral position variation of the circuit, (see Figure 3.13b). Height sensitivity and lateral movement sensitivity performances are depicted in Figure 3.14a and Figure 3.14b. The S_{11} performance for both cases is better than -10 dB and the S_{12} is approximately 0.2 dB, which is still within acceptable efficiency

range.



(a) Simulation result of the RF circuit performance for different floating heights



(b) Simulation result of the RF circuit performance for the lateral movement.

Figure 3.14.

3.3 Diagonal Horn Design

As shown above on the circuit position sensitivity analysis, the possible variation on the THz circuit placement during assembly should not affect the performance within a reasonable tolerance. Achieving the assembly tolerance range of the THz circuit should be possible.

3.3. Diagonal Horn Design

A diagonal horn antenna is integrated with the mixer block with a horn length of $L=3$ mm and aperture diameter of $2a = 0.56$ mm. Since the mixer block has an E-plane split, the horn is placed at the block split to ease the machining process. A diagonal horn antenna inherently incorporates the TE_{10} and TE_{01} modes, as a result, it has high fundamental Gaussian beam coupling, A properly designed diagonal horn antenna will have approximately 84 % Gaussian coupling [35].

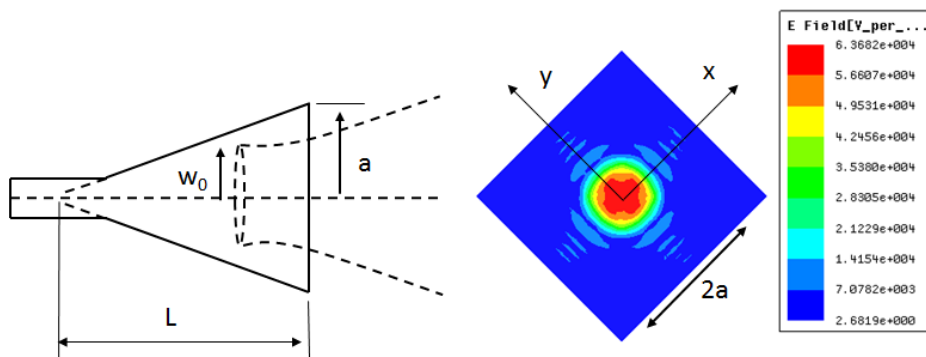


Figure 3.15.: Schematic of diagonal feedhorn

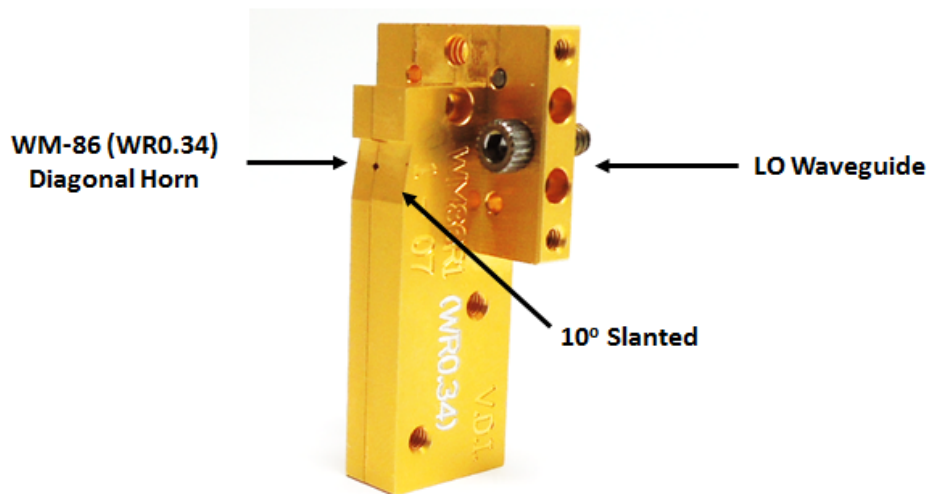


Figure 3.16.: WM-86 (WR0.34) harmonic mixer block

The focused beam radius from the QCL is wider than the aperture size of the horn by a factor of at least 3 (see Section 4.1). As a result, the uncoupled THz beam reflects off the diagonal horn and can create standing waves. To circumvent the standing wave at the horn surface, the mixer block at the horn aperture is slanted by 10 degrees. This will cause the reflected wave at the horn surface to bounce back with an angle. The modified diagonal horn antenna full 3-D structure is simulated and showed a approximately 25 dB gain at 3.2 THz. The Full Width at Half Maximum (FWHM) radius is 6 degrees.

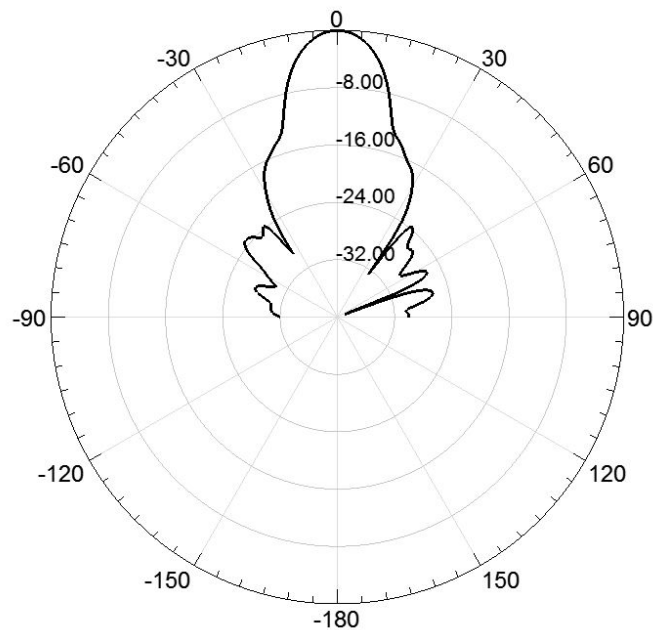


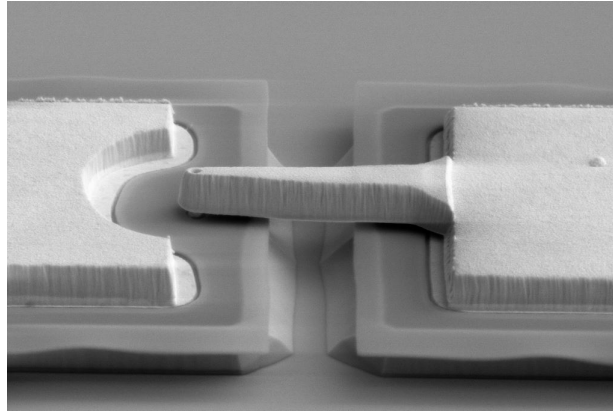
Figure 3.17.: The simulated antenna pattern of the WR0.34 diagonal feedhorn for an angle theta of -90-90 degrees and an angle phi of 180 degree.

3.4. Fabrication of THz Circuits and Integrated Diode

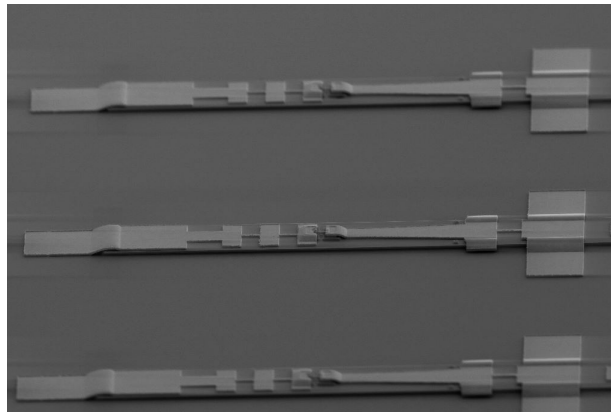
In this Section detail of the THz circuit and diode fabrication is presented, first details of WM-102 (WR-0.4) circuit is discussed and later the fabrication of the GaAs based WM-86 (WR0.34) THz circuit is described. The WM-102 (WR-0.4) harmonic mixer uses a planar Schottky diode with GaAs in its epi-layer and it is integrated onto a quartz microstrip circuit with overall dimensions of 400 μm length by 30 μm width and thickness of 8 μm .

Due to the lower dielectric property ($\epsilon_r = 4$) and higher mechanical strength, a quartz substrate is preferable to make the THz circuit. However, integrating a GaAs-based diode onto a quartz-

based THz circuit is challenging. Therefore, the WM-86 (WR-0.34) harmonic mixer used a GaAs substrate with integrated diode.



(a) WM-86 (WR0.34) THz diode with $0.2 \mu\text{m}$ anode radius and $6 \mu\text{m}$ finger length.



(b) THz circuit

Figure 3.18.: 1.9-3.2 THz circuit with beam lead, the SEM image is taken at the University of Chalmers

The quartz based circuits, such as the LO probe, the IF circuits and the supporting substrate, are fabricated at Virginia Diodes, Inc. The THz circuit that contains the THz diode is based on a GaAs substrate which was fabricated at Chalmers University Terahertz and Millimetre-Wave laboratory department of microtechnology and nanoscience by Jen Stake group. The diode

process is based on electron beam lithography, with a beam spot of less than 5 nm, allowing precise and repeatable anode and air bridge formation.

To achieve a high cutoff frequency and a low conversion loss mixer diode, it is necessary to have high epitaxial doping and small anode size [36]. The THz diode uses a 60 nm thick GaAs-based epitaxial layer for its active region with an n-type doping of $4 \times 10^{17} \text{ cm}^{-3}$. At high frequencies, the shunting effect of the junction capacitance over the junction resistor becomes problematic for the diode performance. As a result, reducing the anode area is necessary to overcome the shunting effect at high frequencies. Therefore, the harmonic mixer contains a THz diode with an anode areas of $0.126 \mu\text{m}^2$ and $0.28 \mu\text{m}^2$ are fabricated for approximately 5-6 μm finger length structures. Scanning Electron Microscope images of the fabricated THz circuit and the THz diode are shown in Figure 3.18.

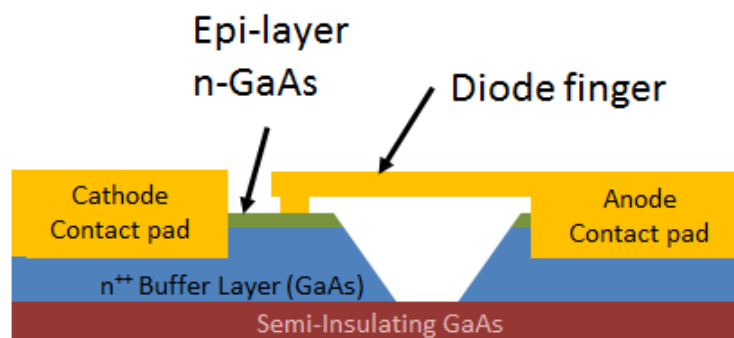


Figure 3.19.: THz Schottky diode structure.

For diodes on a membrane, the starting structure is a semi-insulating GaAs substrate supporting a 3 μm thick GaAs layer sandwiched in between two AlGaAs etch stop layers and a heavily doped n^{++} buffer layer followed by an approximately 60 nm n-type epitaxial layer, (see Figure 3.19). The standard diode fabrication process is started by deposition of a stress-

balanced PECVD SiO_2 layer, followed by patterning of the ohmic contacts Pd/Ge/Au/Pd/Au. Additional steps, such as annealing of the ohmic contacts and patterning of the Schottky contacts by wet etching through the SiO_2 layer and deposition of Ti/Pt/Au Schottky contacts with following lift off process were completed. Moreover, patterning the air-bridge and deposition of Au metallization and isolation of the diode by wet etching was performed.

Finally, formation of the membrane shape and patterning of passive circuitry, such as beam-leads, waveguide probes and filter structures, and deposition of thick Au metallization was applied. Thinning down the sample from the backside to the AlGaAs layer which is then etched away to release the devices completes the THz circuit fabrication process. This process module can also be utilized for sub-micron size anodes and Terahertz Monolithic Integrated Circuits (TMICs) [37]. The DC measurement of the THz circuit and the extracted diode parameters are presented in section 3.6.

3.5. Block Machining and Assembly

The block machining is performed using a Computer Numerical Control (CNC) milling machine. The block was machined into two halves with the E-plane split between the two halves of the block. The THz circuit channel that is found in the base has the smallest dimensions, which is approximately $4 \times 39\mu\text{m}$. A $25\mu\text{m}$ diameter milling tool was used to create the smallest dimensions of the block, (see Figure 3.20). The channels were measured using a Mitutoyo Precision Microscope (MPM) which verified the dimensions are accurate within $1\text{-}4\mu\text{m}$.

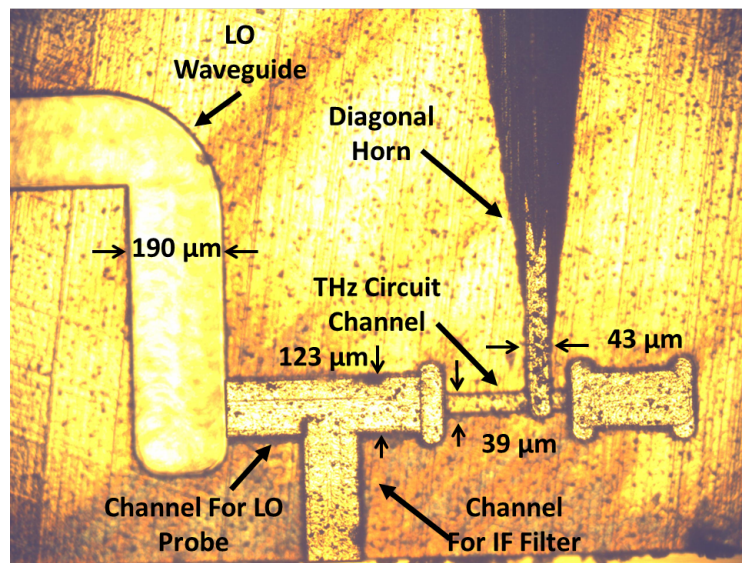


Figure 3.20.: The WM-86 (WR0.34) harmonic mixer block and circuit channels.

	Designed dimensions (μm)	Measured dimensions (μm)
RF Wavguide Width/Hight	86/43	89/44
THz Channel-Base Width/Hight	39/4	36/6
LO Waveguide Width/Height	380/190	377/188.5
LO circuit channel	123/20	121/21
IF circuit channel	123/20	121/21

Table 3.1.: WM-86 (WR0.34) harmonic mixer block channel and waveguide dimensions.

Finally, the mixer is assembled at Virginia Diodes, Inc. under a microscope. First the mixer block is cleaned properly to remove debris remaining from the block machining, followed by mounting the LO probe, IF filter, IF circuit and THz supporting substrate circuits into their proper channels. Bonding the LO probe with the IF circuit and IF filter with IF circuit is done using 16 μm and 24.5 μm bond wires respectively. Once those circuits are stably positioned, the THz circuit is placed on top for the LO probe and the THz supporting circuit and connected using conductive epoxy. Once all the circuits are mounted in a mixer block, the two halves of the block are aligned, fastened together and the block is ready for RF testing.

3.6. Harmonic Mixer Test and Measured Performance

This section presents the experimental test setup and the measured performance of the THz harmonic mixers, such as the current-voltage relationship, RF and LO video responses, 3rd and 4th harmonic mixing, noise temperature and conversion loss using Y-factor method. Even though the harmonic mixer is design to work for 1.8-3.2 THz, due to the lack of wide band RF sources, the characterization presented here is for 1.9-2 THz using a solid state multiplier chain. Furthermore, the harmonic mixer performance above 2 THz is tested using a 2.6906 THz QCL. Initial harmonic mixer testing was performed by measuring the current-voltage relationships of the THz diode using a Keithley 236 Source-Measure Unit. The current-voltage performance of the THz diode is shown in Figure 3.22.

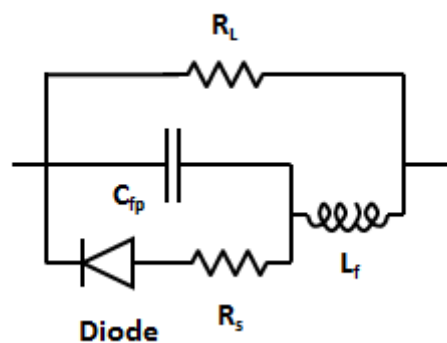


Figure 3.21.: THz diode model

Due to the large substrate leakage resistance, the I-V curve is bent for a voltage bias less than 0.6 V. This can be modeled by inserting a shunt resistance across the ideal diode (R_L) and fitting the measured I-V characteristics to the model yields a substrate leakage resistance of approximately $R_L = 80 \text{ K}\Omega$. For biases greater than 0.65 V, the leakage resistance becomes insignificant and has no impact on the mixing performance but it will affect the small signal

detection mode.

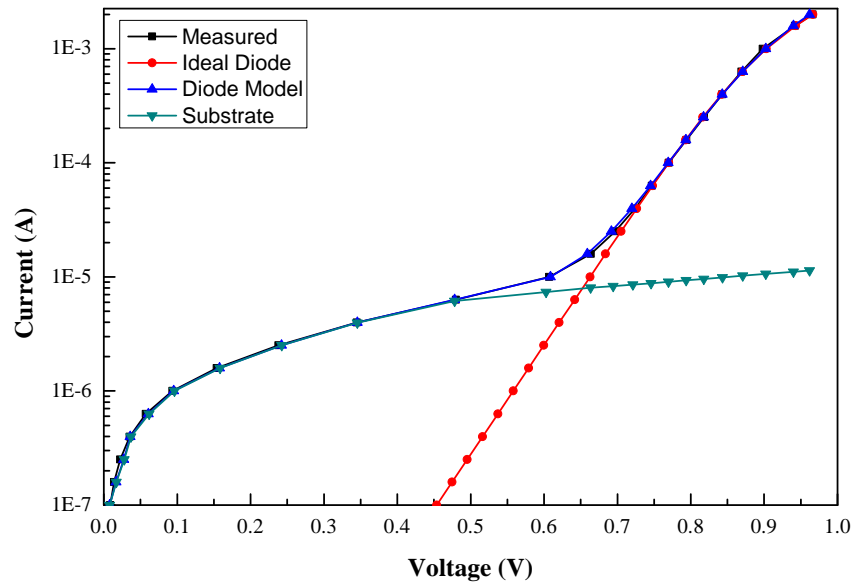


Figure 3.22.: I-V curve of the THz diode

Anode diameter, (μm)	0.5
Ideality factor	1.7
Series Resistance (Ω)	27
Saturation Current (pA)	4.2
Leakage Resistance ($K\Omega$)	80

Table 3.2.: Measured DC parameters of the THz diode

The diode parameters are extracted by performing a curve fitting to an ideal diode for applied voltage greater than 0.65 V, and minimizing the mean square error for accurate representation. The extracted diode parameters are series resistance $R_s = 27\Omega$, ideality factor $\eta = 1.7$ and

saturation current under reverse bias $I_0 = 4.2 \text{ pA}$. The measured DC parameters for the THz diode are given in Table 3.2.

3.6.1. Video Response and Responsivity

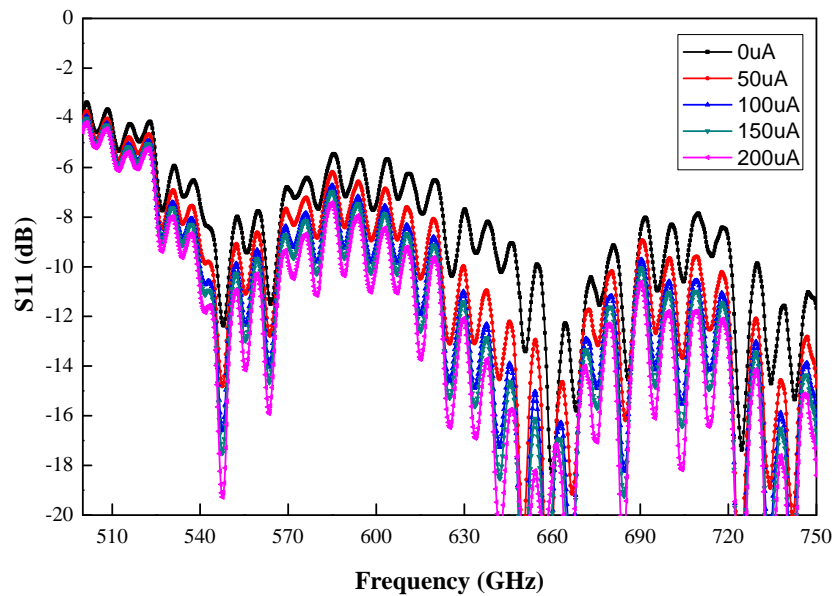


Figure 3.23.: LO return loss measurement using VNA extender calibrated using SOLT.

To characterize the LO probe coupling efficiency and LO power delivery to the diode, LO return loss is measured. Return loss measurements for the harmonic mixer's LO waveguide for different current biases are performed using VDI's WR-1.5 Vector Network Analyzer (VNA) extender calibrated using VDI's standard SOLT calibration kit. The return loss improved for higher current biases, and shows nominal return loss better than 10 dB for frequencies above 620 GHz, the performance is illustrated in Figure 3.23

The LO video response is measured by pumping the mixer with LO power while modulating

3.6 Harmonic Mixer Test and Measured Performance

the LO signal and measuring the output voltage on a lock-in amplifier, (see Figure 3.24). The LO chain is a VDI solid-state varactor based AMC source that has an output frequency of 500-750 GHz with a multiplication factor of $N=48$. The LO source is modulated by a 100 Hz square wave using a function generator that is connected to a pin-switch within the LO chain. The signal from the function generator is split and also used as a reference signal for the lock-in amplifier. The IF chain contains a bias-tee that allows DC bias to the mixer while accessing the modulated video response. The LO video response is tested by pumping the mixer with LO power, while biasing the mixer at different current levels and the modulated video output is fed into the lock-in amplifier and the output voltage is measured. From this test we can determine the LO responsivity that relates the input power and the output voltage, (see Figure 3.25). This test also predicts the LO coupling performance at different frequencies of the mixer. Since the available solid state-based higher frequency multiplier chain source matches perfectly to those LO frequencies for the 3rd harmonic mixing, further characterization of the mixer is performed using those LO frequencies.

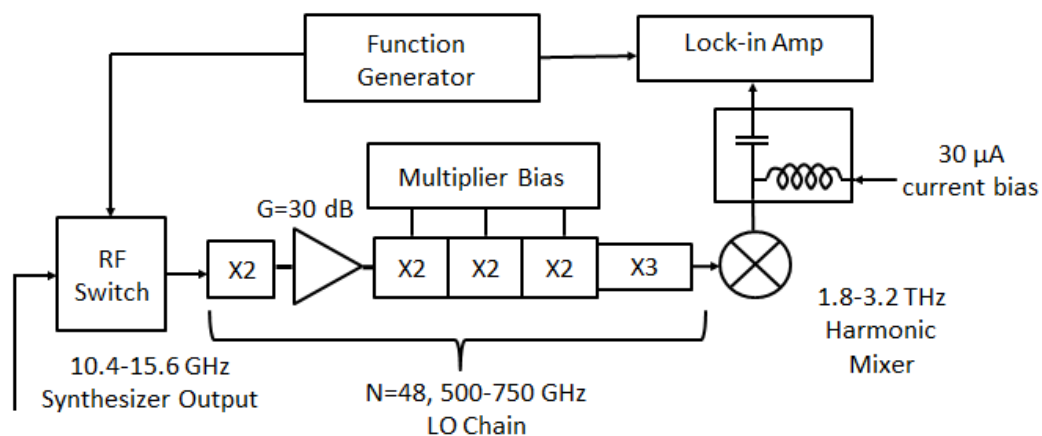


Figure 3.24.: LO video response test setup

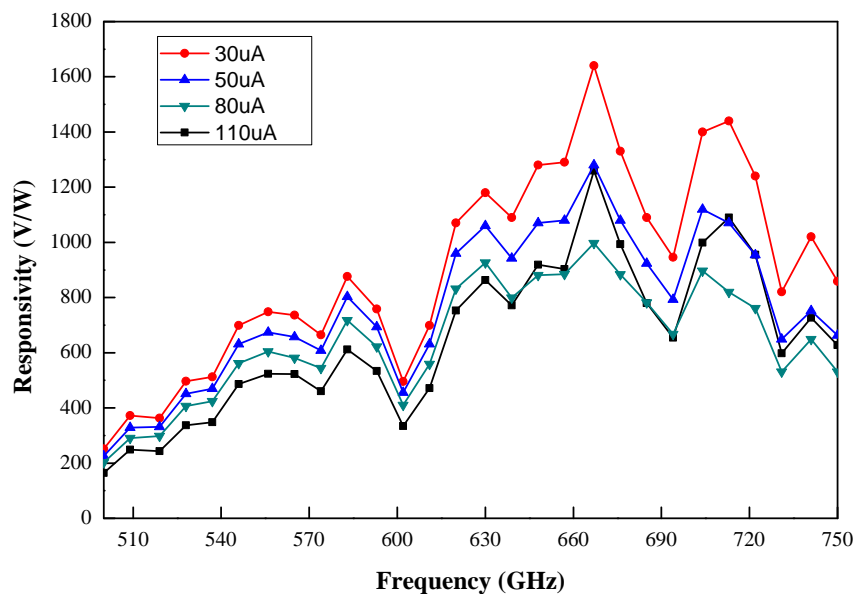


Figure 3.25.: LO responsivity measurement for WM-86 (WR0.34HM) with WM-380 (WR1.5) LO input waveguide for different current biases is shown. Due to the calibrated waveguide connections and higher LO input power, the measurement uncertainty is neglected.

Similarly, the RF video responses for a range of current biases are measured by modulating the RF source using a 100 Hz square wave and monitoring the modulated video response using the lock-in amplifier, (see Figure 3.26). The RF source is a varactor based multiplier chain with a multiplication factor of $N=144$, this multiplier chain has an output frequency of 1.9-2.025 THz. The last stage multiplier of the RF source has an integrated WM-130 (WR-0.51) diagonal horn antenna that transmits a maximum output power of approximately $2 \mu\text{W}$, and the power is measured using an Erickson power meter [38].

3.6 Harmonic Mixer Test and Measured Performance

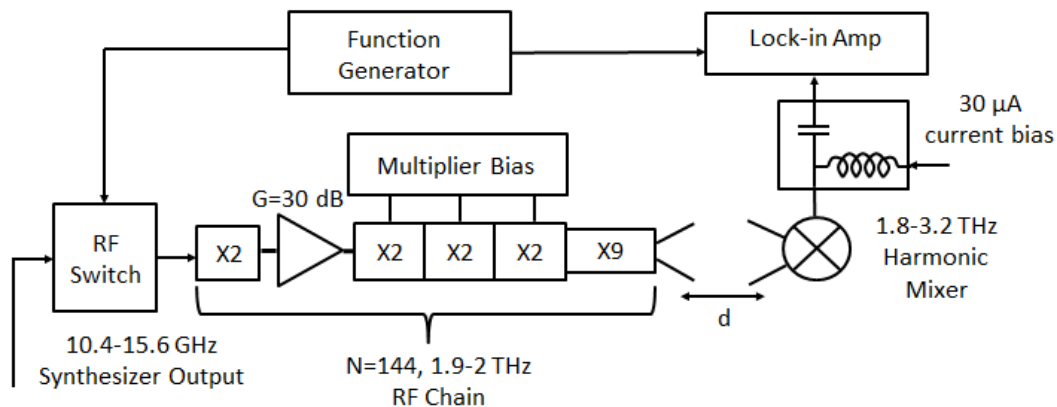


Figure 3.26.: RF video response test setup

The WM-86 (WR-0.34) harmonic mixer is set for a range of current biases $30 - 70 \mu A$, and RF signal is transmitted quasi-optically and the video response is measured. Finally, the responsivity relates the input power and the output voltage is calculated for different current biases. Figure 3.27 depicts the responsivity of the WM-86 (WR-0.34) harmonic mixer when it operates in a detector mode by biasing it at lower currents. $30 \mu A$ gives the relatively best responsivity. Since 1.9 THz is the band edge of the mixer, the responsivity is lower, however, progressing upward in frequency the coupling is better and the responsivity is continuously improving.

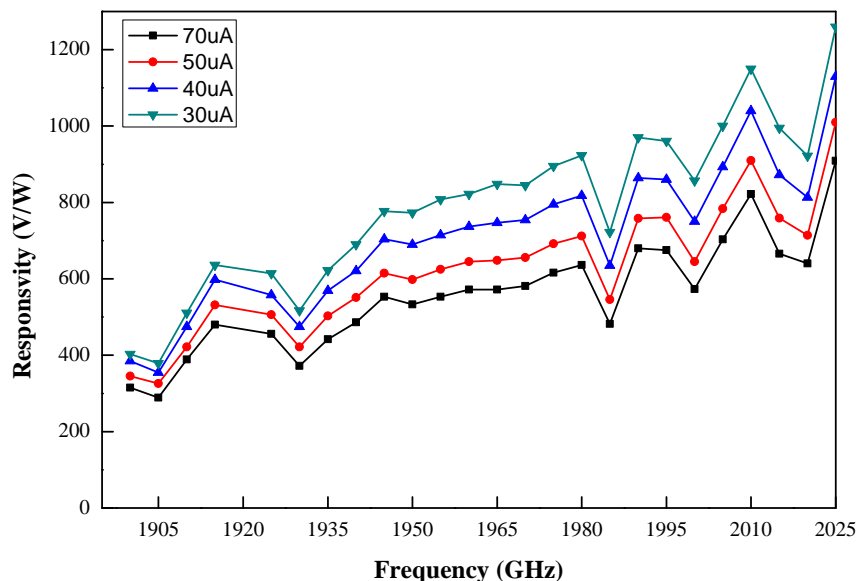


Figure 3.27.: RF responsivity of the WM-86 (WR-0.34) harmonic mixer for different current biases, measurement uncertainty is shown in Table 3.3, adding the uncertainty would change the RF responsivity at 1965 GHz and for a current bias of $50 \mu\text{A}$ to $600 \pm 130 \text{ V/W}$.

Finally, the video response of the mixer at 2.6906 THz is measured using a QCL as a THz source and the responsivity is calculated. The initial test setup is implemented by having two mirrors to collimate and focus the THz beam, (see Figure 3.28). The mixer is positioned 10 mm away from the focal point of the second mirror to optimize the video response. An optical chopper is used at the cryocooler window to modulate the THz beam with 30 Hz modulation rate and used as a reference for the lock-in amplifier. The QCL is biased at different current values between 0.78-0.9 A to generate 2.690-2.6912 THz frequencies with a maximum output power of -11 dBm. Since the focused THz beam radius is larger than the mixer diagonal horn aperture, at 10 mm away from the focal point only up to 20 % of the THz power can be coupled to the THz mixer (see section 4.1.2 for power measurement and coupling efficiency calculations). The output video response recorded from the lock-in amplifier and the input power estimated from

3.6 Harmonic Mixer Test and Measured Performance

Section 4.1.2 are used to calculate the responsivity of the mixer, Figure 3.29 depicts the 2.690-2.6916 THz responsivity at different current biases, and a nominal responsivity of 1200 V/W is observed. From Figure 3.27, 30 μ A yields relatively best responsivity which is also the case for the 2 THz responsivity measurements. This measurement did not account the Gaussian coupling efficiency of the receiving horn antenna and also the loss due to the transition between the RF waveguide to the microstrip circuit. Therefore, the data shown in Figure 3.27 could underestimate the true RF responsivity. From Section 3.3, the WM-86 (WR0.34) diagonal horn antenna has a Gaussian coupling efficiency of 82-87%, that results an approximate of 0.7 dB loss and an additional 1 dB loss due to waveguide to microstrip transition with a total RF loss of 1.7 dB could be accounted to give a measurement tolerance for the responsivity data. Furthermore, atmospheric attenuation needs to be accounted for during the quasi-optical systems setup to estimate the actual input power coupled to the mixer. For the measurements shown above, the atmospheric loss in THz frequencies is accounted for an air with 50 % relative humidity. However, the humidity might be different during the test and it could change the input power. For a short distance THz quasi-optical systems with a relative humidity of 40-60 %, the difference is small and the input power variation due to the relative humidity level can be ignored. In Figure 3.27, for the frequency range of 1.9-2.025 THz an RF responsivity of 300-1200 V/W is shown. Adding the losses discussed above would change the RF responsivity range to 447-1764 V/W.

Parameter	Uncertainty Range	Additional Loss
Gaussian coupling efficiency of the horn (85%)	82-87%	0.6-0.86 dB
Loss due to tilt angle	-	0-0.3 dB
Atmospheric loss: relative humidity (50%)	45-55 %	\pm 1 dB/m
Power measurement accuracy	-	0.2-1 dB

Table 3.3.: Estimated measurement uncertainty.

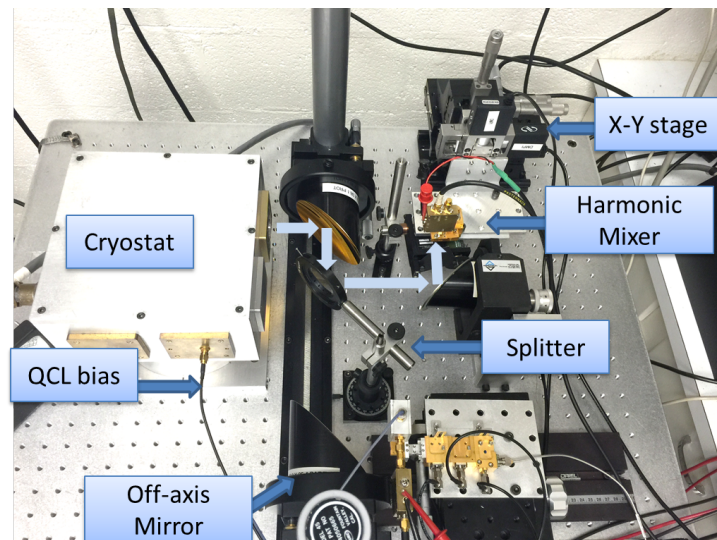


Figure 3.28.: Video response test setup using 2.6906 THz QCL

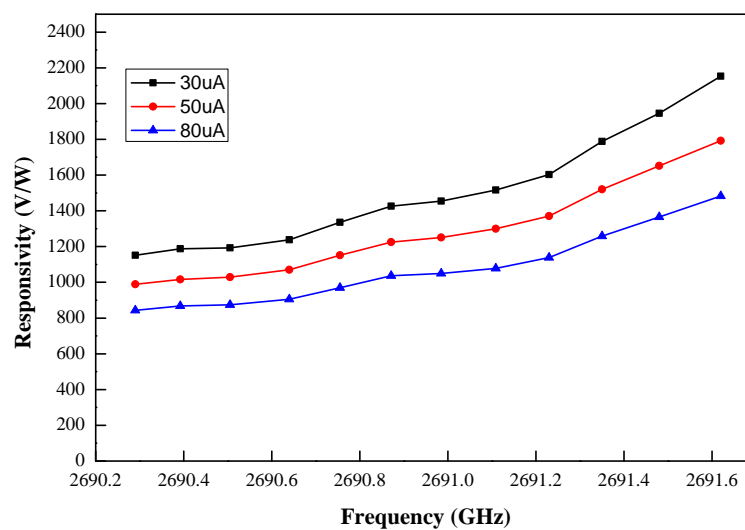


Figure 3.29.: Responsivity performance of the WR0.34 harmonic mixer tested using approximately 2.6906 THz QCL at different current biases, measurement uncertainty is shown in Table 3.3, adding the uncertainty would change the RF responsivity at 2691 GHz and for a current bias of 50 μ A to 1200 ± 400 V/W.

3.6.2. Harmonic Mixing

Due to the lack of a broadband RF source that covers 1.8-3.2 THz, harmonic mixing is tested in two different frequency bands. The first harmonic mixing is performed using VDI's ~2 THz solid state source and the second harmonic mixing is tested using a 2.69 THz QCL.

3.6.2.1. Harmonic Mixing at ~2 THz

Once the RF and LO video response are tested as discussed in Section 3.6.1, selecting the appropriate LO harmonics and RF frequencies based on the video response is straight forward. Harmonic mixing is performed by injecting the RF and LO signal into the mixer and monitoring the output IF signal using a spectrum analyzer, (see Figure 3.30 for mixing test setup). The mixer is biased with different current biases between 150 - 300 μA and the optimal bias range is determined.

Two different harmonic mixers are characterized and their performances are depicted in Fig. 3.32a. Harmonic mixing is applied using a 3rd harmonic of the 654.5 GHz LO signal that mixes with a 1.9634 THz RF signal. Similarly, a 3rd harmonic of the 667.8 GHz LO signal is used to mix with a 2.004 THz RF signal. The down converted 500 MHz IF signal passes through an IF Low Noise Amplifiers (LNA) with a total gain of 30 dB. To eliminate spurious products and to reduce noise bandwidth, a low pass filter is used. The IF signal output power is measured on a spectrum analyzer and the conversion loss is determined. Fig. 3.32b depicts the mixer performance at different LO and RF frequencies for a fixed current bias of 150 μA .

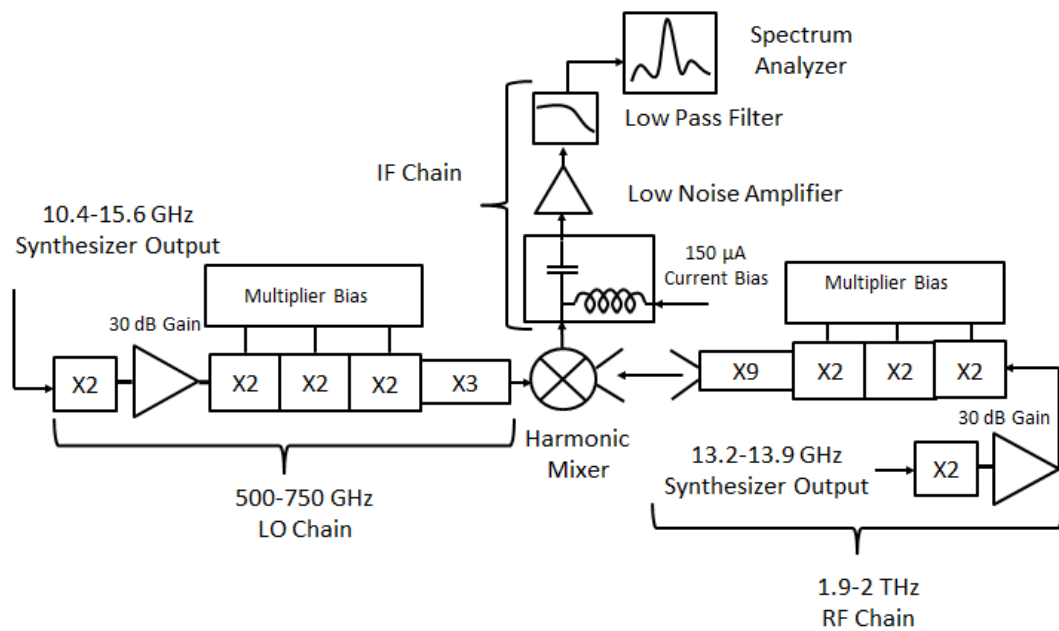


Figure 3.30.: Harmonic mixing test setup.

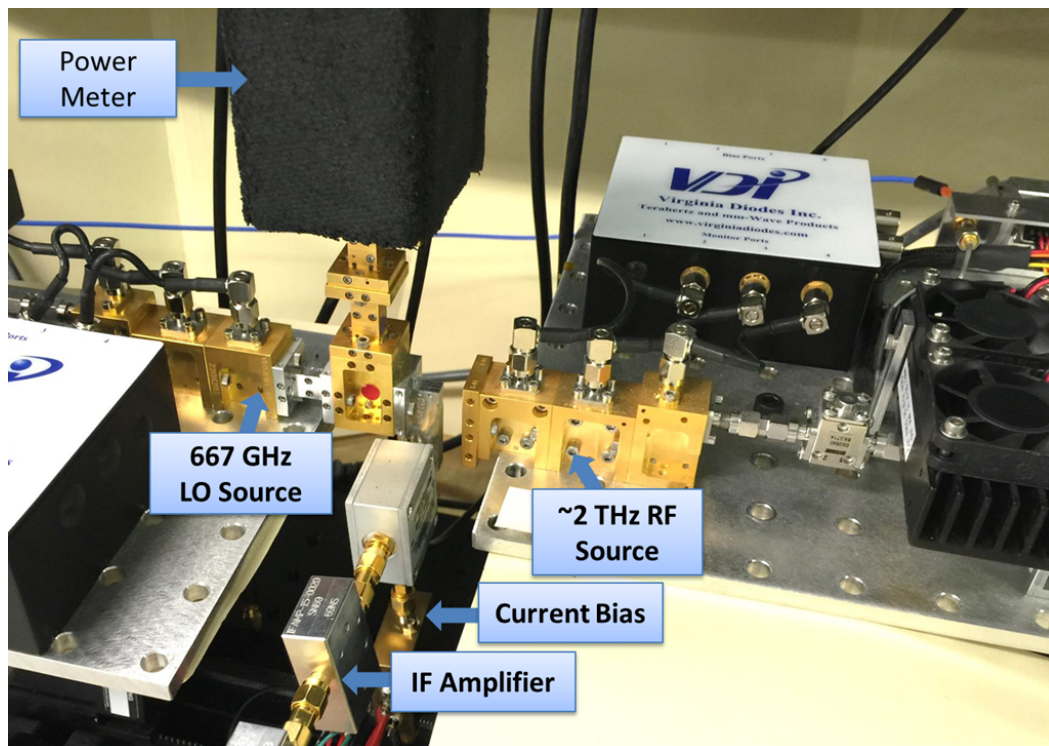
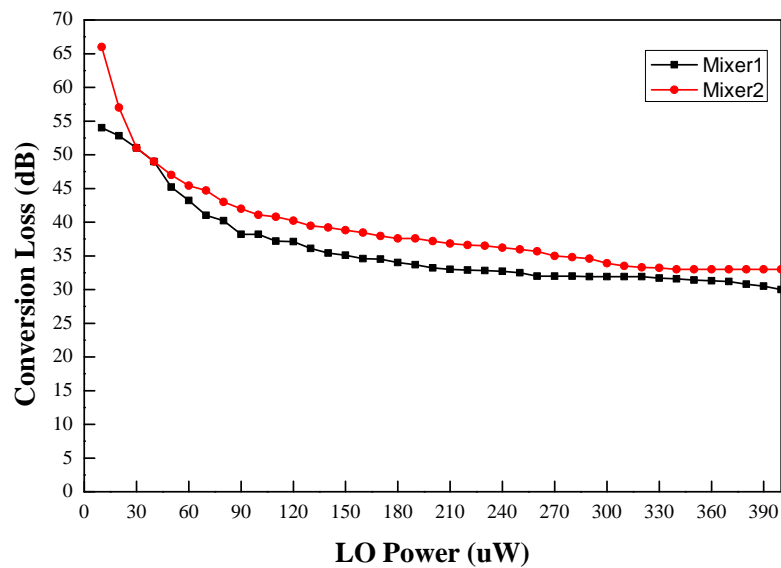
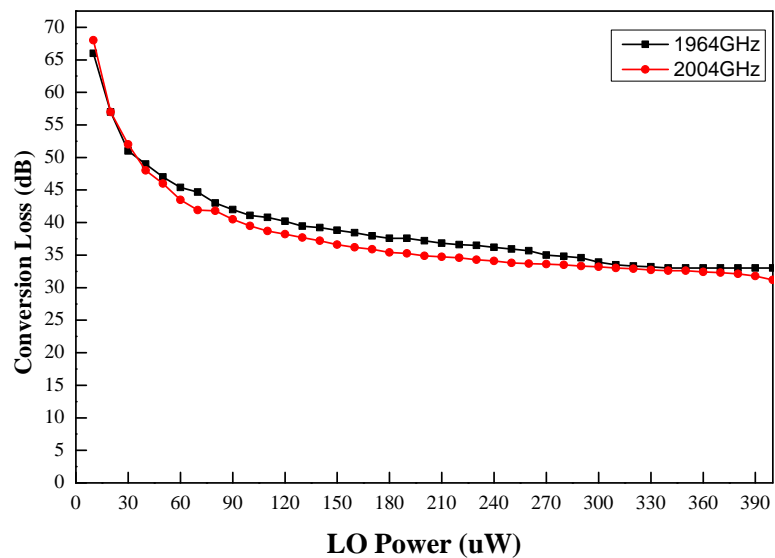


Figure 3.31.: Experimental setup for harmonic mixing at 2 THz using solid state sources.

3.6 Harmonic Mixer Test and Measured Performance



(a) The above graph shows the 3rd harmonic mixing for two different mixers at LO: 2.0035 THz and RF: 2.004 THz for a fixed current bias of 150 μ A.



(b) The above graph shows the 3rd harmonic mixing for LO: 1963.5 GHz, RF: 1964 GHz and LO: 2003.5 GHz, RF: 2004 THz for a fixed current bias of 150 μ A.

Figure 3.32.: WM-86 (WR0.34) harmonic mixer performance (measurement uncertainty is shown in Table 3.3), adding the uncertainty for the 300 μ W LO drive would change the conversion loss to 32.5-35.5 dB.

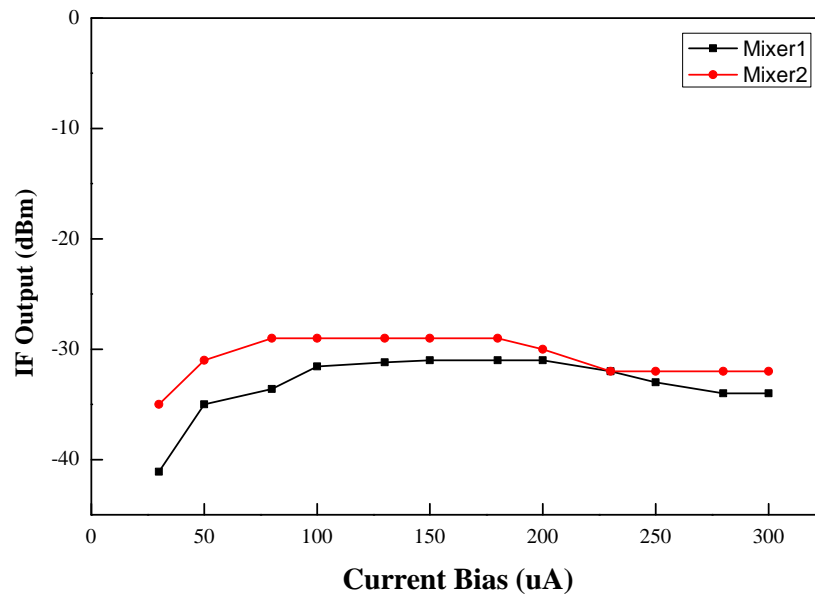


Figure 3.33.: Mixer’s performance (IF output vs. current bias) for $380\ \mu\text{W}$ LO power, measurement uncertainty is shown in Table 3.3, adding the uncertainty for the current bias of $150\ \mu\text{A}$ of the 2^{nd} mixer would change the conversion loss to 27.5-30.5 dB.

The performance of the first mixer at different current biases between $30\text{-}300\ \mu\text{A}$ is investigated while pumping the mixer with an optimal LO power of $380\ \mu\text{W}$. The current bias range of $140\text{-}170\ \mu\text{A}$ is found to provide an optimal IF output power, as shown in Figure 3.33. For a fixed IF frequency of $500\ \text{MHz}$, the single sideband conversion loss is also calculated at different RF frequencies. Figure 3.34 depicts the optimal conversion loss for different frequencies ranging from $1.905\ \text{THz}$ to $2.060\ \text{THz}$ by optimizing the LO power and the current bias at each frequency. Conversion loss of $27\text{-}35\ \text{dB}$ is achieved for the 3^{rd} harmonic mixing which improved the previous WM-102 (WR-0.4) harmonic mixer conversion loss performance by more than $18\ \text{dB}$. Due to the RF horn antenna 85% Gaussian coupling efficiency, an additional of $0.5\text{-}2.5\ \text{dB}$ RF power loss can be accounted to the conversion loss data shown in .

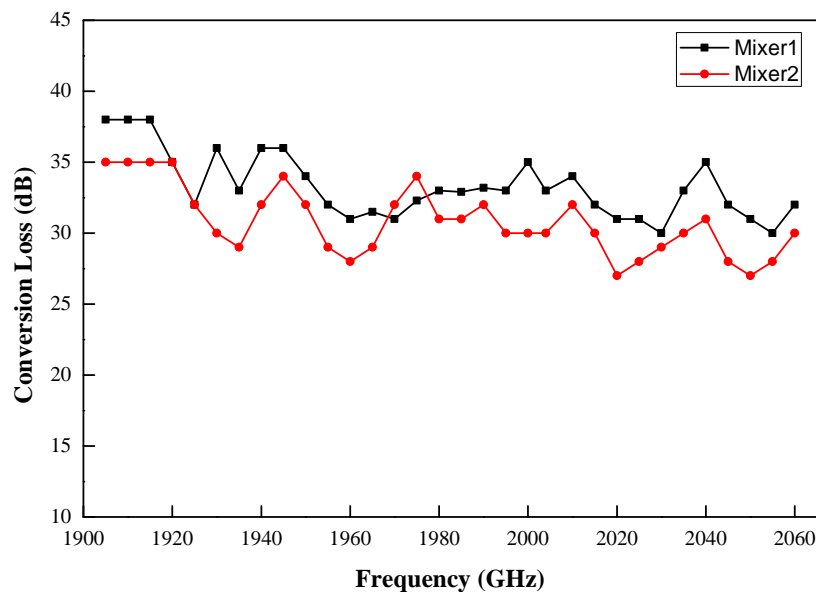


Figure 3.34.: Optimized conversion loss vs. RF frequency, measurement uncertainty is shown in Table 3.3, adding the uncertainty will change the conversion loss by 0.5-2.5 dB across the band.

3.6.2.2. Harmonic Mixing at ~2.69 THz

The WM-86 (WR0.34) harmonic mixer performance at higher frequency is tested using a ~2.69 THz QCL. The mixer is positioned at the focal point of the second parabolic mirror and the input power is estimated based on the beam width of the THz beam and the aperture of the harmonic mixer feed horn (see Figure 3.28 testing setup), (see section 4.1.2 for power measurement and coupling efficiency calculations). To measure a constant 1 GHz down converted IF signal, the 4th harmonic of the LO frequency is varied between 2689-2.690.8 GHz and mixes with the QCL frequency of 2690-2691.8 THz. The down converted 1 GHz IF signal is measured using a spectrum analyzer and conversion loss is calculated.

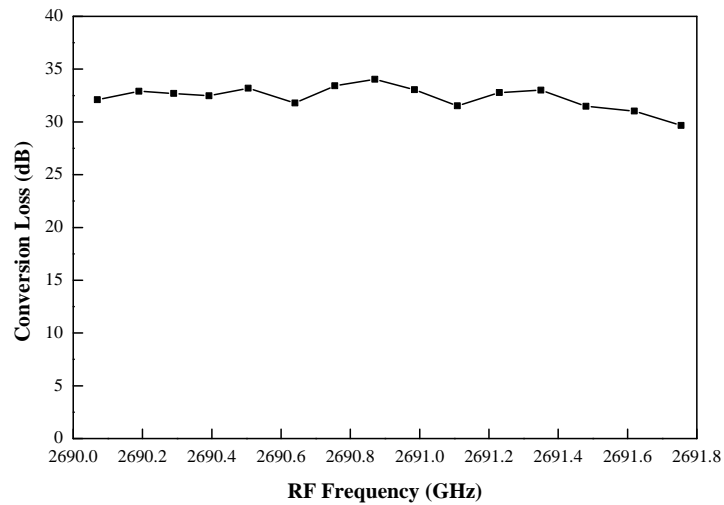


Figure 3.35.: Conversion Loss of the WM-86 (WR0.34) harmonic mixer tested using 2690-2691.8 GHz QCL, measurement uncertainty is shown in Table 3.4, adding the uncertainty will change the conversion loss by 0.9-3.5 dB across the band.

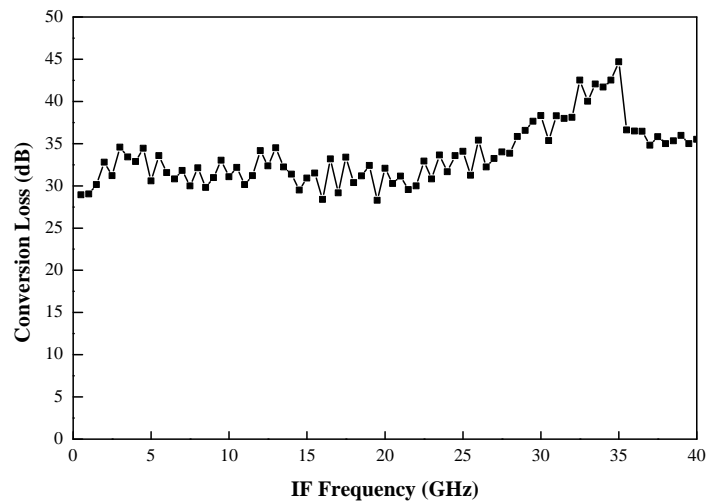


Figure 3.36.: Conversion Loss of a 40 GHz IF bandwidth is tested for a fixed RF: 2690 GHz and LO: 2690.5-2730 GHz, measurement uncertainty is shown in Table 3.4, adding the uncertainty will change the conversion loss by 0.9-3.5 dB.

3.6 Harmonic Mixer Test and Measured Performance

Parameter	Additional Loss
Waveguide overmoding and Gaussian coupling efficiency	1-2 dB
Loss due to tilt angle	0-0.3 dB
Atmospheric loss: relative humidity (45-55 %)	1 dB/m
Power measurement accuracy	0.2-1 dB

Table 3.4.: Estimated measurement uncertainty.

Figure 3.35 depicts the conversion loss performance of the 4th harmonic mixing, and a conversion loss of 31-34 dB is measured. Similarly, to measure the IF bandwidth of the harmonic mixer, the LO frequency is swept for a constant RF frequency of 2690 GHz. The LO frequency is varied between 2690.5-2730 GHz and a response of 0.5-40 GHz IF signal is measured. Figure 3.36 presents the mixer IF bandwidth performance and the mixer has fairly flat conversion loss of 30-35 dB up to an IF of 28 GHz, drops its response between 28-36 GHz and goes back to similar conversion loss up to 40 GHz.

Similar analysis as Section 3.61 could be implemented to account for power losses and to give range to the conversion loss data shown above. Gaussian coupling efficiency of the receiving horn antenna and also the loss due to the transition between the RF waveguide to the microstrip circuit could approximately contribute 1-2 dB and this could underestimate the conversion loss of the mixer. During the RF power measurement, a VDI Erickson power meter with WR10 straight waveguide and a WR10 conical horn is used. Since those waveguides look overmoded for the 2.69 THz QCL output power measurement, other modes could contribute to the power measurement and thus overestimate the conversion loss data. Due to the difficulty of estimating or measuring the power contributions from other modes, it is not accounted in the conversion loss calculation shown above.

Furthermore, atmospheric attenuation needs to be accounted for during the quasi-optical systems setup to estimate the actual input power coupled to the mixer. For the measurements shown above, the atmospheric loss in THz frequencies is accounted for an air with 50 % relative humidity. However, the humidity might be different during the test and it could change the input power. For a short distance THz quasi-optical systems with a relative humidity of 40-60 %, the difference is small and the input power variation due to the relative humidity level can be ignored.

3.6.3. Mixer Noise Temperature and Conversion Loss using Y-Factor Technique

Two important parameters that describe the performance of the mixer are noise temperature and conversion loss. In this section the Y-factor method that is commonly used to characterize mixer's noise temperature and conversion loss is described. The mathematical derivation is formulated at the beginning of the section and the measured result is presented at the end.

The black body radiation is the random motion of electrons due to temperature that produce a non zero RMS voltage value. According to Max Planck's black body radiation law, the output noise voltage (V_n) and output noise power (P_n) of any black body with temperature T is described as [39]:

$$V_n = \sqrt{\frac{4hfBR}{e^{hf/KT} - 1}} \quad (3.1)$$

$$P_n = \frac{hfB}{e^{hf/KT} - 1} \quad (3.2)$$

3.6 Harmonic Mixer Test and Measured Performance

Where h is Planck's constant, f is the center frequency in Hz, B is the bandwidth in Hz, R is the resistance in Ω , K is Boltzmann's constant. Using two different black body sources, a hot load T_h and a cold load T_c , the equivalent noise temperature of a system T_{sys} can be calculated using the Y-factor technique, where $T_h > T_c$. When we supply input noise power to any practical system, the output power consists of the noise generated from the device under test with gain G plus the noise from the source, (see Figure 3.37) [39].

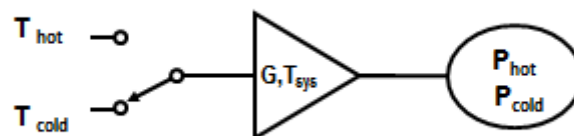


Figure 3.37.: The Y -factor method for measuring the system noise temperature.

$$P_h = \frac{GhfB}{e^{hf/KT_h} - 1} + GT_{sys}KB \quad (3.3)$$

$$P_c = \frac{GhfB}{e^{hf/KT_c} - 1} + GT_{sys}KB \quad (3.4)$$

Y-factor is the ratio between the noise power due to hot load and cold load:

$$Y = \frac{P_h}{P_c} \quad (3.5)$$

From this, we can calculate system equivalent noise temperature T_{sys} :

$$T_{sys} = \frac{hf}{k(1-Y)} \left[\frac{Y}{(e^{hf/KT_c} - 1)} - \frac{1}{(e^{hf/KT_h} - 1)} \right] \quad (3.6)$$

Eqn. (3.6) can be used to calculate system noise temperature at any frequency. For cascaded systems that contain a mixer and IF chain, it is necessary to identify the noise due to IF chain in order to measure noise temperature of the mixer T_{mix} . The total noise temperature of the system can be calculated as, (see Figure 3.38), [39]:

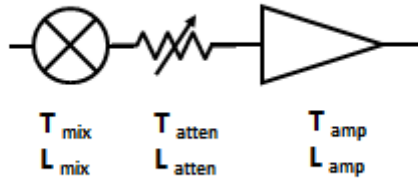


Figure 3.38.: Noise temperature of a cascaded system.

$$T_{sys} = T_{mix} + L_{mix}T_{atten} + L_{mix}L_{atten}T_{amp} \quad (3.7)$$

$$T_{sys} = T_{mix} + L_{mix}[T_{atten} + L_{atten}T_{amp}] \quad (3.8)$$

$$T_{IF} = T_{atten} + L_{atten}T_{amp} \quad (3.9)$$

$$T_{sys} = T_{mix} + L_{mix}T_{IF} \quad (3.10)$$

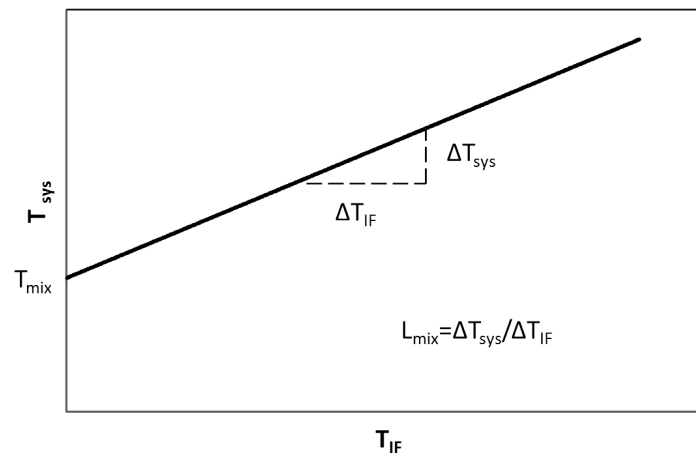


Figure 3.39.: T_{sys} versus T_{IF}

The above equation is a straight line with slope L_{mix} (mixer's conversion loss) and y-intercept T_{mix} (mixer's noise temperature). Where T_{IF} is the noise temperature of the IF chain that is characterized beforehand. The IF chain contains a programmable attenuator at the first stage, a low noise amplifier followed by a filter and an amplifier with a total amplifier gain of 50 dB. The narrow bandwidth filter is used to reduce the noise bandwidth, therefore, the IF chain is designed to operate within a 1 GHz bandwidth at a center frequency of 1 GHz. A square law detector is connected at the end of the IF chain to measure the noise voltage. During an IF calibration, the input of the IF chain is exposed to the hot and cold loads and at the end of the the IF chain the square law detector produces a DC voltage that is proportional to the input noise power and a Y-factor can be obtained by taking the voltage ratio. Noise temperature of the IF chain that is collected during the experiment is depicted in Table 3.5.

Attenuation (dB)	IF Chain Noise temperature (K)
0	98
1	199
2	327
3	489
4	686
5	940

Table 3.5.: Measured noise Temperature of the IF chain

The experimental noise temperature setup of the harmonic mixer contains a chopper to switch between the hot load from room temperature and the cold load from the liquid nitrogen bath at a rate of 30 Hz. This modulation signal is used as a reference for the lock-in amplifier to detect the down converted 1 GHz signal. During the mixing test, the output of the detector contains an RMS voltage corresponding to the AC signal due to the chop between the hot and cold loads that is displayed on a lock-in amplifier. Moreover, the DC offset from the detector is also monitored and recorded. The detector output of the AC signal and the DC offset are related to the input noise power as;

$$P_{hot} = V_{DC} + \frac{1}{2}V_{pp} \quad (3.11)$$

$$P_{cold} = V_{DC} - \frac{1}{2}V_{pp} \quad (3.12)$$

Taking the ratio between Eqn. (3.11) and Eqn. (3.12) provides a Y-factor of the system. By adjusting the attenuation values of the programmable attenuator at the first stage, a number of T_{sys} values can be collected. Using Eqn. (3.10), the relationship between T_{IF} and T_{sys} can be determined and T_{mix} and L_{mix} can be extracted.

3.6 Harmonic Mixer Test and Measured Performance

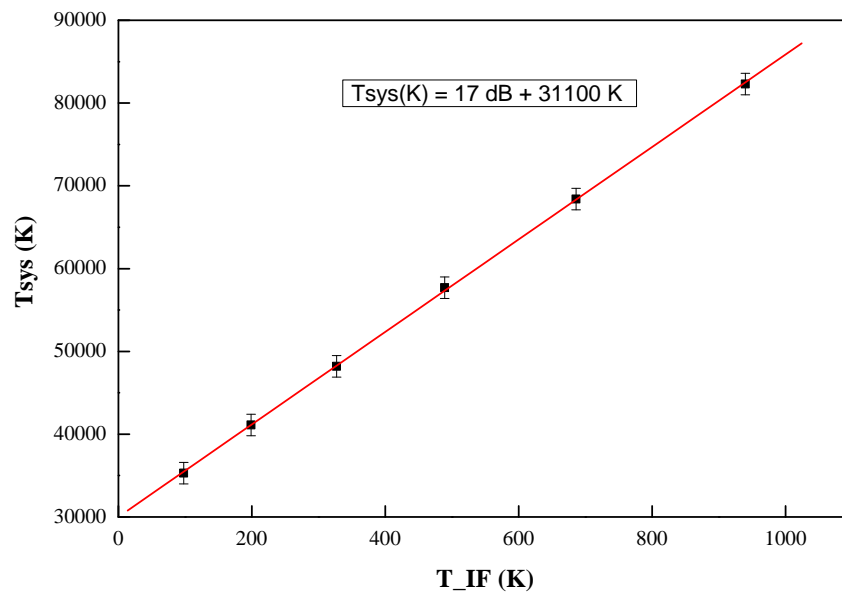


Figure 3.40.: Noise temperature measurement of the WR0.34 harmonic mixer

Y-factor measurement of the WM-86 (WR0.34) harmonic mixer is implemented by pumping the mixer using the 3rd harmonic of the 667 GHz LO signal. The LO power is set to approximately -4 dBm and the mixer is current biased at 150 μ A. A nominal double side band noise temperature of 31100 K with a standard deviation of 1359 K is obtained and a conversion loss of 17 dB with standard deviation of 0.7 dB is measured for a consecutive three measurements, (see Figure 3.40). For an equal side band conversion loss, the single side band conversion loss is 3 dB more than the double side band conversion loss. Therefore, the Y-factor technique indicates that the WM-86 (WR0.34) harmonic mixer has approximately 20 dB single side band conversion loss. This result introduced a 7 dB discrepancy between the previous technique discussed in section 3.6.2 using two tone measurement. When the harmonic mixer is pumped at 667 GHz LO signal, higher harmonics will be created. Those harmonics might mix with the broad band noise above the feed horn cutoff frequency (1.74 THz) and produces an IF signal

that adds power to the intended IF signal due to the 3rd harmonic and underestimate the true conversion loss result. To validate this assumption, and eliminate the RF power contribution from the higher harmonics, a 9.8 % bandwidth 2 THz mesh filter is used and the Y-factor is tested, and similar noise temperature is obtained. Furthermore, another reason that could cause the discrepancy between the Y-factor technique and the two tone measurement described in section 3.6.2 is that the single side band conversion loss calculation does not account the Gaussian coupling efficiency of the transmitting and receiving WM-86 (WR0.34) diagonal horn. This could underestimate the conversion loss measurement tested at 2 THz using two tone measurements and the 7 dB discrepancy might be from that.

3.7. Comparison of Test and Simulation Results

Nonlinear simulation is implemented to compare the measured performance with the simulation data and to correct design parameters and to implement a better harmonic mixer in the future. The harmonic balance analysis is performed using ADS nonlinear simulator. The diode parameters that are extracted by performing a curve fitting to an ideal diode, such as series resistance $R_s = 27\Omega$, saturation current $I_s = 4.2\text{ pA}$ and ideality factor $\eta = 1.7$ are used to run the harmonic balance simulation.

Similarly, the finger inductance $L_f = 3.2\text{ pH}$ and the finger to pad capacitance $C_{fp} = 1.3\text{ fF}$ are determined from the HFSS structural simulations, and used to estimate the harmonic mixer performance.

3.7 Comparison of Test and Simulation Results

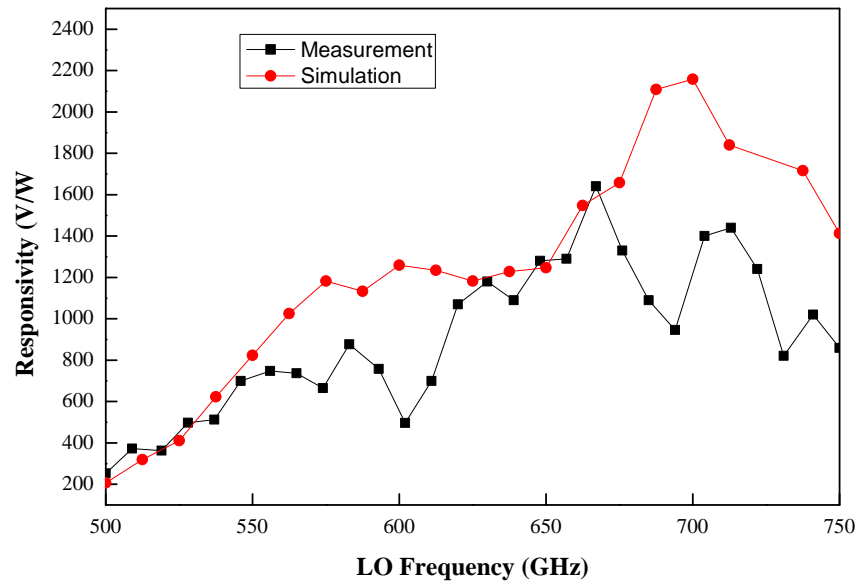


Figure 3.41.: Comparison of the simulated and measured performance of the WM-86 (WR0.34) LO responsivity at a current bias of $30\ \mu\text{A}$.

Furthermore, the LO, RF and IF waveguides and circuits are designed on HFSS, the data is imported to the HFSS designer to predict the LO responsivity. Figure 3.41 shows the LO responsivity comparison of the simulated and measurement result. The responsivity results are in close agreement at the lower and center frequency, however, there are few difference at the higher frequency. The difference could be due to few different reasons, such as positioning the LO probe during assembly, and the connection between the LO and RF circuit could cause reflection.

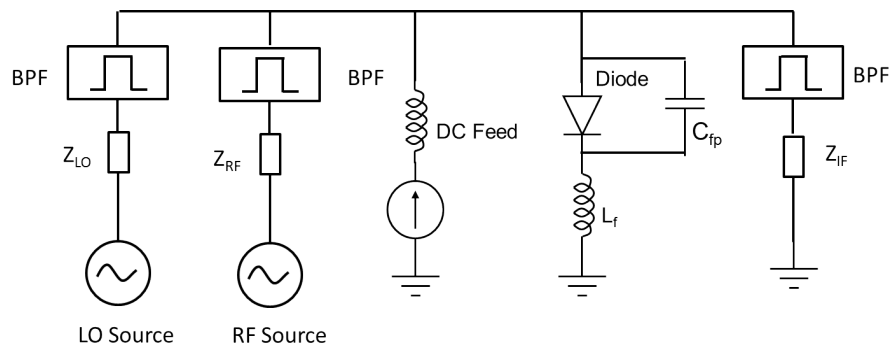
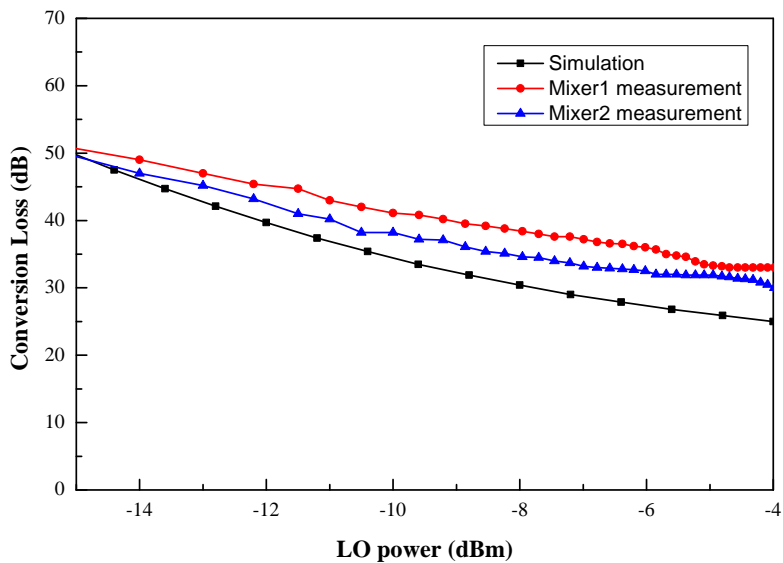


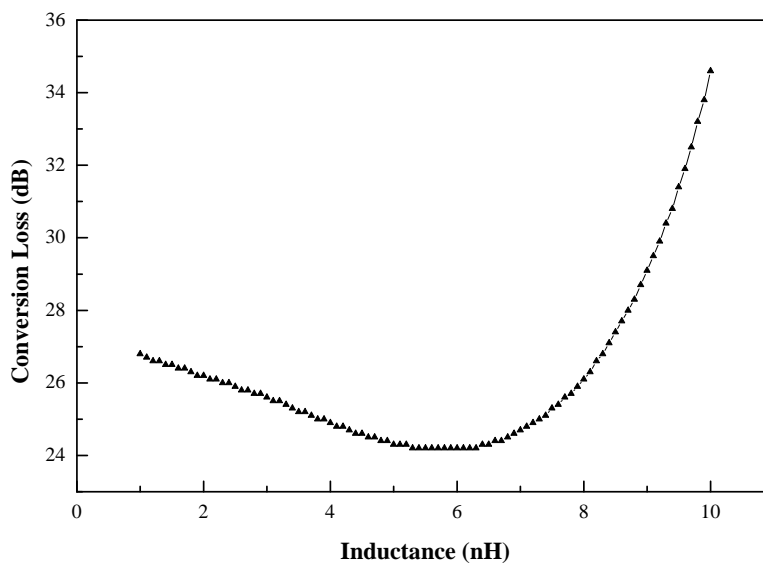
Figure 3.42.: ADS simulation circuit model

An RF source at 2001 GHz and an LO source of 667 GHz is used to drive the diode during the simulation. For the circuit model, $50\ \Omega$ impedance is used to terminate all sources and the IF circuit. Ideal band pass filters are used for each source to allow the source frequency only and to block the others. The optimal current bias ($150\ \mu\text{A}$) that is found during the WM-86 (WR0.34) harmonic mixer measurement is used to bias the diode and the harmonic balance is simulated from -15 dBm to -4 dBm LO power.

3.7 Comparison of Test and Simulation Results



(a)



(b)

Figure 3.43.: (a) Comparison of the simulated and measured performance of the WM-86 (WR0.34) harmonic mixer for RF: 2 THz, IF: 1 GHz, and current bias of $150\ \mu\text{A}$, measurement uncertainty is shown in Table 3.3, adding the uncertainty will change the conversion loss by 0.5-2.5 dB, (b) Inductance vs. conversion loss.

Figure 3.43a depicts increasing the LO power to -4 dBm reduces the conversion loss significantly. The general simulated conversion loss curve for the lower LO power matches the measured data. At LO power of -4 dBm, the simulated conversion loss is 2-4.5 dB below the measured data using two tone technique and approximately 4 dB above the result of Y-factor technique (see section 3.6.3). Therefore, the simulated data might be in a close agreement with the true conversion loss data which is bounded between the two techniques. The difference between the simulated data and the measured data could also be due to the waveguide to microstrip transition loss and circuit losses that are not accounted during the conversion loss calculation.

In general $1 \mu\text{m}$ corresponds to approximately 1 pH inductance [40]. From Figure 3.43b, the simulated conversion loss vs. finger inductance is shown and an optimal conversion loss is obtained for an inductance of 5-6 pH. This is due to the simulation setup that was intended for 2 THz. However, for a WM-86 (WR0.34) harmonic mixer with a center frequency of 2.8 THz, the optimal inductance will be 3-5 pH and these corresponds to finger inductance of $3\text{-}5 \mu\text{m}$.

3.8. Room Temperature Schottky based Receiver

Room temperature Schottky based THz receivers are good candidates for different applications in 1-3 THz where cryogenics are difficult or impossible to use. Specially, for applications where compactness and low power consumption is a requirement. One of the largest High Elevation Antarctic Terahertz Telescope (HEAT) 0.5-2 THz project to study the formation of interstellar clouds and their evolution is using VDI's 1.4 THz Schottky based receiver [41]. This receiver has a noise temperature of 1400 K (DSB) at room temperature test and a noise temperature of 3500 K when the receiver is operating at 75 K, (more discussion is presented in Section 5.2.3).

3.8 Room Temperature Schottky based Receiver

The mixer in conjunction with the LO chain can be used to produce a Schottky-based THz receiver. Furthermore, if the harmonic mixer performance (noise temperature and conversion loss) improves at cryogenic as suggested in section 5.2.3, it would have further advantage. This approach is not intended to replace superconductive based receivers, however, to present an alternative options for the applications where Schottky based receivers are suited

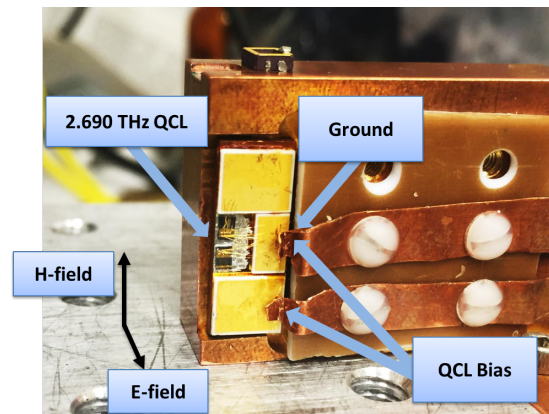
4. Characterizing and Phase Locking of Quantum Cascade Lasers

This chapter starts by characterizing the free running 2.582 THz and 2.691 THz QCLs and their current bias and output frequency linearity are determined. Additional characterization of the far field and focused beams are mapped using an X-Y scanner. Furthermore, a room temperature based terahertz focal plane array microbolometer THz camera is used to observe the THz beam from the QCL at different current bias levels. The output power of the QCL near the facet and the usable output power after splitting the THz beam and focusing it using off-axis mirrors is measured using an Erickson power meter. The THz signal is also down converted using a 1.8-3.2 THz WM-86 (WR0.34) harmonic mixer and observed on a spectrum analyzer. In addition, a gap fee with 85 MHz bandwidth real-time spectrum analyzer is used to observe the down converted IF signal stability when the QCL is free running. Moreover, the down converted signal is compared with a stable 100 MHz reference and used to phase lock the 2.5 THz and the 2.7 THz QCLs. At the end of this chapter, phase noise of the down converted signal and long term frequency drift is discussed and the data are presented.

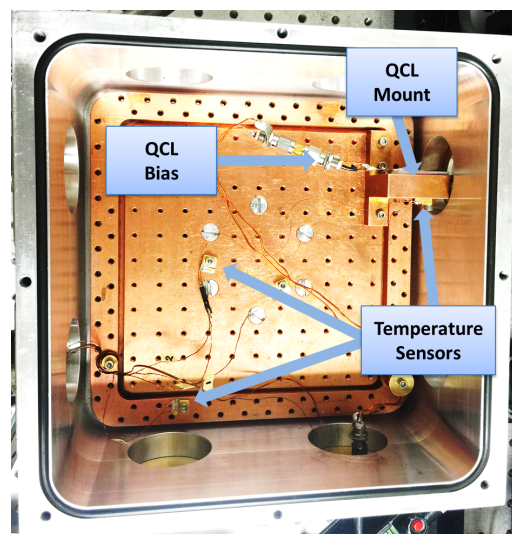
4.1. Characterizing Quantum Cascade Laser

The 2.5 THz and the 2.6905 THz QCLs used in this work are a type of semiconductor laser which uses epitaxially grown GaAs/AlGaAs quantum wells formed with molecular beam epitaxy (MBE). The QCLs are based on a 15 μm and 12.5 μm thick bound-to-continuum active region, grown on a ~ 150 μm -thick GaAs substrate. The active regions were processed using conventional photolithography and wet-etching techniques into a gold semi-insulating single-plasmon ridge waveguide configuration with contacts consisting of a thin layer of evaporated AuGeNi. The QCLs have a 200 μm waveguide ridge width and are cleaved into 1 mm long Fabry-Perot resonator laser bars, (see section 2.5 for more QCL discussions). For better thermal coupling, the laser bars are indium soldered on a copper carrier and the QCL facet is accurately positioned as close as possible to the carrier edge to reduce reflections.

To supply a maximum of 1 A bias current, four 1 mil gold bond wires are used to connect the top contact of the device to the QCL carrier biasing pads. Finally, spring bias lines are formed to create an electrical contact to the external bias supply and to hold the QCL biasing pads to the copper mount. In order to use the QCL, it must be kept below 40 K, therefore, the QCL is mounted in a two-stage 4.2 K closed-cycle cryogenic system to characterize the DC response, map the beam profile and to stabilize the output frequency and magnitude by phase locking the QCL, (see Figure 4.1). A two stage closed cycled SRDK-415D cryogenic system from Sumitomo is used to keep the QCL mount temperature at less than ~ 20 K. The cryocooler consists of a cold head, compressor and high pressure helium gas to provide continuous closed cycle refrigeration at temperature depending upon the heat load imposed. Characterizing the QCL is done by performing an I-V test while the cold head stage and the QCL-mount temperatures are monitored, and to determine the heat load of the cryocooler due to the heat dissipation of the QCL.



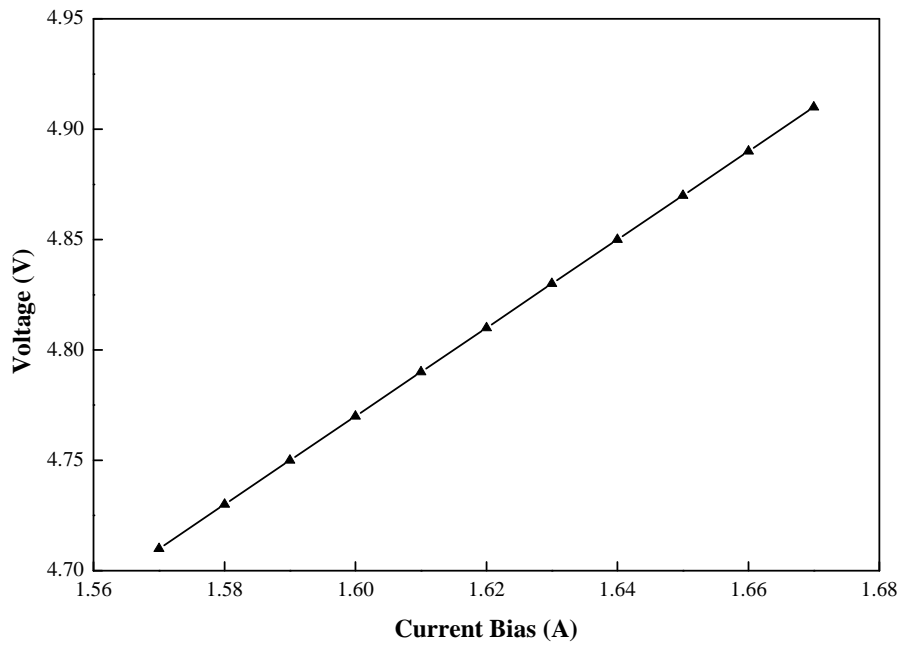
(a) QCL on a copper mount with a bias lines.



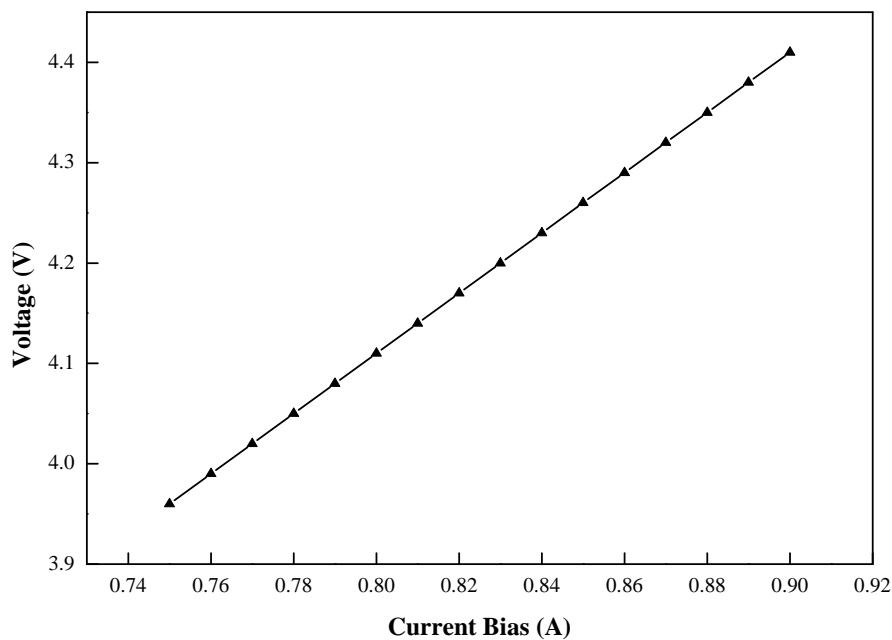
(b) 4.9 K cryocooler cold head stage and temperature sensors.

Figure 4.1.

By applying Apizon N thermal grease between the QCL mount and the second stage cryogenic system, effective heat transfer is achieved and the temperature differential is less than 3 K. When the 2.691 THz QCL is not biased, the QCL mounting temperature is 7.2 K and when the bias is applied to the QCL during operation, it dissipates approximately 3.6 W DC power and the QCL mount temperature becomes approximately 10.8 K which is still a safe temperature to operate the QCL, (see Fig. 4.2a and Fig. 4.2b).

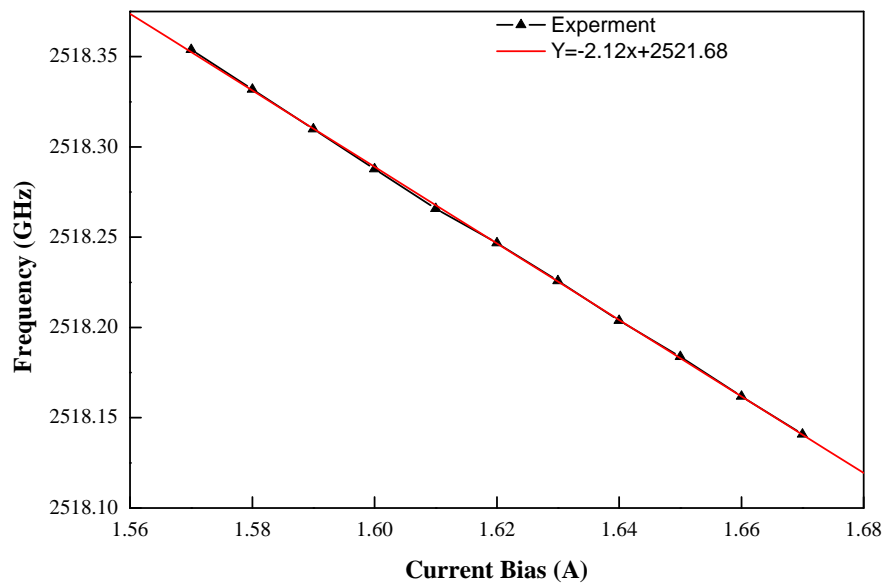


(a) The measured 2.5 THz QCL current bias versus voltage is shown. 7.86 W dissipated power is produced at a current bias of 1.63 A and the cryocooler temperature is raised to 15.2 K.

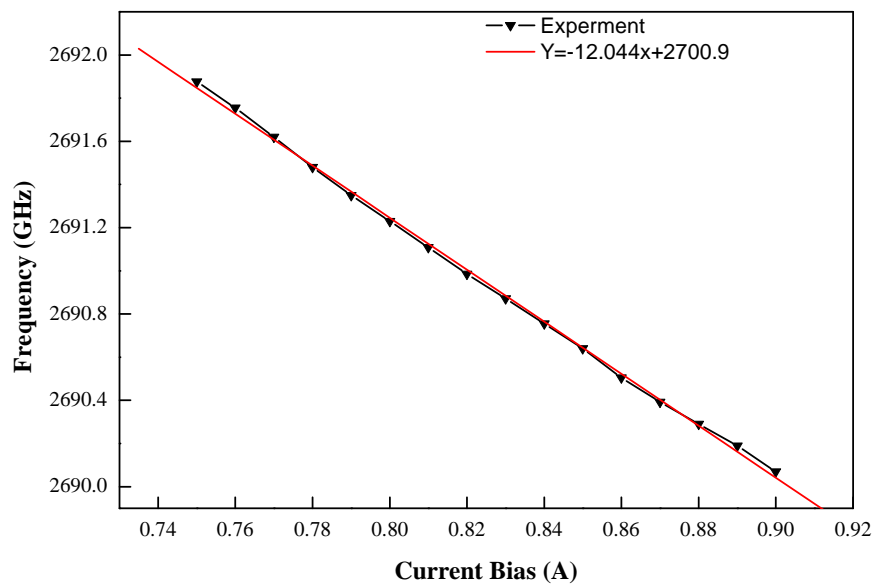


(b) The measured 2.6905 THz QCL current bias versus voltage is shown. 3.6 W dissipated power is produced at a current bias of 0.85 A and the cryocooler temperature is raised to 10.8 K.

4.1 Characterizing Quantum Cascade Laser



(a) A 2.5 THz QC current bias versus output frequency with current tuning factor of $\Delta f/\Delta I = -2.12$ GHz/A at 15.2 K.



(b) A 2.690 THz QC current bias versus output frequency with current tuning factor of $\Delta f/\Delta I = -12.044$ GHz/A at 10.8 K.

Figure 4.3.

Current Bias (A)	Frequency (GHz)	Mounting Temperature
0.77	2691.62	10.15
0.78	2691.48	10.2
0.79	2691.35	10.25
0.8	2691.23	10.3
0.81	2691.109	13.35
0.82	2690.985	10.4
0.83	2690.871	10.46
0.84	2690.755	10.53
0.85	2690.64	10.6
0.86	2690.505	10.68
0.87	2690.392	10.75
0.89	2690.29	10.82
0.9	2690.19	10.89

Table 4.1.: Current bias and frequency versus 2.69 THz QCL mounting temperature

The resonant frequency of the QCL Fabry–Pérot cavity is given by:

$$f = mc/2nL \quad (4.1)$$

We can differentiate the resonant equation and normalize to get the fractional change

$$\frac{1}{f} \frac{df}{dT} = -\left(\frac{1}{n} \frac{dn}{dT} + \frac{1}{L} \frac{dL}{dT}\right) \quad (4.2)$$

where m is the mode number, L is the length, $\frac{dL}{dT}$ is the coefficient of thermal expansion, n is the effective refraction index of the gain media and $\frac{dn}{dT}$ is temperature dependent index of refraction. Material index of refractive in the gain media of the QCL is a function of both the temperature and the electric field across the device (i.e. Stark tuning).

For GaAs active layer at 10 K, $\frac{1}{n} \frac{dn}{dT} = 6.17 \times 10^{-5}/K$ and $\frac{1}{L} \frac{dL}{dT} = 5.6 \times 10^{-6}/K$ [42].

At lower operational temperatures approximately 10 K, the coefficient of linear expansion

4.1 Characterizing Quantum Cascade Laser

should be negligible and length variation within the Fabry-Pérot is not expected Eqn. (4.2). However, temperature dependent index of refraction will change within the cavity. Moreover, the 2.691 THz QCLs have a temperature sensitivity of approximately -2 GHz/K, (see table Table 4.1), therefore the output frequency can be controlled by changing the bias current. Additional characterization is implemented to investigate the bias current and frequency relationship of the QCLs by mixing down the THz radiation with a known LO signal using a THz harmonic mixer, (Fig.[1], Fig.[5]).

A linear shift in frequency is obtained for currents in the 1.56–1.68 A range for the 2.518 THz QCL, with a tuning coefficient of -2.12 GHz/A (Fig. 4.3a). Similarly, the 2.690 THz QCL is linear for a current bias of 0.75–0.9 A, with a tuning coefficient of -12.1 GHz/A (Fig. 4.3b). A wider range linear relationship between current bias and frequency is desirable to produce a tunable QCL THz source.

Using the current-voltage and current-temperature relationship, the thermal resistance that characterize the QCL's resistance to the heat flow to the cold finger can be calculated as:

$$R_T = \left(\frac{dP}{dT}\right)^{-1} = \left[\frac{dI}{dT}\left(I\frac{dV}{dI} + V\right)\right]^{-1} \quad (4.3)$$

Using $I = 0.85A$, $V = 4.26V$, $dV/dI = 3$, $dI/dT = 0.16$, the calculated thermal resistance of the 2.691 THz QCL is $R_T = 1K.s/J$. From this, we can estimate the thermal time constant that measures how fast the QCL response to the change in temperature:

$$\tau = \frac{\rho C_p V}{1/R_T} \quad (4.4)$$

Parameter	Values
Density (GaAs)	$\rho = 5.307 \text{ g/cm}^3$,
Specific heat capacity (GaAs)	$C_p = 1 \times 10^{-3} \text{ J/g.K}$
Volume (QCL)	$V = 1 \times 10^{-4} \text{ cm}^3$.
Thermal Resistance	$R_T = 1 \text{ K.s/J}$

Table 4.2.: Parameters used to calculate thermal time constant.

The calculated thermal time constant is $\tau = 0.5307 \mu\text{s}$ and the cutoff frequency is $f_c = 1/2\pi\tau = 300 \text{ KHz}$. From this analysis, we can deduce the system loop bandwidth to phase locking the 2.69 THz QCL should be slower than the thermal time constant so that the feedback circuit can compensate the temperature change using the voltage bias.

4.1.1. THz Beam Characterization

The free running ~2.690 THz QCL beam image is taken using a IRV-T0831 THz camera from NEC corporation, at different current biases. The camera is a small sized terahertz imager which incorporates an uncooled terahertz focal plane array of microbolometers. The array contains 320 (horizontal) X 240 (vertical) pixel and each pixels is $23.5 \mu\text{m}^2$.

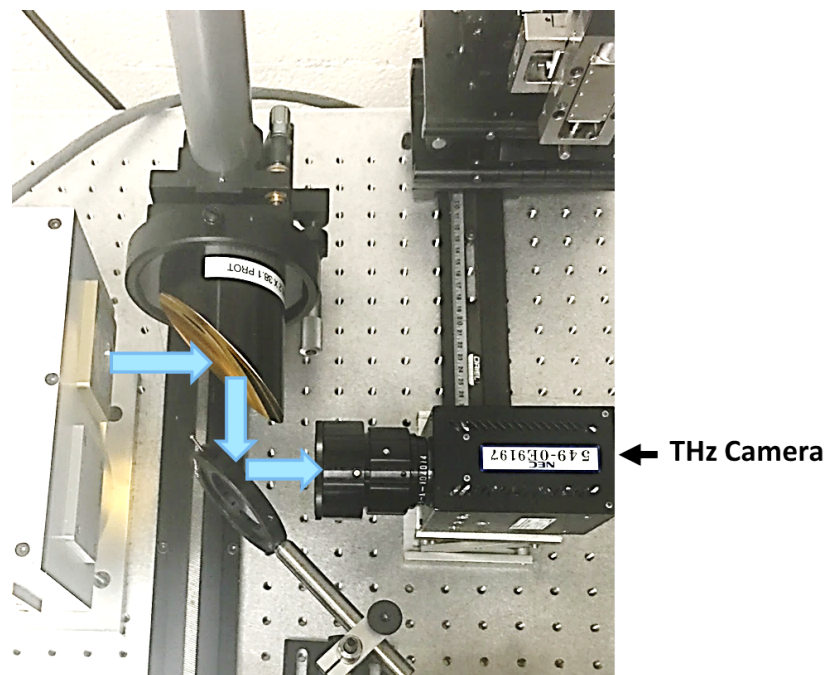


Figure 4.4.: THz focal plane array of the microbolometer-based camera setup with a beam splitter to image the QCL beam.

The 2.690 THz signal from the QCL passes through a polyethylene cryocooler window and reflects off of the first off-axis parabolic mirror and the reflected beam becomes collimated. A 2 mil Mylar beam splitter splits the THz beam and reflects a portion of the THz power to the THz camera and the rest of the THz power goes to the harmonic mixer (Figure 4.4), [43]. The ~2.690 THz beam image is taken for different current biases and the images are presented in Figure 4.5

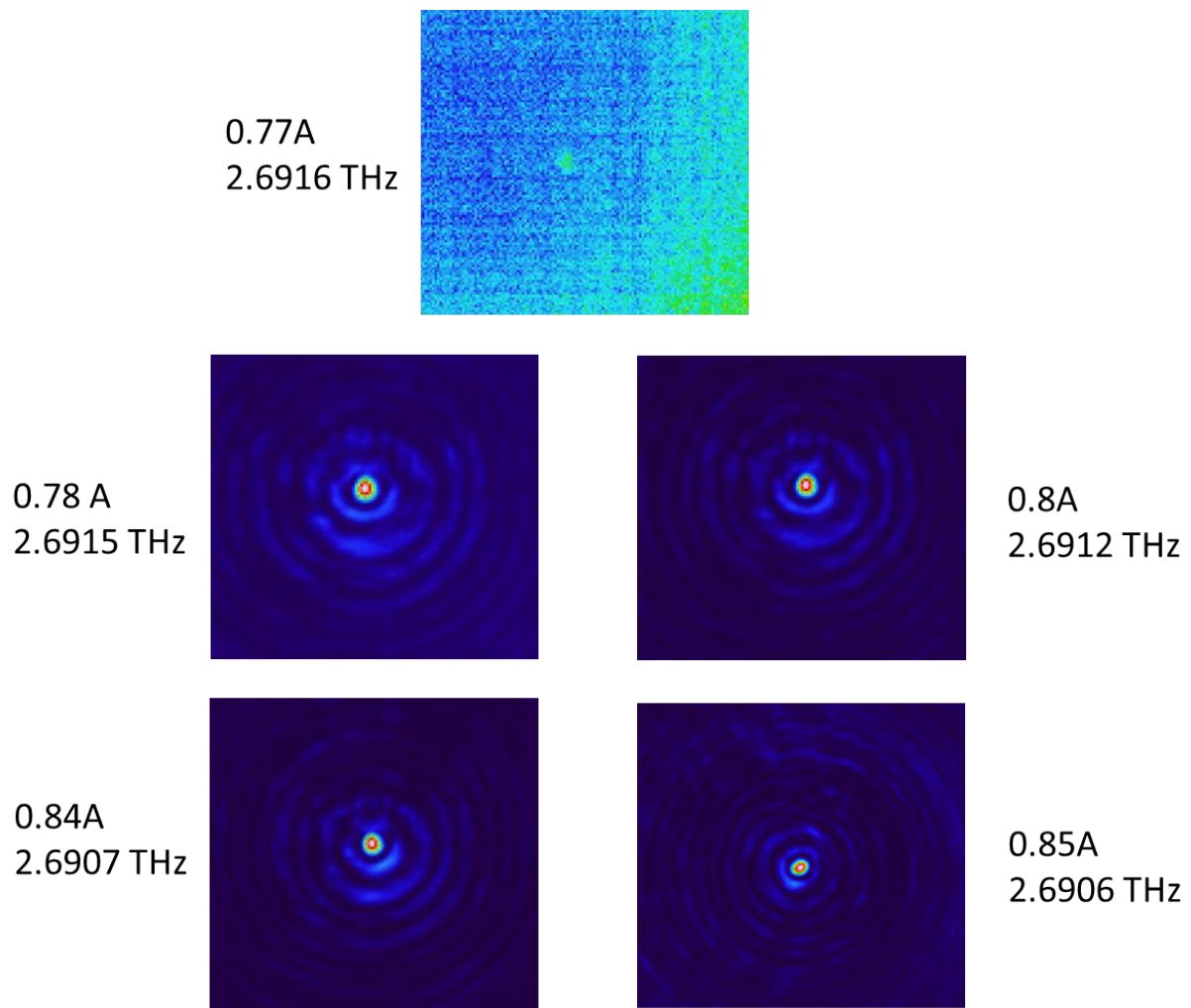


Figure 4.5.: Image of the THz beam at different current biases is taken using IRV-T0831 THz camera.

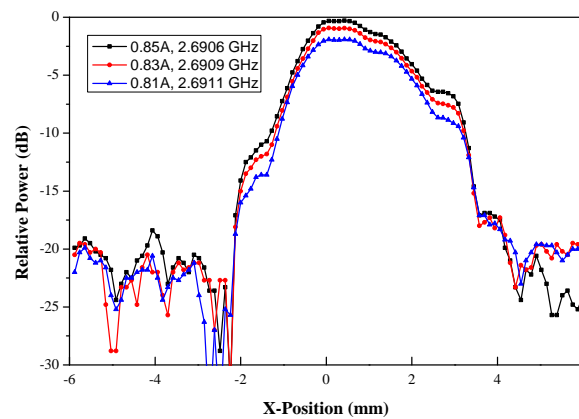
For a 0.77 A current bias, the QCL is not fully turn on and the THz beam is dominated by the background noise. Increasing the current bias to 0.78 A turns on the QCL, which emits a strong main beam with multiple side lobes. Further characterization of the 2.691 THz QCL is implemented using a current bias of 0.85 A, which is approximately 0.08 A above the threshold to maintain the laser output to nearly a single mode beam (lower right). In general most QCLs with Metal-Metal (M-M) waveguide have highly diverging and non symmetrical beams,

however QCL's with Semi-Insulating Surface Plasmon (SI-SP) based waveguide provides better beam patterns. This is due to the SI-SP waveguide is quite leaky, and the near-field mode spreads deep into the device substrate (not just the ~ 12.5 μm active region) and the near-field pattern is fairly circularly symmetric. The far-field pattern is, therefore, also fairly symmetrical [44]. Adding Distributed Feedback (DFB) gratings for a single mode operation also have shown improvement to the beam quality [45].

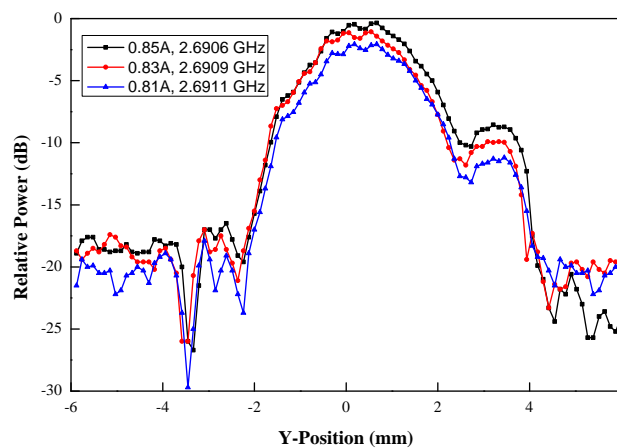
Moreover, the near field beam and the focused THz beams are mapped using a X-Y scanner. To perform the beam mapping, the THz mixer is used as a detector with a lower current bias $30 \mu\text{A}$ to stay within a square-law range, (more discussion on detection and video testing is in chapter 3). The THz radiation is modulated using an optical chopper and the reference signal is fed to a lock-in amplifier. The harmonic mixer video response due to the THz radiation from the QCL is measured using the lock-in amplifier and the output is normalized to the maximum output.

During the beam profiling measurement, the THz mixer is placed at a z -distance of 25 mm from the QCL, and the X-Y stage changes the X and Y position of the THz mixer in 0.015 mm steps for a total distance of 12 mm. Fig. 4.6a and Fig. 4.6b show the measured H-plane and E-plane radiation patterns. The full width at half maximum (FWHM) spatial radius of the THz beam for X-position scanning is approximately 1.3 mm; this corresponds to in-plane angle θ of approximately 3 degrees. For the E-plane beam, 0.6 mm is the radius where the relative power drops by $1/e^2$ is 0.6 mm. Similarly, the FWHM radius for the Y-position scanning is approximately 1.22 mm, and this corresponds to an elevation angle ϕ of 2.8 degrees and the power drops by $1/e^2$ at 0.55 mm. A Gaussian distribution is used to fit the data and extract the beam radii and the center of the peak in the X and Y positions. From the curve fitting, the exponential beam radius at distance $z=25$ mm is approximately 2.13 mm in the E-plane and

2.03 mm in the H-plane. Furthermore, Fig. 4.6a and Fig. 4.6b present beam patterns at different QCL frequencies and the beam shape is similar but the power increases almost by 2 dB at lower frequency 2.6906 THz when the QCL is biased at 0.85 A.



(a) E-plane radiation pattern measurements for a ~ 2.6906 THz QCL relative output power versus X-position for different current biases.



(b) H-plane radiation pattern measurements for a ~ 2.6906 THz QCL relative output power versus Y-position for different current biases.

Figure 4.6.

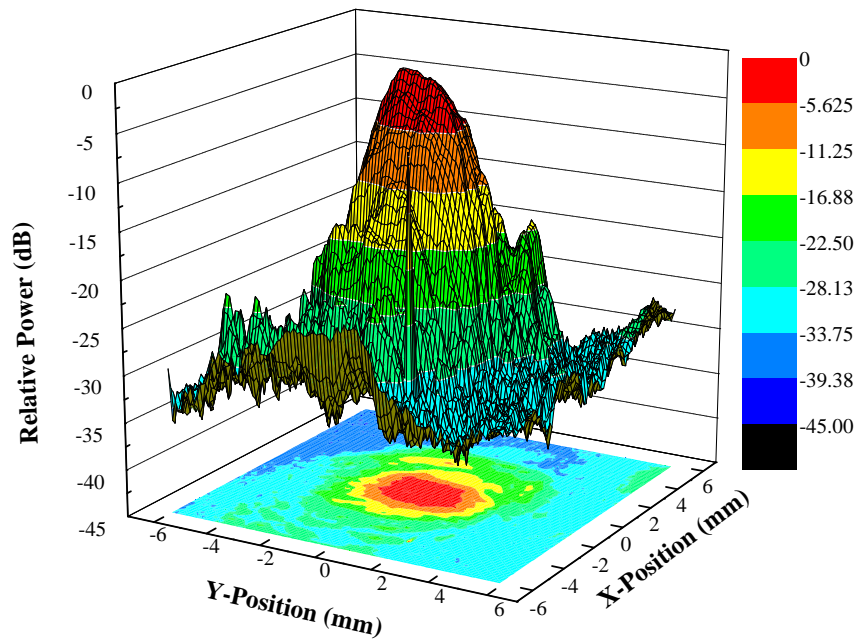


Figure 4.7.: A ~ 2.6906 THz normalized power versus 2D beam pattern at 0.85 A current bias.

In addition, the far field 2-D beam pattern is measured using 100×100 grid from the X-Y scan. The detector is placed approximately 25 mm away from the QCL, Figure 4.7 depicts the 2-D X-Y scan for the 12 mm by 12 mm dimensions and the Z axis shows the relative power. From the projected beam pattern on the X-Y plane, the beam is nearly symmetric with beam radius of approximately 2.1 mm.

From the beam patterns presented in Figure 4.6, the E-plane and H-plane beam pattern radii are similar, therefore it is reasonable to approximate the beam with Gaussian shape and calculate the beam area at the FWHM. Similarly, the aperture area of the diagonal horn at the beam waist is calculated and the ratio is compared to the beam FWHM area. The diagonal horn area at the beam waist is approximately 3% of the incoming beam FWHM when the detector is placed

25 mm distance away from the QCL. For a perfect power coupling to occur, the incoming beam radius and the receiving aperture waist radius need to be equal with no gap between the two. This simple analysis indicates that the THz beam is too wide and focusing mirrors are needed to reduce the beam spot size to improve coupling. Moreover, at a given distance, the power coupling coefficient at 2.691 THz can be estimated using Eqn. (4.6). To apply this equation, the beam waist radius of the THz beam needs to be determined. Therefore, consecutive beam profile measurements are implemented at different locations along the optical axis and the minimum beam waist radii are extracted by least square fit to Eqn (4.5).

$$W(z) = W_0 \sqrt{1 + \left(\frac{\lambda z}{\pi W_0^2}\right)^2} \quad (4.5)$$

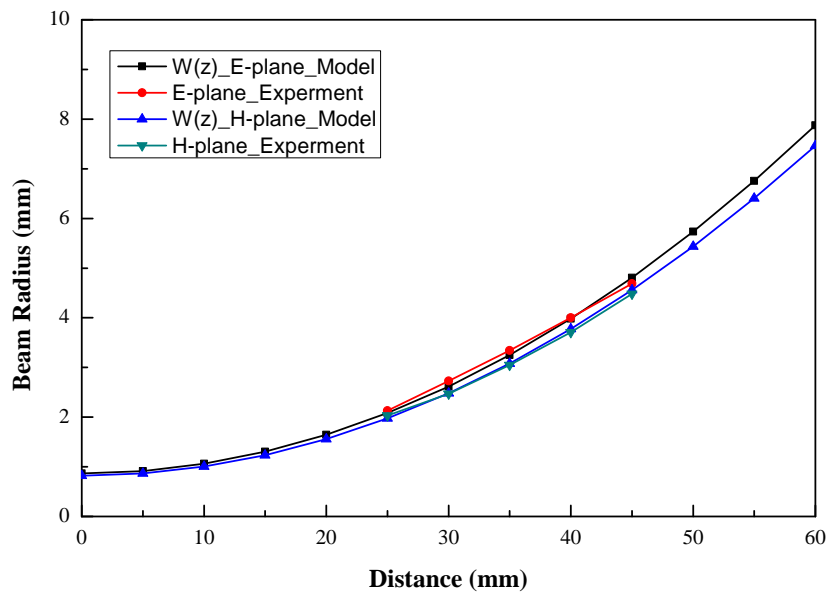


Figure 4.8.: The 2.6906 THz beam radii at different locations in the optical axis.

4.1 Characterizing Quantum Cascade Laser

Figure 4.8 depicts the experimental E-plane and H-plane beam radii at locations between $z = 25 \text{ mm}$ to $z = 45 \text{ mm}$ and their model Gaussian beam radii are presented up to $z = 60 \text{ mm}$. The y-intercept in the figure are the minimum beam radii, therefore, $W_{0a-x}=0.865 \text{ mm}$ would be the beam waist radius of the E-plane beam and $W_{0a-y}=0.82 \text{ mm}$ would be the beam waist radius of the H-plane beam.

The two dimensional power coupling in the E-plane and the H-plane are the magnitude squared of the field coupling coefficients for the two orthogonal coordinates [46]. However, if the E-plane and H-plane beams are assumed to be symmetric, Eqn. (4.6) can be used to calculate the power coupling coefficient of the 2.6906 THz beam at the far field, where the beam waist radius is $W_{0a-x} \simeq W_{0a-y} = W_{0a} = 0.865 \text{ mm}$, the detector minimum waist radius is $W_{0b} = 0.21 \text{ mm}$ at a $\Delta z = 25 \text{ mm}$ distance.

$$K = \frac{4}{(W_{0a}/W_{0b} + W_{0a}/W_{0b})^2 + (\lambda \Delta z / \pi W_{0a} W_{0b})^2} \quad (4.6)$$

$$K = \frac{4}{(W_b/W_a + W_a/W_b)^2 + (\pi W_a W_b / \lambda)^2 (1/R_a - 1/R_b)^2} \quad (4.7)$$

$$R(z) = z + \frac{(\pi W_0^2 / \lambda)^2}{z} \quad (4.8)$$

Alternatively, using Eqn. (4.7), an arbitrary plane of reference between the THz beam and the aperture can be taken to find the THz beam radii and radius of curvature and Eqn. (4.8) can be used to calculate the coupling coefficient. Using both approaches, the power coupling is calculated at a $\Delta z = 25 \text{ mm}$ distance and it is approximately 9 %.

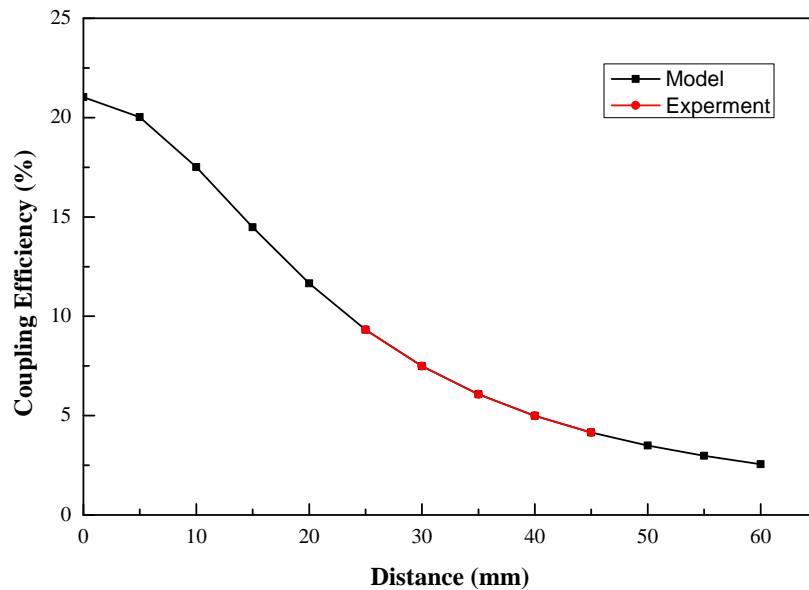


Figure 4.9.: Power coupling efficiency at different distance along the optical axis.

Figure 4.9 depicts the power coupling at different distances in the optical axis. Because of the beam divergence, when the mixer is positioned away from the source, the efficiency decreases as expected. For the experimental test setup, the mixer is positioned $z = 25 \text{ mm}$ to $z = 45 \text{ mm}$ distance away for the QCL and the efficiency drops from 9 % to 5 %.

To further quantify the far field beam quality of the THz beam, important beam parameters, such as divergence angle, beam parameter product and beam quality factor are determined.

In Figure 4.8, the angle between the beam radii and the optical axis is the divergence angle of the beam, the divergence angle is calculated by differentiating the beam radii shown in Eq.4.5 with respect to the axial position in the far field. The divergence angle extracted from the experiment is approximately 8.4 degree. Furthermore, the total angular spread of the beam far from the waist can be calculated by multiplying the divergence angle by factor of 2.

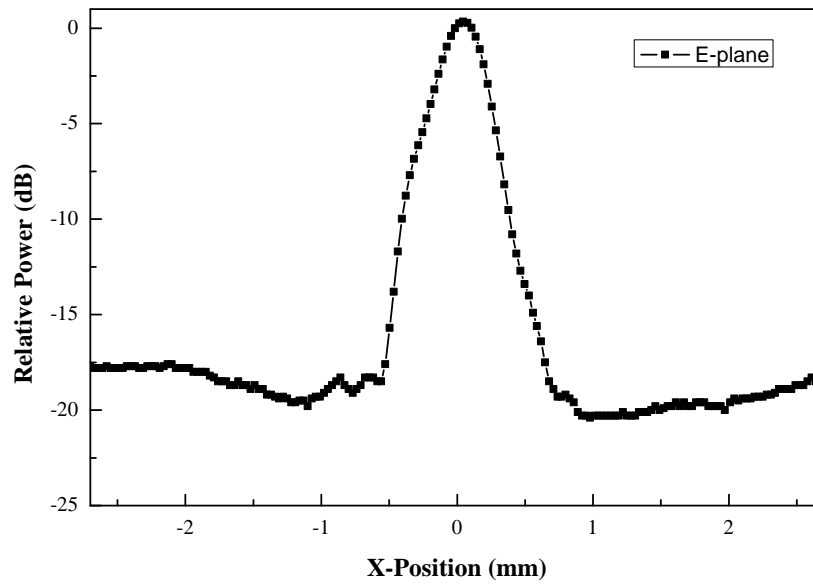
Beam parameter product (BPP) is the product of the beam waist radius and the far field beam divergence half angle. Usually a lower quality beam has higher beam parameter product. From Figure 4.8, the 2.6906 THz beam waist is approximately 0.865 mm and for the divergence angle of 8.4 degree, the BPP is 0.12 rad.mm. Beam quality factor (M^2) or beam propagation factor is also a common measurement of the beam quality and the value is the normalization of the BPP against a Gaussian diffraction limited beam at 2.6906 THz. M^2 describes the deviation of the laser beam from a theoretical Gaussian beam that has M^2 of 1.

$$BPP_0 = \frac{\lambda}{\pi} \quad (4.9)$$

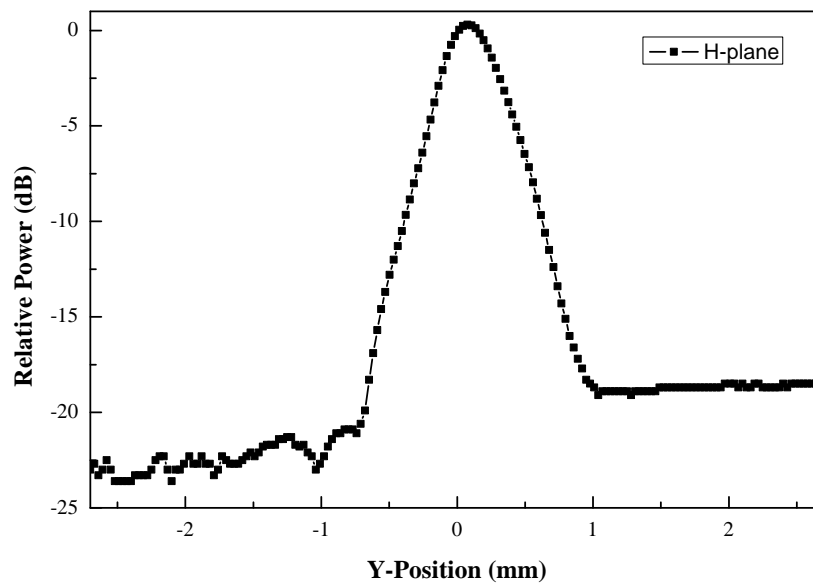
$$M^2 = \theta_{w0} \frac{\pi}{\lambda} = \frac{BPP}{BPP_0} \quad (4.10)$$

Using Eqn. (4.9), the diffraction limited beam parameter product at 2.6906 THz is $BPP_0 = 0.035$, and Eqn. (4.10) yields a beam quality factor of $M^2 = 3.4$.

To use the THz radiation for different applications, such as pumping HEB based receivers, the system needs to include focusing mirrors and a beam splitter to use part of the QCL radiation for phase locking and the rest as an LO source. Furthermore, using focusing mirrors will improve the power coupling efficiency by reducing the beam spot size as shown in Figure 4.9; therefore, 90 degree off axis mirrors are used with effective focal length of 72.6 mm and the focused beam is mapped using the X-Y stage for a current bias of 0.85 A, (see Figure 4.11 for the testing setup).



(a) A ~ 2.6906 THz QCL focused beam normalized output power verses X-Position for 0.85 A current biases.



(b) A ~ 2.6906 THz QCL focused beam normalized output power verses Y-Position for 0.85 A current biases.

Figure 4.10.

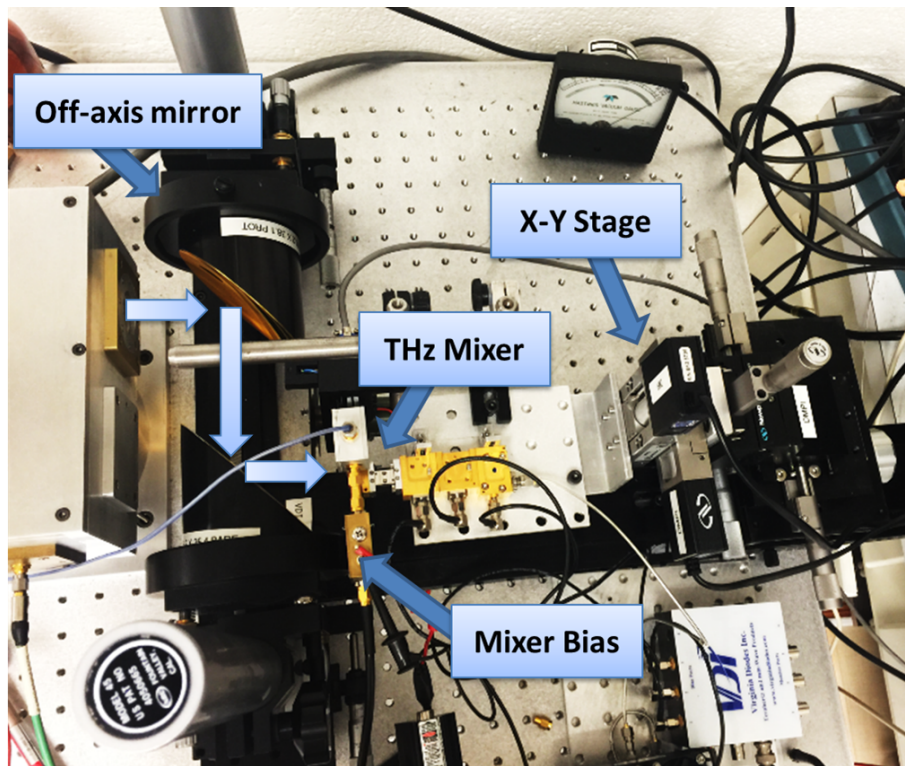
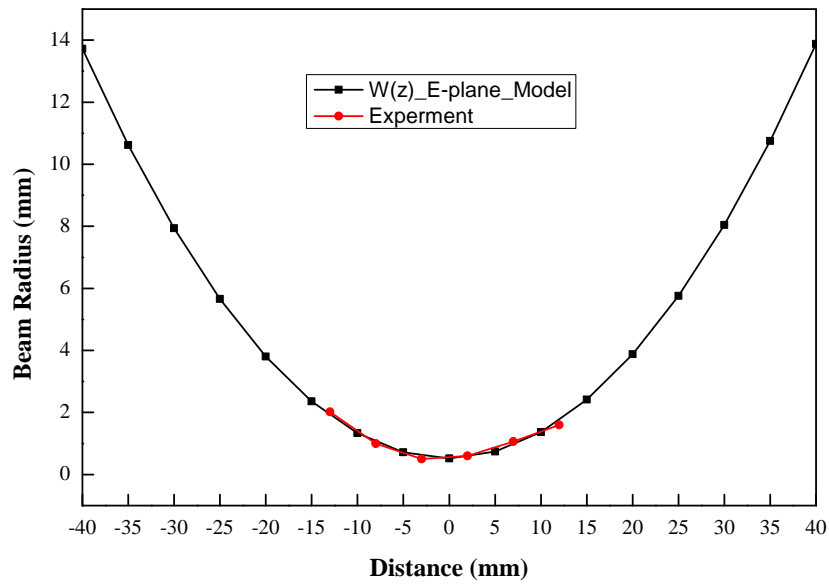
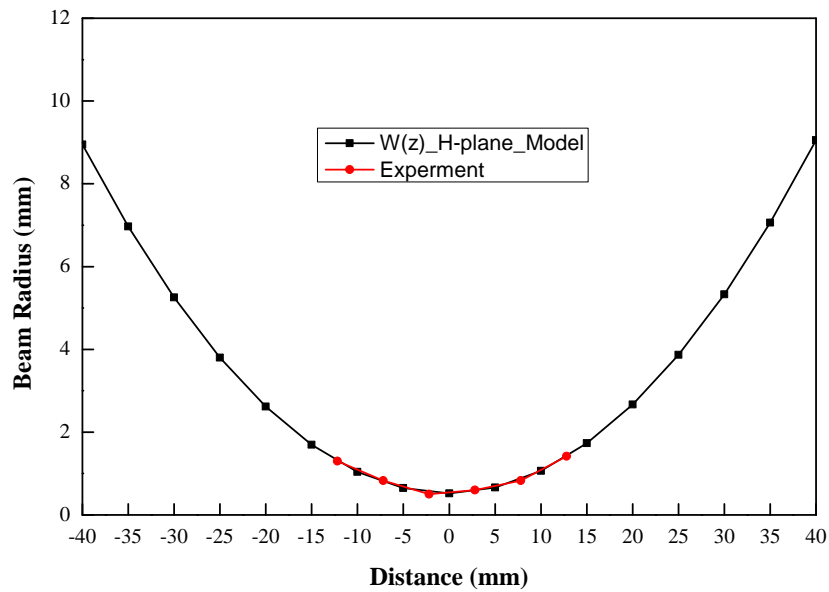


Figure 4.11.: Experimental setup to map the focused beam using X-Y stage.

Fig. 4.10a and Fig. 4.10b demonstrate that using the off-axis mirrors significantly reduced the beam size; the FWHM of the THz beam in the X-Position is approximately 0.52 mm and 0.51 mm in the Y-Position. Using a similar approximation, the diagonal horn area at the beam waist becomes 16 % of the incoming beam FWHM at the focal position of the second off-axis mirror. Moreover, consecutive beam mapping is implemented at different positions in the optical axis and minimum focused beam waist radii are extracted by fitting to Gaussian beam radii Eqn. (4.5).



(a)



(b)

Figure 4.12.: The 2.6906 THz focused beam radii at different locations in the optical axis.

4.1 Characterizing Quantum Cascade Laser

The detector is positioned between -13 mm to 13 mm away from the minimum beam waist location. Figure 4.12 depicts the beam radius increase when the detector is positioned closer to the focusing mirror and also the beam radius increased when the detector is kept farther from the minimum beam waist. From this experiment, the minimum focused beam radius is determined and it is approximately 0.55 mm for the E-plane beam pattern and 0.52 mm for the H-plane beam pattern.

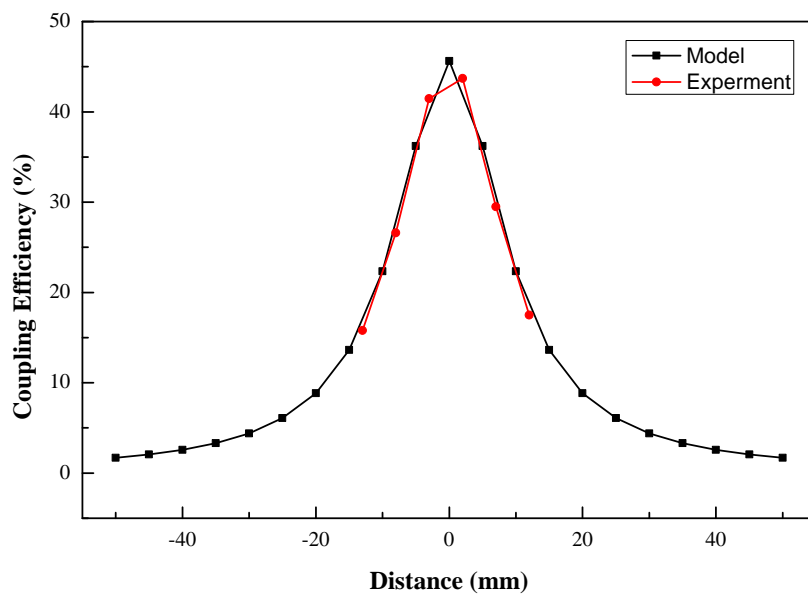


Figure 4.13.: A ~2.6906 THz QCL focused beam coupling efficiency at different position.

Using this result, the coupling coefficient is calculated using Eq.4.6 for the nearly symmetric focused beam radius of $W_{0a-x} \simeq W_{0a-y} = W_{0a} = 0.55 \text{ mm}$ and the mixer minimum radius of $W_{0b} = 0.21 \text{ mm}$ at different distances in the optical axis. The maximum coupling efficiency of the focused beam improved to 43 % and the coupling efficiency decreased to 14 % when the mixer

is positioned 13 mm away from the minimum beam radius location. Since the THz harmonic mixer requires less than $10 \mu\text{W}$ power to produce a down-converted beat signal with sufficient power to phase lock, a significant amount of the available THz power can be split for other uses. Despite the advantage of using off-axis mirrors discussed above, aligning the off-axis mirror is difficult and needs careful attention.

4.1.2. QCL Output Power Measurement

The output power of the QCL is measured using an Erickson calorimeter from VDI [38]. The power meter has a WM-2540 (WR10) waveguide input to direct the power to the power meter sensor, therefore a WM-2540 (WR10) conical horn is used to couple the THz radiation from the QCL. The power meter is placed 5 mm away from the 2.6906 THz QCL and the position is aligned with the QCL to achieve optimal power coupling. Figure 4.14. illustrates the output power measured at different frequencies. Higher frequency corresponds to the lower current bias that produces lower output power. When the current bias increases above 0.82 A, more than -5 dBm power is measured. According to a VDI power measurement calibration document found in VDI's website, power correction needs to be implemented for higher frequencies due to the loss of straight waveguide used at the input of the power meter [47]. Approximately a 2 dB final power correction is added and the power correction factor and corrected power is presented in Table 4.3 and Figure 4.14 respectively.

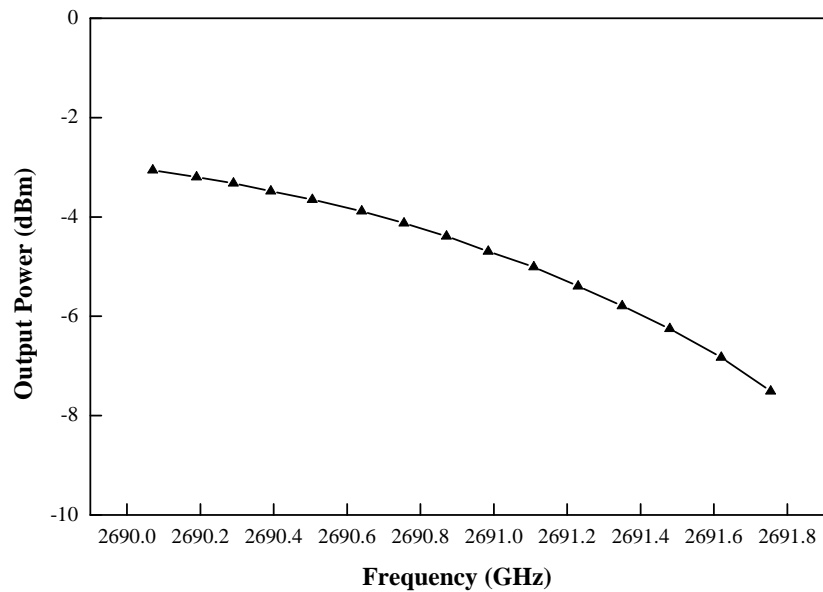


Figure 4.14.: Output power of the 2.6906 THz QCL measured using Erickson power meter (2dB correction is added), measurement uncertainty is shown in Table 4.4, adding the uncertainty would change the output power by approximately 0.9-3.5 dB.

Frequency (GHz)	Atmospheric Attenuation (dB/m)	Conductor Loss (dB)
2690-2691.8	1 dB	1 dB

Table 4.3.: Power correction factors for near field.

Parameter	Additional Loss
Waveguide overmoding and Gaussian coupling efficiency	1-2 dB
Loss due to tilt angle	0-0.3 dB
Atmospheric loss: relative humidity (45-55 %)	1 dB/m
Power measurement accuracy	0.2-1 dB

Table 4.4.: Estimated measurement uncertainty.

Additional measurement of the usable THz power for experiment is implemented by using off-axis mirrors and a 3 dB beam splitter [43]. The beam splitter is positioned approximately 45 degree from the first off-axis mirror and it reflects the power off of the splitter and the beam hits the second off-axis mirror to focus to the power meter. The rest of the THz power goes to the harmonic mixer and will be used to phase lock the QCL. Since the WM-2540 (WR10) conical horn has an aperture input diameter of 16.3 mm, which is bigger than the beam spot size of the focused THz beam, most of the THz beam is within the aperture area. However, proper alignment of the off-axis mirrors and the beam splitter is critical to achieve optimal coupling.

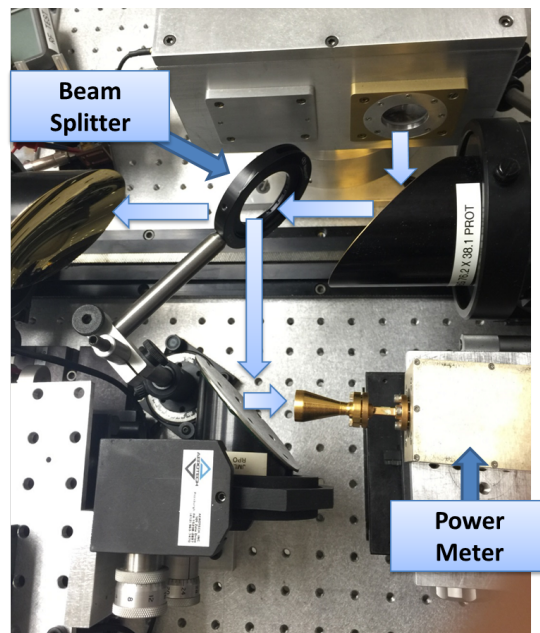


Figure 4.15.: Usable THz power measurement setup using an Erickson power meter.

4.1 Characterizing Quantum Cascade Laser

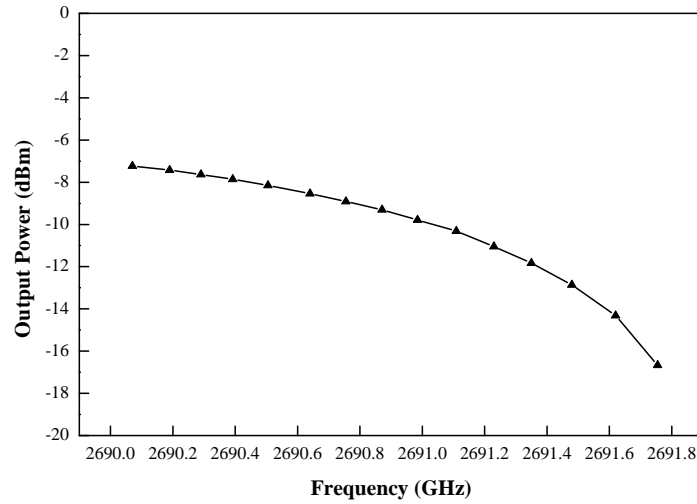


Figure 4.16.: Usable THz power measured using an Erickson power meter, measurement uncertainty is shown in Table 4.4.

Frequency (GHz)	Measured Power (dBm)	Atmospheric Attenuation (dB/m)	Conductor Loss (dB)	Corrected power (dBm)
2691.755	-23.45	10.92	1	-16.66
2691.62	-21.18	11.16	1	-14.32
2691.48	-19.79	11.41	1	-12.86
2691.35	-18.85	11.67	1	-11.83
2691.23	-18.14	11.94	1	-11.04
2691.109	-17.49	12.22	1	-10.31
2690.985	-17.05	12.51	1	-9.78
2690.871	-16.66	12.82	1	-9.3
2690.755	-16.37	13.14	1	-8.91
2690.64	-16.1	13.47	1	-8.53
2690.505	-15.82	13.82	1	-8.15
2690.392	-15.64	14.19	1	-7.86
2690.29	-15.52	14.57	1	-7.62
2690.19	-15.44	14.97	1	-7.43
2690.07	-15.36	15.39	1	-7.23

Table 4.5.: Measured available THz power and correction factors used, measurement uncertainty is shown in Table 4.4, adding the uncertainty would change the RF available THz power by approximately 0.9-3.5 dB.

Figure 4.15 shows the setup used to measure the available THz output power for other uses. The output power measurement is performed about 300 mm away from the QCL using two off-axis mirrors. Due to high absorption from water lines, $\sim 12\text{dB/m}$ for the 2.690-2.692 THz frequency range and other conductor losses in the waveguide used, power correction is implemented and the output power is less than 4.2 dB from the initial close-in measurement. The power loss is due the splitter $\sim 3\text{ dB}$ and power lost due to misalignment of the off-axis mirrors and the beam might be tilted with respect to the horn on the power meter which is not accounted during the power correction.

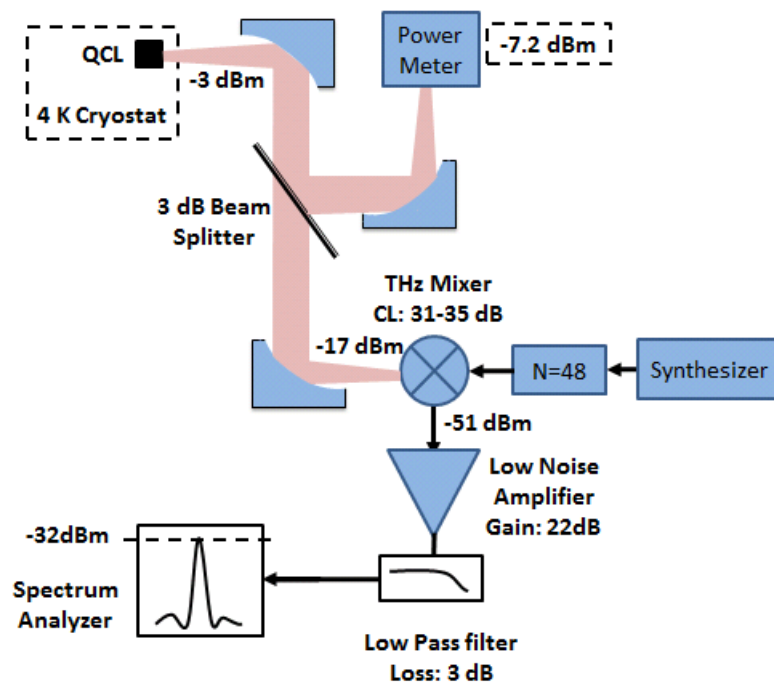


Figure 4.17.: System test setup and output power in each stage.

When the the harmonic mixer is positioned approximately $\Delta z = 15\text{ mm}$ away from the focal point for the second parabolic off-axis mirror, the coupling efficiency becomes 14% and the coupled power is approximately -17 dBm at 2.69064 THz. Due to the 30-35 dB conversion

loss of the 4th harmonic mixer, the output power from the mixer is approximately -51 dBm. Furthermore, because of the power gain from the amplifier and the losses from the low pass filter and splitter, the spectrum analyzer display an output power of -32 dBm. Since the 3 dB power splitter is used at the end of the IF chain, an equal amount of power that is shown on the spectrum analyzer will be split and supplied to the phase detector to perform phase locking of the QCL, Figure 4.21.

4.1.3. Real-Time Spectrum

Before phase locking the QCL and analyzing the phase locked down converted IF signal, we used gap free real time spectrum analyzer to study the down converted IF signal when the QCL is free running. The N9030A real time spectrum analyzer uses Application Specific Integrated Circuit (ASIC's) and Field Programmable Gate Array (FPGA) to convert the down converted IF into signal spectral at high rate, approximately 300, 000 spectra per second for 85 MHz gap free bandwidth [48]. The real time spectrum analyzer also allows to measure the density map (Spectrogram), which is the summary of an accumulation over an acquisition time interval up to 600 traces being displayed at any one time. Therefore, the density display uses a color code to show the number of times a frequency and amplitude point is hit during a capture, which is the time a signal spends at each frequency and amplitude point in a given time.

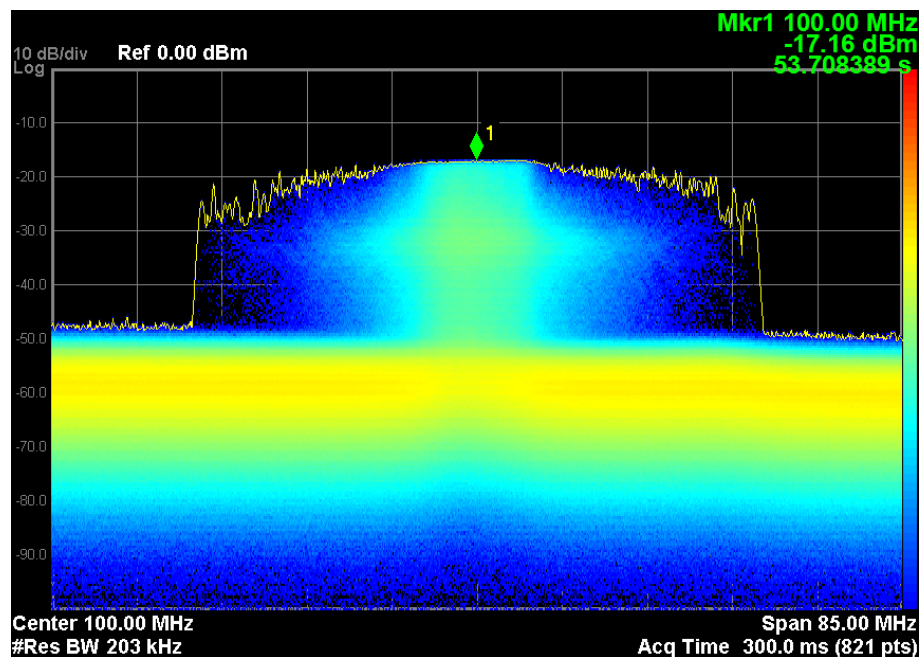


Figure 4.18.: Real time spectrum view of a 2.6906 THz QCL down converted signal is shown for a 85 MHz span and 300 ms acquisition time.

In the above Figure 4.18, the X axis represents the gap free frequency span, the Y axis represents amplitude and the color code indicated on the right represents the number of hits in a single capture. The down converted signal jitters predominantly around 100 MHz within a span of 20 MHz for the 300 ms acquisition time; moreover, the down-converted signal change its frequency within approximately 50 MHz span. The free running 2.6906 THz QCL frequency instability produces a spectral resolution of $\frac{f}{\Delta f}$, approximately 50×10^3 , with which is difficult to do astronomical studies. Therefore, phase locking of the QCL using room temperature technique stabilizes the QCL output frequency and it is advantageous to build high resolution spectroscopy with a spectral resolution of greater than 10^{10} .

4.2. Phase Locking of 2.518 THz and 2.6905 THz QCL

Two types of WM-86 (WR0.34) harmonic mixers that are tuned for different frequency bands are used as part of an ambient temperature receiver to enable phase locking of the 2.5182 THz and 2.6906 THz QCLs. The THz harmonic mixer is used to down convert the QCL radiation down to a lower frequency to compare its phase with a stable 100 MHz reference. For the 2.518 THz QCL down conversion, a 13.115 GHz phase locked referenced to the same 100 MHz signal microwave synthesizer is used as an LO source to drive a Virginia Diodes, Inc. (VDI) Amplifier Multiplier Chain (AMC) with a multiplication factor of $N=48$. The AMC produced a 629.46 GHz signal with an output power of 1.5 mW. When the LO source pumps the 1.8-2.5 THz harmonic mixer, it generates the 4th harmonic at 2.5181 THz and mixes with the 2.5182 THz QCL radiation resulting in a 100 MHz beat note, (see Figure 4.19, Figure 4.20).

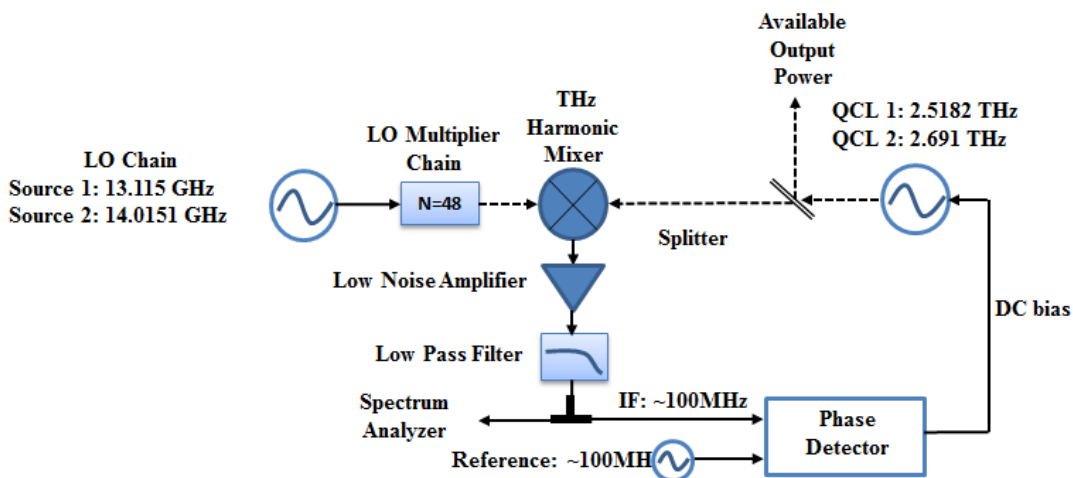


Figure 4.19.: Schematic of the setup for phase locking a QCL.

Similarly, for the 2.6906 THz QCL down conversion, a 14.0151 GHz phase locked microwave synthesizer is used to drive the LO chain with a multiplication factor of $N=48$. The LO system

produces a 672.62 GHz signal with an output power of 1.2 mW. When the LO pumps the 2.3-3.2 THz harmonic mixer, it produces the 4th harmonic at 2.6906 THz and mixes with the 2.6906 THz QCL radiation and produces a 100 MHz IF signal, which is used to phase lock the QCL.

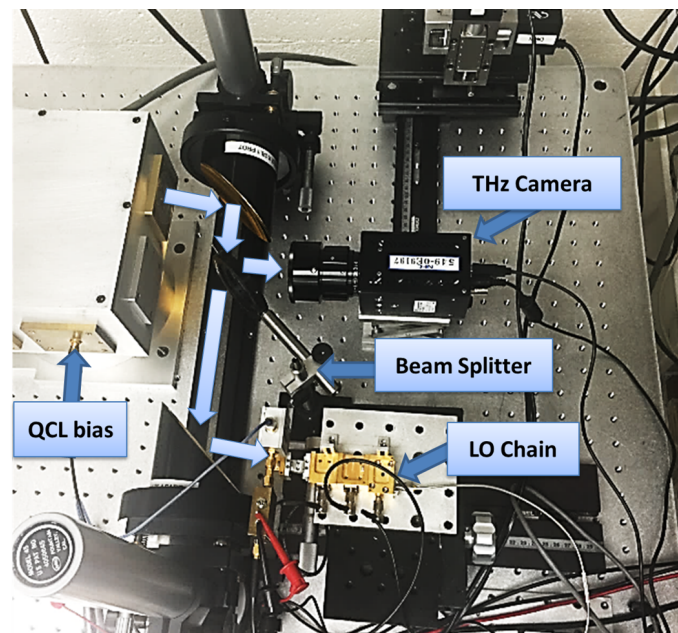


Figure 4.20.: Experimental setup to down convert the QCL; beam splitter and THz camera is used to monitor the QCL output.

Before implementing phase locking, sufficient amount of IF power should be set; therefore, the beat signal from the THz harmonic mixer is fed into a low noise amplifier with a gain of 22 dB and a noise figure of 1.4 dB with a final output power of -29 dBm. The amplified IF signal goes through a low-pass filter with a cutoff frequency of 190 MHz, which is used to remove unwanted inter-modulation products and to set the noise bandwidth that goes to the phase detector. Using a 3 dB splitter, the IF signal is split and the down converted signal is monitored on a spectrum analyzer and the rest of the down converted IF signal is fed into XL Microwave 800A-801 phase locking module. The phase locking module has a maximum output

4.2 Phase Locking of 2.518 THz and 2.6905 THz QCL

voltage of 10.5 V and a maximum current of 0.5 A. Since the QCL requires a maximum current bias of more than 0.8 A, a home made current amplifier is developed using Bipolar Junction Transistor (BJT) from ON Semiconductor. The 2N6042G PNP transistor is setup on a common collector mode and voltage output from the lock-in module is used as base voltage. The load resistor (QCL) is connected to the emitter terminal and the current through the emitter which bias the QCL is achieved by applying voltage (V_{cc}) at the collector node.

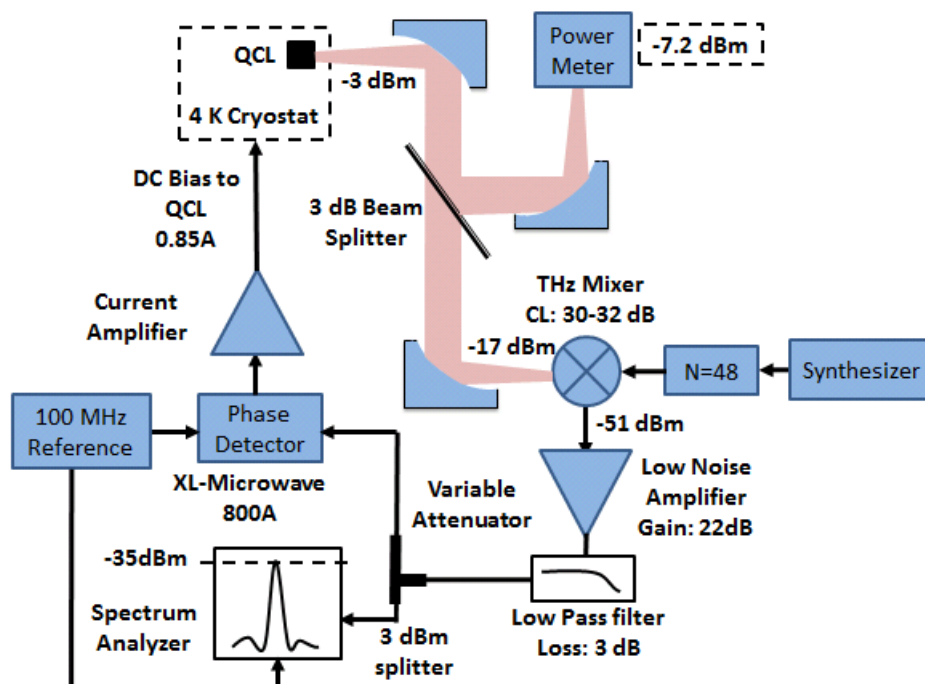
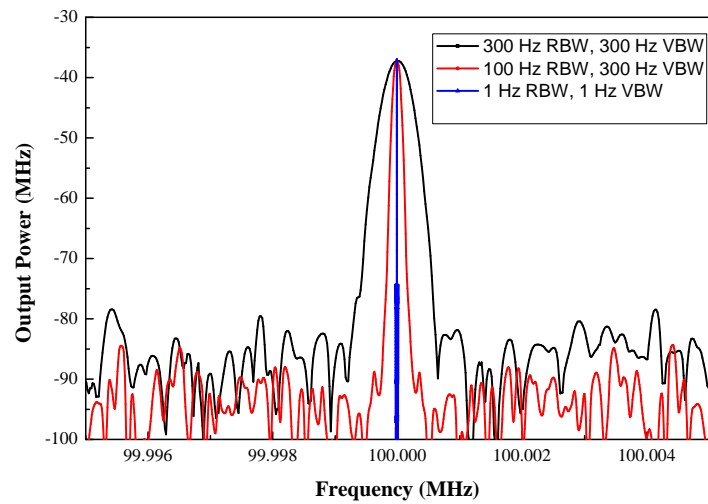


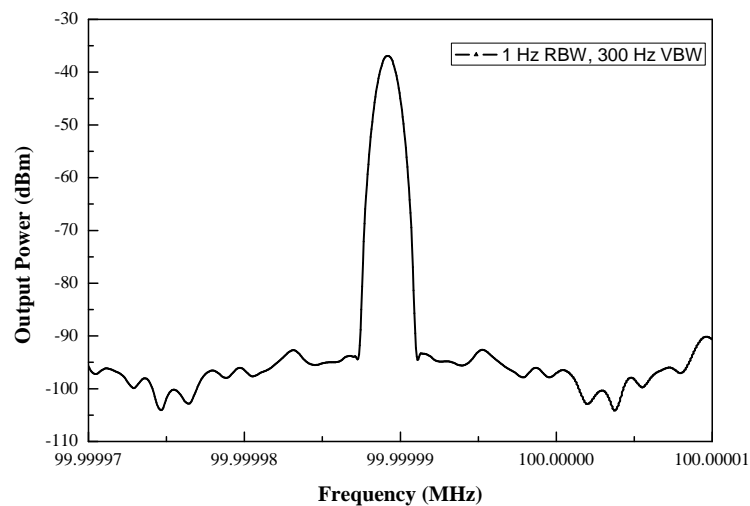
Figure 4.21.: QCL phase locking loop test setup.

In general, before the phase locking loop starts tracking the phase of the input signal, initial phase locking conditions need to be fulfilled. Since the down-converted IF frequency is different from the reference signal, the bias voltage and current must be set in the vicinity of the desired THz frequency. Once the operating bias is set, the sweeper circuit injects a current into the integrator amplifier to sweep the operating voltage of maximum 0.4 V above and below the

nominal bias voltage that was initially set.

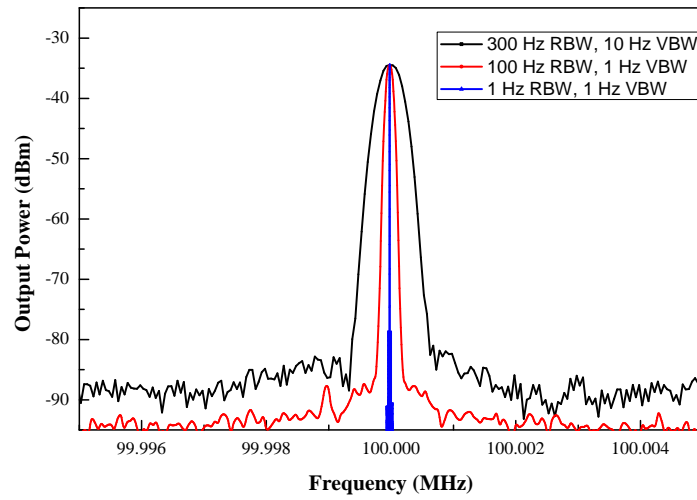


(a) Power spectra of the beat signal of the phase locked 2.51825 THz QCL recorded by spectrum analyzer with RBW of 1 Hz, 100 Hz and 300 Hz and VBW of 1 Hz and 10 Hz.

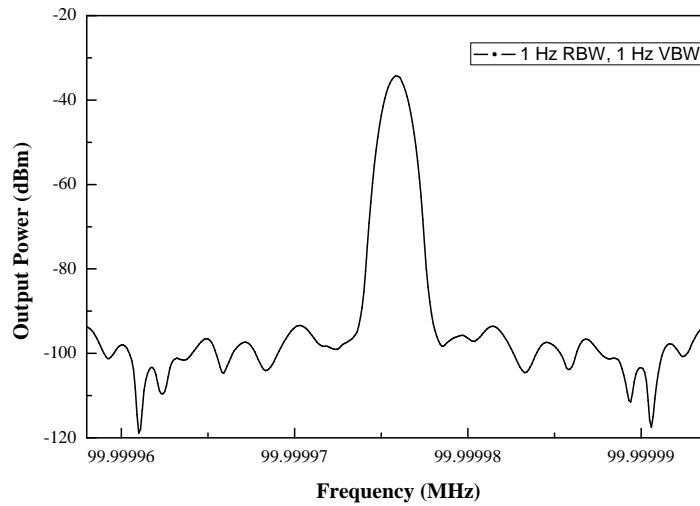


(b) Power spectra of the beat signal of the phase locked 2.5182 THz QCL recorded by spectrum analyzer with 1 Hz RBW and VBW of 1 Hz.

Figure 4.22.



(a) Power spectra of the beat signal of the phase locked 2.6906 THz QCL recorded by spectrum analyzer with RBW of 1 Hz, 100 Hz and 300 Hz and VBW of 1 Hz.



(b) Power spectra of the beat signal of the phase locked 2.6906 THz QCL recorded by spectrum analyzer with 1 Hz RBW and VBW of 1 Hz.

Figure 4.23.

When the down converted IF frequency becomes equal to the reference frequency, locking will occur. This generates a DC voltage that is proportional to the phase difference between the two signals. The DC voltage is applied to the loop filter with less than 1 MHz bandwidth. The loop bandwidth characteristics determine the range in which the phase-locked loop tracks the signal, sets the locking range and suppresses the noise and unwanted output from the phase detector. The DC produced output is amplified and fed back into the QCL to complete the phase locked loop (Fig. 4.22a, Fig. 4.22b, Fig. 4.23a and Fig. 4.23b). Phase locking of a free running QCL compensated approximately a 50 MHz instability due to bias, temperature fluctuation and cryocooler vibrations to sub-hertz accuracy.

4.3. Phase Locking System

The phase lock loop is a nonlinear feedback system that tracks the phase of the input signal. It contains a phase detector, loop filter and the QCL that is used as a voltage controlled oscillator. The phase detector produces an error signal that is proportional to the phase error between the down-converted signal and the reference signal.

$$K_D = \frac{V_e}{\phi_{ref} - \phi_{IF}} \quad (4.11)$$

Phase detector's gain K_D is determined by setting the reference signal and the IF signal same frequency and changing the phase difference between the two signals. Since it is difficult to isolate the phase detector's response from the integrated XL-Microwave phase locking module circuits, the total response of the phase detector and the steady state loop filter response is

4.3 Phase Locking System

measured and the combined gain is $K = -18.3 \text{ mV/deg}$ [49].

Similarly, the oscillator tuning factor is determined in Section 4.1 and found $K_{QCL} = -4.0146 \text{ GHz/V}$.

The change in QCL output frequency in deg/sec due to a 1-deg change is $K_V = KK_{QCL} = 461 \times 10^6 \text{ deg/s}$.

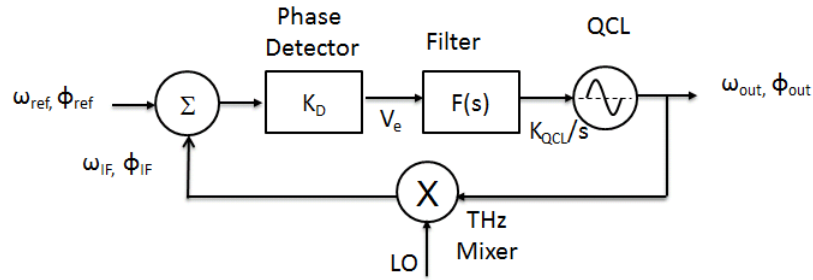


Figure 4.24.: Phase locking loop diagram

From Figure 4.24, the open loop transfer function can be written as:

$$T(s) = \frac{KK_{QCL}F(s)}{s} = \frac{K_V F(s)}{s} \quad (4.12)$$

Figure 4.25 shows the phase locking circuit of the XL-Microwave module with third-order type 2 phase lock loop; it contains an integrator design with additional pole at the output to obtain a steeper rolloff frequency response.

The open loop transfer function $G(s)$ is calculated as below [49]:

$$G(s) = \frac{K_V}{s} \frac{s\tau_2 + 1}{s\tau_1(s\tau_3 + 1)} = \frac{K_T}{s} \left(1 + \frac{1}{s\tau_2}\right) \frac{1}{1 + s\tau_2/b} \quad (4.13)$$

where $\tau_1 = R_1C_1$, $\tau_2 = R_2C_1$, $\tau_3 = R_3C_2$, $K_T = K_V \tau_2/\tau_1$, $b = \tau_2/\tau_3$.

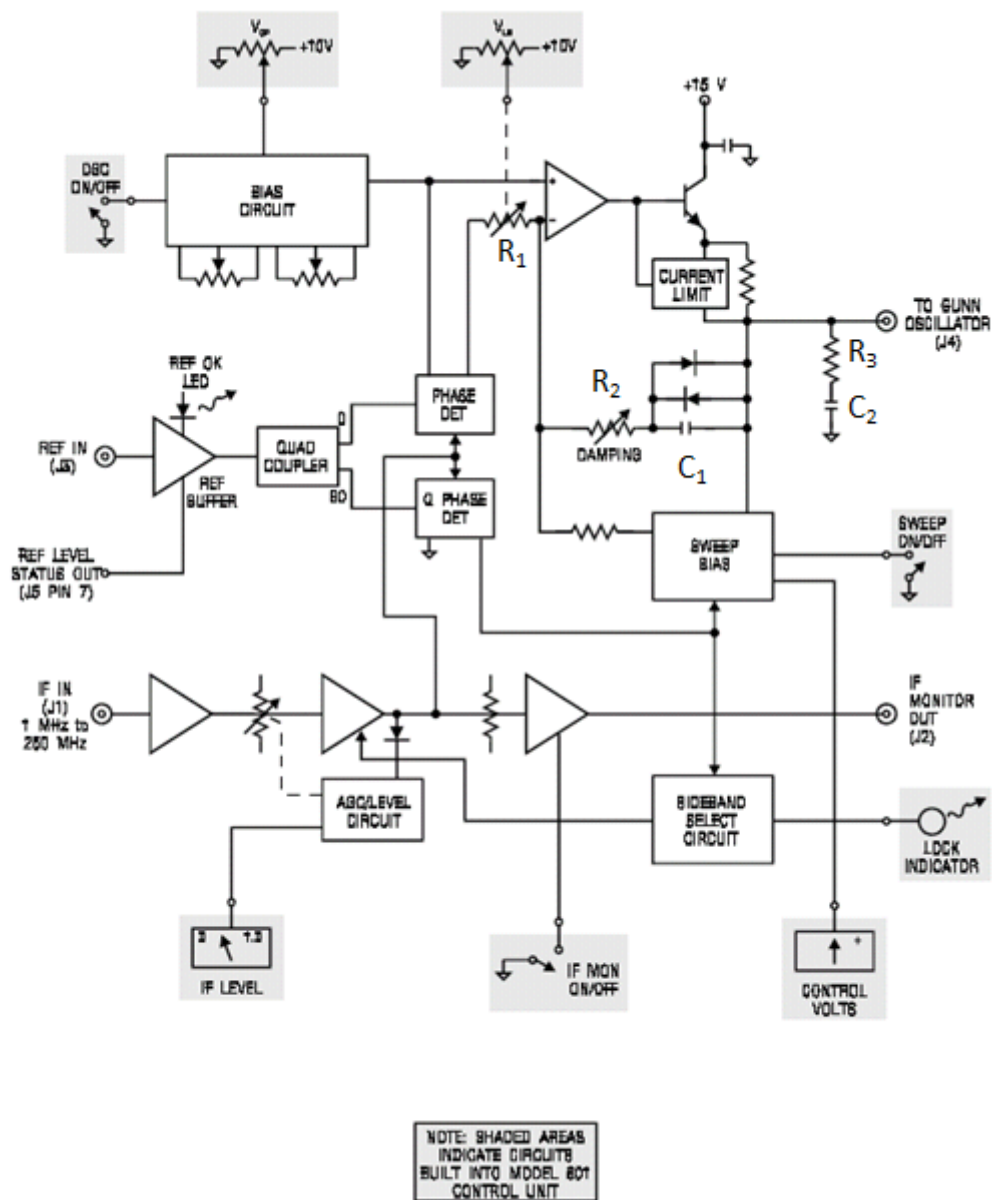


Figure 4.25.: XL-Microwave phase locking module circuit

From this, the normalized transfer function can be expressed as:

$$H(p) = \frac{K'(p+1)}{p^3/b + p^2 + K'p + K'} \quad (4.14)$$

where $K' = K_T \tau_3$ and $p = s\tau_2$.

For large values of K' , an approximate transfer function for high frequencies $H_H(p)$ (for small $|p|$) and for low frequencies $H_L(p)$ (for large $|p|$) become [49].

$$H_H(p) = \frac{K'(p+1)}{p^2 + K'p + K'} \quad (4.15)$$

$$H_L(p) = \frac{K'}{p^2 + K'p + K'} \quad (4.16)$$

From Eqn. (4.16 and 4.15), we can determine the natural frequency and damping of the system.

$$\omega_L \tau_2 = \sqrt{K'}, \quad \xi_L = \frac{1}{2}\sqrt{K'} \quad (4.17)$$

$$\omega_H \tau_2 = \sqrt{bK'}, \quad \xi_H = \frac{1}{2}\sqrt{\frac{b}{K'}} \quad (4.18)$$

The XL-Microwave-800A phase locking module has tunable resistors of $R_1 \Rightarrow 1 - 100\Omega$, $R_2 \Rightarrow 20\Omega - 10\text{K}\Omega$, $R_3 = 1\text{K}\Omega$, $C_1 = 47\mu\text{f}$, $C_2 = 1\text{nf}$ and a given output gain of 10^5 . For a faster loop speed with a natural frequency of greater than 1 KHz, Eqn.(4.18) provides a range of natural frequency of $\omega = 2 - 1200\text{KHz}$ and damping of $\xi = 0.1 - 5$. Furthermore, the 3 dB loop bandwidth is determined using the natural frequency and the damping based on the overshoot and settling time requirements.

The noise from the oscillator can be analyzed by looking at the ratio of the output of the oscillator and the down converted signal.

$$\frac{\phi_{out}}{\phi_{QCL}} = \frac{s^2/K_v}{\frac{s^2}{K_v\omega_1} + \frac{s}{\omega_2} + 1} \quad (4.19)$$

Eqn. (4.19) shows a closed loop high pass filter characteristics, therefore, phase noise from the QCL is filter out within the loop bandwidth. However, outside the loop bandwidth, the phase noise is unattenuated.

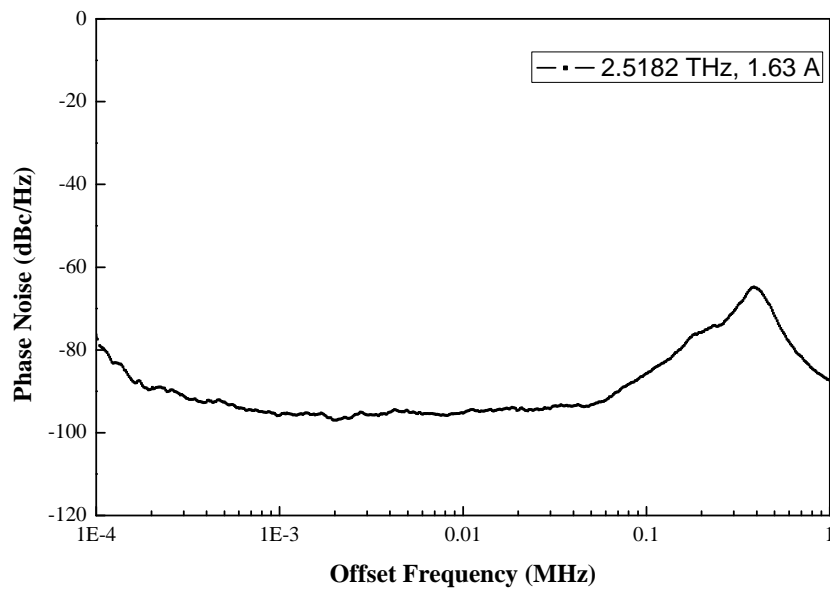
4.3.1. Frequency Tuning of the THz QCL

The phase locked 2.6906 THz QCL output frequency is tuned approximately for 1 GHz in the linear range of 2.6903-2.6913 THz and current bias of 0.8-0.88 A. The frequency tuning experiment is demonstrated by adjusting the LO driver synthesizer frequency 14.15947368 GHz with a step size of 100 Hz. The LO multiplier chain has a frequency factor of N=192, therefore, the frequency step changes of the LO driving synthesizer changes the LO final frequency by 19.2 KHz. Since the difference between the QCL output frequency and the 4th harmonic of the LO driver is within the loop bandwidth, the phase lock loop will pull the voltage controlled oscillator (QCL) to maintain phase locking. The rate of the LO frequency changing to tune the QCL within the linear range can be fast and the QCL will stay phase locked. A step change greater than 19.2 KHz could throw the signal outside the locking range. However, as soon as the phase locking stops tracking the THz signal, the sweeper in the locking module will turn on to regain phase locking, and it will achieve phase locking. Therefore, reasonably larger frequency steps to tune the QCL frequency can only cause delay in the frequency tuning process. The tunable THz source can be used for many applications in astronomy and other fields to produce a tunable spectroscopy with high spectral resolution and compact local oscillators to pump HEB based receivers.

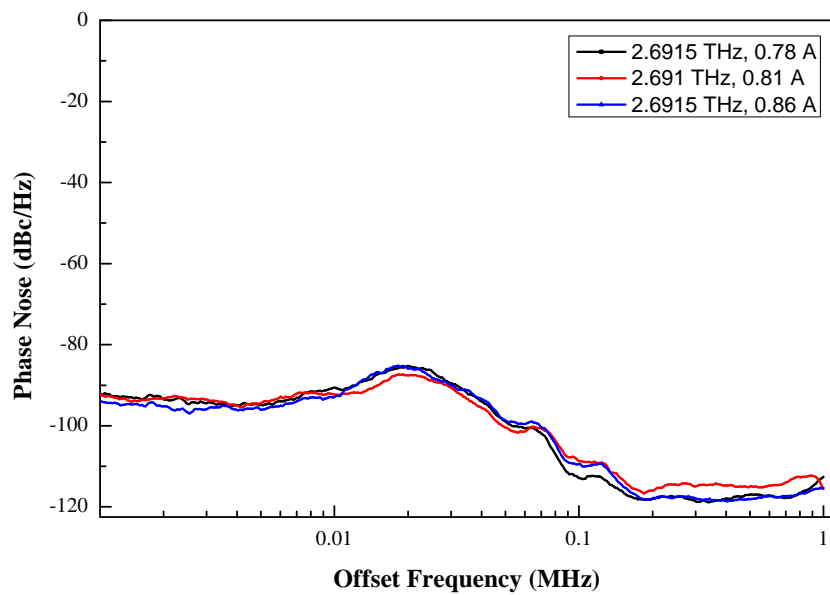
4.4. Phase Noise and Long Term Frequency Drift

To further demonstrate the phase locking of the free running QCL, the single sideband phase noise of the down converted beat signal is measured by coupling the beat signal while it is phase locked. Due to the jitter and frequency instability of the down converted signal of the free running QCL, performing a phase noise measurement without phase locking is challenging. Precise phase noise measurement is only implemented for a phase locked beat note. The phase noise of the phase locked 2.5182 THz and 2.691 THz QCL beat signal is approximately 95 dBc/Hz at 1 KHz offset. The phase noise results shown in Fig. 4.26a and Fig. 4.26b are similar to a typical stable phase locked VDI's Synthesizer. Fig. 4.26b illustrates that the phase noise of the down converted beat signal due to different THz frequency of the QCL is also similar.

In addition to the noise performance, the single sideband phase noise data provides the loop bandwidth information of the phase locked loop. As shown in Figure 4.26b, due to the loop bandwidth high pass filter characteristics, the down converted close-in phase noise is reduced below -80 dBc/Hz for the offset frequency below 0.36 MHz, (see Section 4.3). For above 0.36 MHz offset frequency, the broadband phase noise of the QCL dominates and the phase noise drops significantly. Similarly, the down converted single sideband phase noise due to the 2.691 THz QCL indicates that the loop bandwidth of the phase locking system is approximately 20 KHz. Since the thermal time constant of the 2.691 THz QCL is greater than the loop bandwidth by more than a factor of 10, increasing the loop bandwidth further would affect the close-in phase noise performance.



(a) Single side phase noise of the down converted 100 MHz IF signal of a 2.5182 THz QCL.



(b) Single side phase noise of the down converted 100 MHz IF signal of a ~2.6905 THz QCL.

Figure 4.26.

The down converted IF signal phase noise of the correlated signals (when the LO and the RF signals are phase locked to the same reference) contains the phase noise and stability information of the reference signal. In order to measure the actual phase noise of the QCL, a second mixer driven by an independent synthesizer that is not phase locked to the same reference oscillator is required. The down converted signal phase noise of the second mixer contains phase noise of the LO and RF signals. The phase noise of the LO at ~13 GHz can be measured using spectrum analyzer and its phase noise of the LO at THz should be $20 \cdot \log(N)$, and a second mixer can be used to down convert the signal and look at the IF phase noise and the phase noise of the QCL can be extracted. To apply this technique and determine the true phase noise of the QCL, the QCL phase noise should be worse than the LO phase noise. However, if the phase noise of the QCL is better than the LO, the IF only shows the LO phase noise.

An important question that needs to be addressed within the phase locking system is the minimum signal-to-noise ratio required to achieve phase locking. Understanding the minimum signal-to-noise ratio is important for future work to stabilize high frequency QCLs, such as 4.7 THz. To phase lock such a high frequency QCL, a 4.7 THz harmonic mixer needs to be developed and that would require a higher harmonic factor to extend the LO harmonic frequency to the vicinity of the QCL's signal. As a result, the signal-to-noise ratio of such a higher frequency harmonic mixer is inherently lower due to the higher conversion loss and noise temperature performance, (see chapter 3 for more discussion).

There are two approaches used to address the minimum signal-to-noise ratio that is required to phase lock the 2.691 THz QCL. The first approach is reducing the down converted IF power using a variable attenuator to decrease the signal-to-noise ratio for a given loop bandwidth that is going to the phase locking module. The attenuator is placed after the low noise amplifier and low pass filter to eliminate additional noise due to the attenuator. The second technique is

decreasing the signal-to-noise ratio by reducing the THz power using an optical attenuator.

The signal-to-noise ratio and phase noise depicted in Fig.(4.26b) can be related using the expression below. The rms value of the phase jitter or the square of the rms phase noise is expressed by using Eqn.(4.20) [50]:

$$\bar{\theta}_{n_i}^2 = \frac{P_n}{2P_s} = \frac{1}{2(SNR_i)} \quad rad^2 \quad (4.20)$$

where, p_n is the noise power and p_s is the signal power.

Eqn.(4.20) shows that at the input of the phase lock loop, the square of the phase noise is inversely proportional to the signal-to-noise ratio. From the noise theory, the spectral density of the noise is given as:

$$\overline{\Theta_{n_i}^2(j\omega)} = \Phi = \frac{\bar{\theta}_{n_i}^2}{B_i/2} \quad rad^2 Hz^{-1} \quad (4.21)$$

where B_i is the input noise bandwidth.

The phase noise at the output can be calculated by integrating the spectral density over the phase lock loop bandwidth.

$$\bar{\theta}_{n_o}^2 = \int \overline{\Theta_{n_o}^2(j\omega)} df = \frac{\Phi}{2\pi} \int |H(s)|^2 ds \quad (4.22)$$

$\bar{\theta}_{n_o}^2$ is the area under the phase noise curve shown in Figure 4.26b; this can also be calculated by integrating the transfer function described in Section 4.3 within the loop bandwidth.

At the output, the signal-to-noise ratio can be calculated as:

$$SNR_o = SNR_i \frac{B_i}{2B_o} \quad (4.23)$$

Eqn.(4.23) shows that the phase locking loop improves the output signal-to-noise ratio by a factor of $\frac{B_i}{2B_o}$; thus, narrower loop bandwidth improves the output signal-to-noise ratio. The total output phase noise exceed the signal when a signal-to-noise ratio is unity, therefore phase lock-in process will not occur.

Using Eqn.(4.22), integrating the phase noise data shown in Figure 4.26b provides the signal-to-noise ratio of 45 dB at the state of phase locking the 2.691 THz QCL. By continuously decreasing the signal-to-noise ratio using both techniques described above, phase locking the QCL is attempted and the dynamic range of 22 dB and the minimum signal-to-noise ratio that is required to phase lock the 2.691 THz QCL was found to be 23 dB. This value is higher than the state of the art phase locking module's minimum signal-to-noise ratio requirement at least by 15 dB, therefore further investigation of the XL-Microwave phase locking module is required [50].

One reason that the system temporarily loses locking is due to the instantaneous noise power blip that is slower than the thermal constant. Increasing the input signal-to-noise ratio will reduce the probability of unlocking and increase the time interval between two unlocking events. The probability of unlocking for a given signal-to-noise ratio can be determined by experimentally relating the number of lock-outs and the time interval between the unlocking events.

4.4.1. Frequency Drift

Once the QCL is phase locked, the long term drift of the down-converted beat signal is compared to the stable reference signal and analyzed by continuously tracking the signal using

a spectrum analyzer that shares the same 100 MHz reference oscillator with the whole phase locked system. The 100 MHz reference oscillator that is used in this experiment is quartz based from Wenzel Associate Inc. with phase noise of -165 dBc/Hz at 1 KHz offset and a long term stability of 5×10^{-10} per day. Once the QCL is properly phase locked, it expected to be stable within the stability of the reference oscillator.

To measure a frequency drift of the down converted signal compared to the reference signal, signal tracking is used to track the signal by periodically reacquiring the carrier signal and calculating the delta frequency. Figure 4.27 and Figure 4.28 depicts the drift frequency of the down-converted beat signal of the 2.5182 THz and 2.69 THz QCL for a long term test. Once the QCL is phase locked, the initial down-converted frequency is recorded, and the drifted signal is tested periodically every 3 hours for a 9 hours continuous test. For a 100 MHz carrier frequency, the down-converted beat signal showed a sub-Hertz drift. This data proves that the phase lock loop is successfully phase locked the QCL and the down converted signal is tracking the reference signal precisely. This result implies that the down converted signal has similar stability as the reference oscillator. To further increase the stability of the QCL, a highly stable microwave reference, such as rubidium based oscillators, can be used which could provide a stability as high as as part in 10^{12} .

4.4 Phase Noise and Long Term Frequency Drift

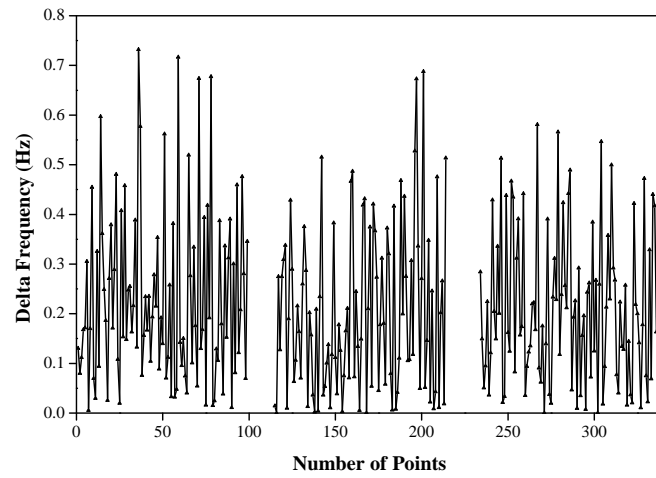


Figure 4.27.: Phase locked 2.5182 THz QCL beat signal long term stability test using signal tracking.

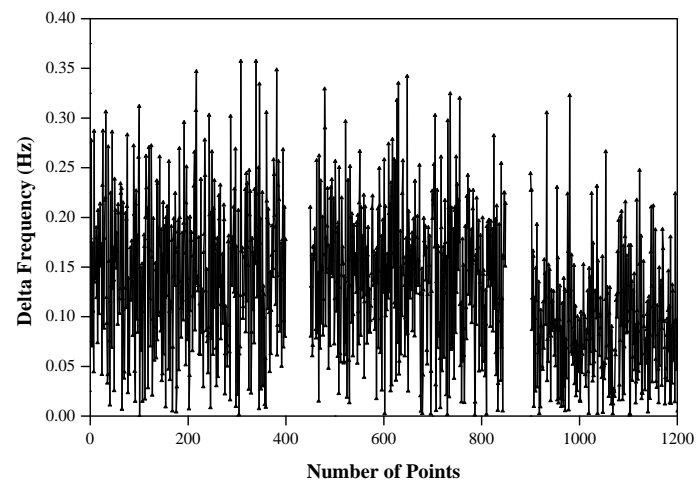


Figure 4.28.: Phase locked 2.6906 THz QCL beat signal long term stability test using signal tracking.

5. Conclusion and Future Work

The goal of this thesis is divided into two parts. The first part involves the design and characterization of the THz harmonic mixer. The second part involves the use of a THz harmonic mixer to phase lock THz Quantum Cascade Lasers. Section 5.1 and Section 5.2 provides a conclusion on the harmonic mixer design and discusses future work to improve the conversion loss of the mixer. Similarly, Sections 5.3 and 5.4 summarize the work on phase locking THz Quantum Cascade Lasers and provide ideas for future work.

5.1. Conclusion on THz Harmonic Mixer

The initial work is started by designing a broad band harmonic mixer to improve the modified harmonic mixer's performance. The WM-86 (WR0.34) harmonic mixer contains quartz based LO and IF circuit and a GaAs based THz circuit with integrated diode. The THz diode uses a 60 nm thick GaAs-based epitaxial layer for its active region with an n-type doping of $4 \times 10^{17} \text{ cm}^{-3}$ with an anode areas of $0.126 \mu\text{m}^2$ and $0.28 \mu\text{m}^2$ for approximately 5-6 μm finger length structures. The THz circuit also contains a beam-lead to support the circuit $4 \mu\text{m}$ above the ground plane. Due to the transmission line between the IF/DC ground and the RF probe,

coupling 1.8-3.2 THz was challenging; hence, two types of RF probes are designed to optimize the coupling of 1.8-2.6 THz and 2.3-3.2 THz bands.

The mixer housing is machined using a Computer Numerical Control (CNC) milling tool. The block was machined into two halves with the E-plane split between the two halves of the block. The harmonic mixer block contains an integrated WM-86 (WR0.34) diagonal feed horn with aperture diameter of 0.51 mm, LO waveguide, IF and THz circuit channels. The base of the THz circuit channel dimension is $39\ \mu\text{m} \times 4\ \mu\text{m}$. Due to the small features in the THz blocks, assembly is challenging; thus, position sensitivity analysis is performed and the design is adjusted to accommodate assembly errors.

Due to the large substrate leakage resistance, the I-V curve is bent for a voltage bias less than 0.6 V. Therefore, diode parameters are extracted by performing a curve fitting to an ideal diode for applied voltage greater than 0.65 V, and minimizing the mean square error for accurate representation. The extracted diode parameters are series resistance $R_s = 27\ \Omega$, ideality factor $\eta = 1.7$ and saturation current under reverse bias $I_0 = 4.2\ \text{pA}$.

The LO video response is measured by pumping the mixer with LO power while modulating the LO signal and measuring the output voltage on a lock-in amplifier. This test also predicts the LO coupling performance at different frequencies of the mixer. The harmonic mixer required LO power and current bias performance is characterized and an optimal LO power of $300 - 350\ \mu\text{W}$ and a current bias of $150\ \mu\text{A}$ are determined.

RF performance of the mixer is tested using a 1.9-2.06 THz solid state AMC source and RF video responsivity of 800 V/W and a conversion loss of 27 dB for 3rd harmonic mixing is measured. Similarly, the harmonic mixer performance is tested using a 2.6906 THz QCL and a responsivity of 1200 V/W and a conversion loss of 30 dB for 4th harmonic mixing is measured. This result shows a conversion loss improvement of 18 dB from the WM-102 (WR0.4) modified

harmonic mixer.

5.2. Harmonic Mixer Future Work

Future work on the harmonic mixer includes having a balanced mixer design using more than one diode in antiparallel or antiseriess fashion to improve the noise performance of the mixer and extending the frequency of operation to 3-5 THz.

5.2.1. WM-52 (WR0.22) Harmonic Design

There is high demand for a 3-5 THz room temperature direct detector-harmonic mixer to characterize THz sources, such as THz QCL or gas lasers. Thus, the development of a WM-52 (WR0.22) harmonic mixer is in progress. The WM-86 (WR0.34) harmonic mixer design is adjusted and scaled to WM-52 (WR0.22) for 3-5 THz operation. Since the WM-86 (WR0.34) harmonic mixer uses a $3\ \mu\text{m}$ thick GaAs substrate, there is a substrate thickness scaling limitation due to material strength. Hence, the WM-52 (WR0.22) design contains a GaAs substrate thickness of $2\ \mu\text{m}$ and width of $18\ \mu\text{m}$ is underway.

The WM-52 (WR0.22) harmonic mixer contains a WR1.0 LO waveguide that allows 750-1100 GHz signal and couples to the quartz based LO probe. Figure 5.1 and Figure 5.2 depict the internal circuitry and the machined block of the WM-52 (WR0.22) harmonic mixer.

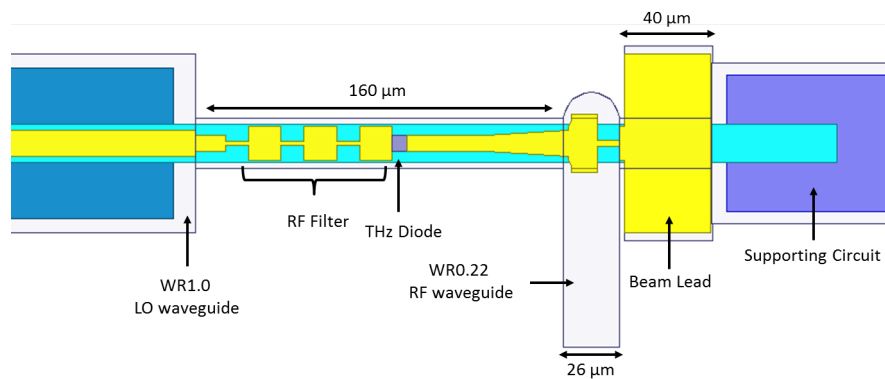


Figure 5.1.: WM-52 (WR0.22) harmonic mixer design.

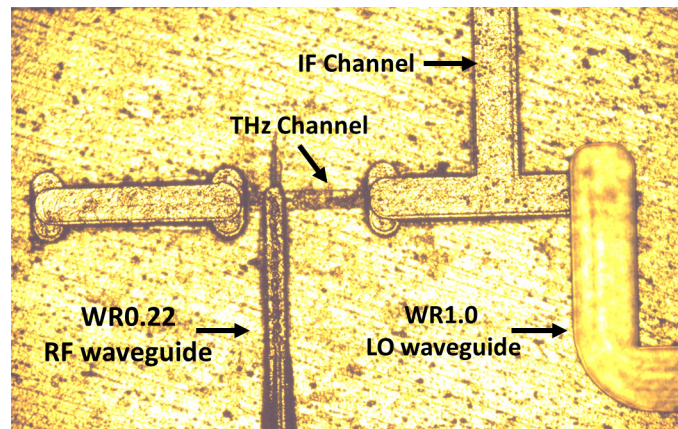


Figure 5.2.: WM-52 (WR0.22) harmonic mixer block.

5.2.2. Double Balance Design

Since the WM-86 (WR0.34) harmonic mixer uses a single diode for harmonic mixing, all harmonics are accessible. However, providing an idler for the unused harmonics to improve the single ended mixer is challenging. As a result, noise associated with those harmonics affects the performance. To alleviate these challenges, balanced types of harmonic mixer design can be implemented. Balanced topology involves two diodes with 180 degree phase difference. This

can be achieved by orienting the diodes in antiparallel/antiseriess fashion or using a quadrature coupler. The resulting IF output from the balanced design is only the desired even or odd harmonics. Some of the advantages that could be gained by having balanced design are:

- Cancellation of half of the mixing product
- Grounding the diode is not required for the LO current return
- AM noise is eliminated due to circuit balance

For future harmonic mixer design work, balanced types of harmonic mixers could improve the mixer's performance.

5.2.3. Schottky based THz Receiver

The WM-86 (WR0.34) harmonic mixer with its LO driver chain can be used as a 1.8-3.2 THz receiver for different applications. As discussed in section 3.7, the receiver has a noise temperature of approximately 31000 K. For highly sensitive applications such as astronomy, this noise temperature could be too high. To further improve the noise temperature and conversion loss, the receiver can be operated at cryogenic temperature. Reducing the ambient temperature of the Schottky based receivers below 100 K will give approximately 4-5 times improvement in noise temperature performance compare to a room temperature measurement [51]. Cooling a Schottky based receiver also enhances the efficiency of the LO driver chain that approximately doubles the available power to increase the number of pixels in the receiver. Increasing the number of pixels in a receiver will enhance the resolution of astronomical measurements. Schottky based cooled receivers with more pixels can be implemented by using a single LO chain at lower frequency (~600 GHz) and splitting the power into different mixers (based on the number of pixels and the available power). Since the WR0.34 harmonic mixers only re-

quire approximately $300 - 350 \mu W$ input power, state of the art 650 GHz LO chain from VDI is expected to produce 5 mW power at cryogenic temperature and this could be used to pump a receiver with up to six pixels.

VDI in collaboration with University of Arizona performed a test on a 1.4 THz Schottky receiver at cryogenic temperature [51]. The data shows that decreasing the dewar ambient temperature from 300 K to 50 K reduces the receiver's noise performance by a factor of more than 4. Similarly, reducing the dewar ambient temperature to 50 K increases the LO power by a factor of more than 2.

Summary of the advantages that can be gained by implementing this approach are:

- 1) Compactness: by using a single LO chain and splitting the power to pump each pixel will reduce the number of high frequency LO chains and associated components that drive each pixel.
- 2) Wider IF Bandwidth: Schottky diode based cooled receivers have wider IF bandwidth and flat response compare to HEB-based receivers.
- 3) Operational temperature: maintaining the required ambient temperature of ~ 4 K for superconductive types of receivers is challenging and expensive. Schottky based receivers at cryogenic temperature can be operated at any ambient temperature (5 K, 40 K, 100 K. . .) based on the minimum noise requirement of the receiver and the availability of the cooling temperature in the cryocooler.
- 4) Cost: reducing the number of LO chains and associated components decreases the cost. Additionally, decreasing the number of components in the systems that have limited life time will reduce the cost associated with repairing the receiver.
- 5) Sensitivity: the Schottky diode based receiver at cryogenic temperature improves the noise

temperature performance by a factor of 4-5 times compared to the room temperature receiver. Therefore, when a Schottky based receiver at cryogenic temperature is sensitive enough for certain applications, it can be an alternative choice to build a sensitive THz receiver with more pixels and wider IF bandwidth at lower cost.

5.3. Conclusion on Phase Locking a THz QCL

Initial testing of the QCL is performed by characterizing the bias current and the output frequency relationship using the WM-86 (WR0.34) harmonic mixer. The harmonic mixer is also set in a detector mode to further quantify the far field beam quality of the THz beam. Important beam parameters such as divergence angle, beam parameter product and beam quality factor are determined. The free running ~2.690 THz QCL beam image is taken using a IRV-T0831 THz camera from NEC corporation at different current biases. Furthermore, the output power of the QCL is measured using an Erickson calorimeter from VDI, [38]. The power meter is placed 5 mm away from the 2.6906 THz QCL and the position is aligned with the QCL to achieve optimal power coupling. Similarly, the output power of the QCL is measured after the beam is collimated and focused using off-axis parabolic mirrors. Using the QCL beam pattern data and the total power measurement, power coupling efficiency at different positions in the optical axis is predicted.

The THz harmonic mixer is used to down convert the QCL radiation to a lower frequency and the conversion loss of the mixer at the 4th harmonic mixing is estimated. From this, a conversion loss of 31-35 dB and an IF bandwidth of 27 GHz is measured.

Finally, the down converted signal phase is compared with a stable 100 MHz reference signal using a digital phase detector. This generates a DC voltage that is proportional to the phase dif-

ference between the two signals. The DC voltage is applied to the loop filter with 1 MHz loop bandwidth. The loop bandwidth characteristics determine the range in which the phase-locked loop tracks the signal and sets the locking range. The DC voltage produced due to the phase difference feeds back into the QCL to complete the phase locked loop. Using this technique, a 2.518 THz and a 2.691 THz QCLs are phase locked with high spectral resolution. Phase locking of a free running QCL compensated approximately a 50 MHz instability due to bias and temperature fluctuation and cryocooler vibrations to sub-Hertz accuracy. To further characterize the phase locked down converted signal, phase noise and frequency drift is measured. The phase locked 2.6906 THz QCL output frequency is tuned approximately for 1 GHz, which can be used to produce tunable spectroscopy for different applications.

5.4. Phase Locking a THz QCL Future Work

Utilizing the 3-5 THz WM-52 (WR0.22) harmonic mixer to phase lock a 4.7 THz QCL is one future project proposed. Furthermore, integrating the QCL within the mixer block could also improve issues related with optical coupling. Those two topics are discussed in the next Sections.

5.4.1. Phase Locking of a 4.7 THz QCL

There is an astronomical important OI line at 4.7448 THz Thus, there is a high need to develop a stable heterodyne spectroscopy. Currently, the Stratospheric Observatory for Infrared Astronomy (SOFIA) is the only heterodyne spectroscopy at this frequency [21]. This project uses a ~4.7THz QCL for the LO chain to pump HEB based mixers. The QCL is relatively stabilized using a Stirling cooler, dedicated heat sink and a low-noise current source. However, for

highly sensitive astronomical measurements, such as the SOFIA project, the 4.7 THz QCL can be phase locked using WR0.22 harmonic mixer and achieve great stability. Hence, the future work includes developing the WM-52 (WR0.22) harmonic mixer and phase locking of QCLs within the WR0.22 harmonic mixer band, particularly ~4.7 THz.

5.4.2. Integrating QCL within a Mixer Block

Due to the small size of the QCLs, the output beam is divergent and non-Gaussian. Thus, coupling power from the QCL with high coupling factor becomes difficult. For efficient radiation out-coupling, a metallic waveguide device can be machined and the output beam can be guided to become a Gaussian beam. Few groups have shown improvement of a QCL output beam by using a metallic guide, [52], [53].

Fabry-Pérot types of QCLs radiate out THz beam in both longitudinal directions, but in most cases only one side is used. Thus, the QCL can be mounted within the harmonic mixer block and one side of the longitudinal output radiation can be used to couple to the harmonic mixer and phase lock the QCL, and the other side of the longitudinal output would be available externally as a THz source for different applications. Additionally, integrating the QCL within the harmonic mixer could be advantageous to avoid atmospheric loss and to circumvent challenges with optical coupling, beam splitting and aligning off-axis mirrors.

A. Schottky Diode

Schottky diode is a contact between metal and semiconductor on an atomic scale with no impurities or surface charges at the contact. At equilibrium there is a built-in voltage V_{bi} across the Schottky interface and depletion extended into the semiconductor, the depletion width of a schottky diode is given as W .

$$w = \sqrt{\frac{2K_s\epsilon_0}{qN_D}(V_{bi} - V_A)} \quad (\text{A.1})$$

For a given doping, the epitaxial layer is chosen based on the zero bias ($V_A = 0$) depletion width with an additional 20 % thickness. The thermionic emission current resulted from majority carrier electron over the Schottky potential is given as:

$$I = I_s(e^{\frac{V}{V_0}} -) \quad (\text{A.2})$$

$$I_s = AA^{**}T^2 e^{\frac{-q\phi}{kT}} \quad (\text{A.3})$$

I_s is the saturation current, V is the applied voltage at the junction, $V_0 = \eta kT/q$ is the thermal voltage, ϕ is the work function of the material and A is the area of the anode. The exponential

term dominates at the forward bias and the total current becomes $I \rightarrow I_s e^{V/V_0}$, for reverse bias the exponential term become negligible and the total current becomes $I \rightarrow -I_s$. Usually the value of the ideality factor η is greater than unity due to other effects such as tunneling and surface imperfection. The junction conductance $1/R_j$ can be drive from the above equation.

$$\frac{1}{R_j} = \frac{dI}{dV} = \frac{\eta KT}{q(I_{dc} + I_s)} \quad (\text{A.4})$$

I_{dc} represent the forward DC current.

A.1. Diode Parasitic Elements

The ideal diode equation is not including the parasitic elements such as R_s and C_j , to get accurate diode representation it is important to add those therns.

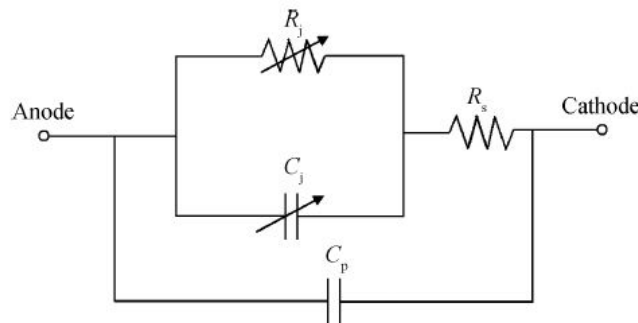


Figure A.1.: Schottky diode equivalent circuit.

Series resistance of a Schottky diode includes undepleted epitaxial layer resistance, spreading resistance in the buffer layer and ohmic resistance.

$$R_s = R_{epi} + R_{spreading} + R_{ohmic} \quad (\text{A.5})$$

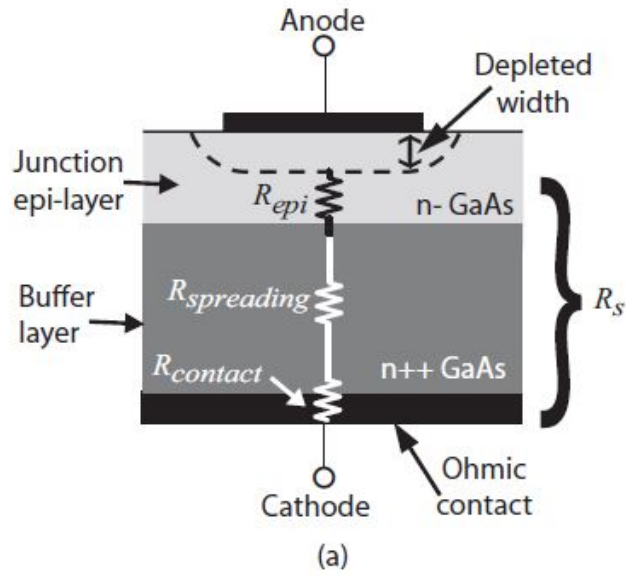


Figure A.2.: Schottky diode equivalent circuit, image is taken from [6].

For a THz diodes the epitaxial layer thickness is usually less than 500 nm. The epitaxial layer resistance is due to undepleted junction epitaxial layer and is calculated as:

$$R_{epi} = \frac{t_{epi} - W}{A\sigma_{epi}} \quad (\text{A.6})$$

$$\sigma_{epi} = q\mu_{n-epi}N_{n-epi} \quad (\text{A.7})$$

Where t_{epi} is the thickness of the epitaxial layer, W is the depletion width, A is the anode area, μ_{n-epi} is an electron mobility of the epitaxial layer and N_{n-epi} is the doping of the epitaxial layer. Since the depletion width is smaller for highly forward bias, the epitaxial layer resistance is maximized. Similarly, the DC spreading resistance is due to the resistance in the buffer layer and is calculated as:

$$R_{spreading} = \frac{1}{2\sigma_{buffer}d} \quad (\text{A.8})$$

Where d is the diode diameter and σ_{buffer} is the substrate conductivity. The series resistance of the diode due to the ohmic contact and the finger is calculated as:

$$R_{Ohmic} = \frac{\sigma_{ohmic}}{A_{ohmic}} \quad (\text{A.9})$$

Where A_{ohmic} is the ohmic contact area of the diode and σ_{ohmic} is the ohmic contact material conductivity.

The junction capacitance can be modeled as a parallel plate compactor with plate separation distance equal to the depletion width.

$$C_j = \frac{\epsilon_{epi}A}{W} \quad (\text{A.10})$$

The zero bias capacitance of a diode is given by:

$$C_{j0} = \frac{\epsilon_{epi}A}{\sqrt{\frac{2\epsilon_{epi}}{qN_D}V_{bi}}} \quad (\text{A.11})$$

where N_D is the doping of the epitaxial layer and ϵ_{epi} is the dielectric constant of the epitaxial layer.

B. WM-102 (WR0.4) Harmonic Mixer Performance

There are two types of WM-102 (WR0.4) harmonic mixer designs for two different LO bands. The first harmonic mixer has a WR4.3 waveguide to allow an LO frequency of 170-260 GHz. The WR4.3 LO band is intended to mix with 8th, 9th and 10th harmonic with a 1.9-2.8 THz RF source. Similarly, the second harmonic mixer uses a WR1.5 waveguide to allow 500-750 GHz LO frequencies for the 3rd and 4th harmonic mixing. Each of these mixers are tested and the data is presented in the next section.

B.1. Block Design

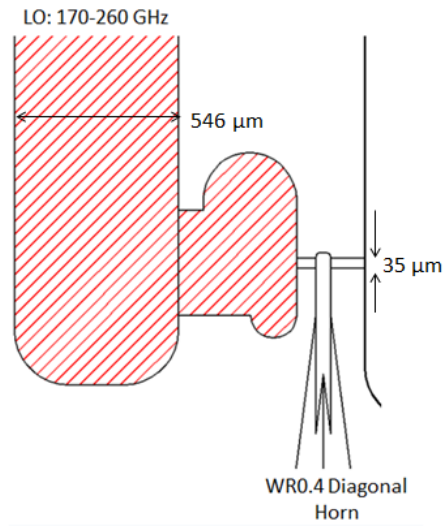


Figure B.1.

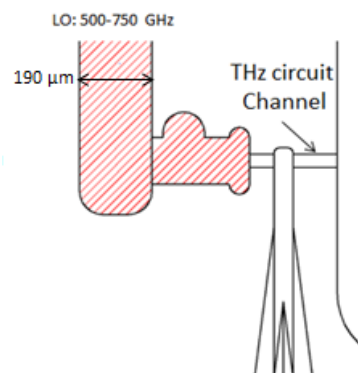


Figure B.2.

B.2. LO Return Loss and Video Response

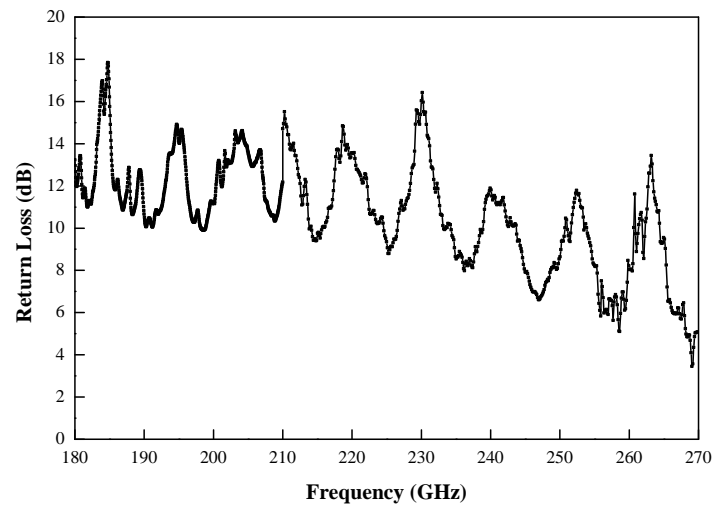


Figure B.3.

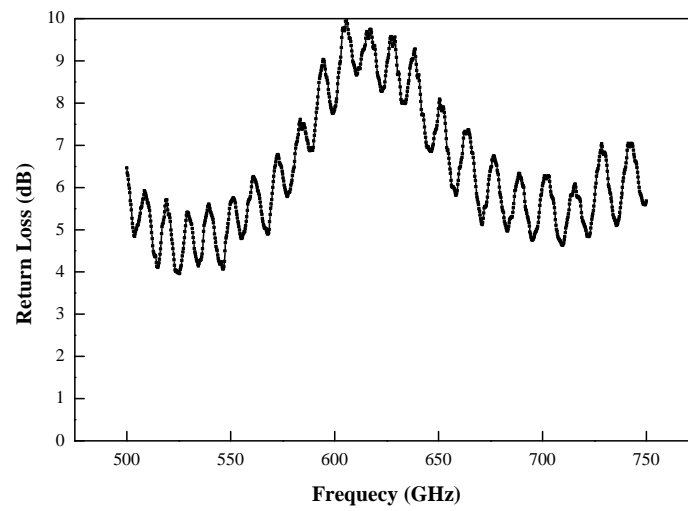


Figure B.4.

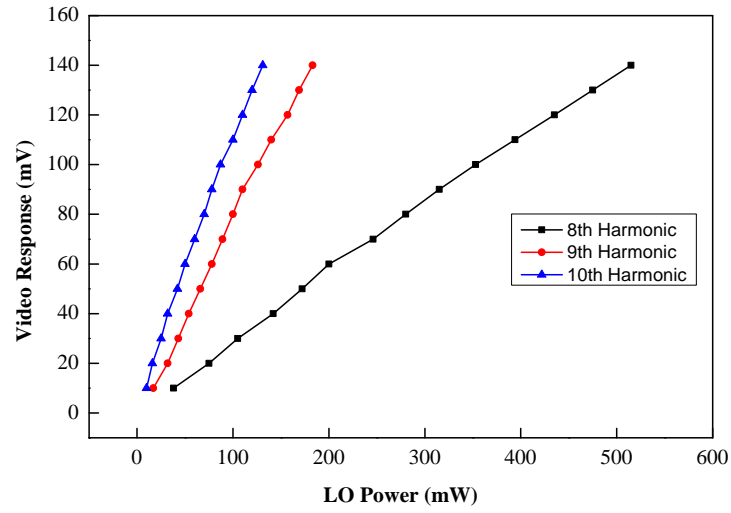


Figure B.5.

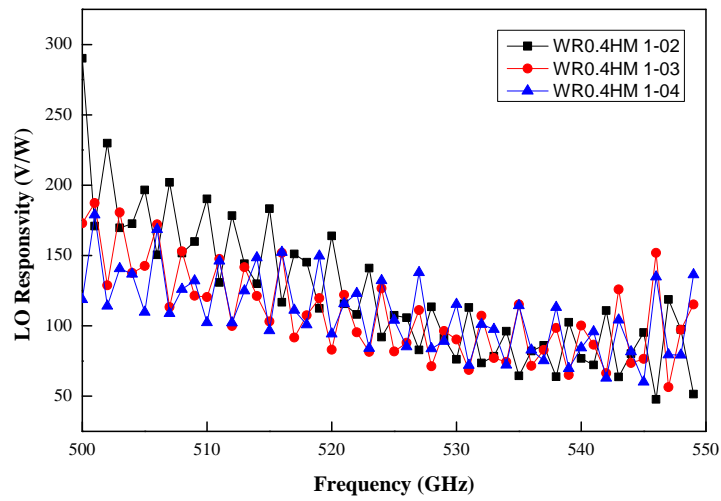


Figure B.6.

B.3. Conversion Loss

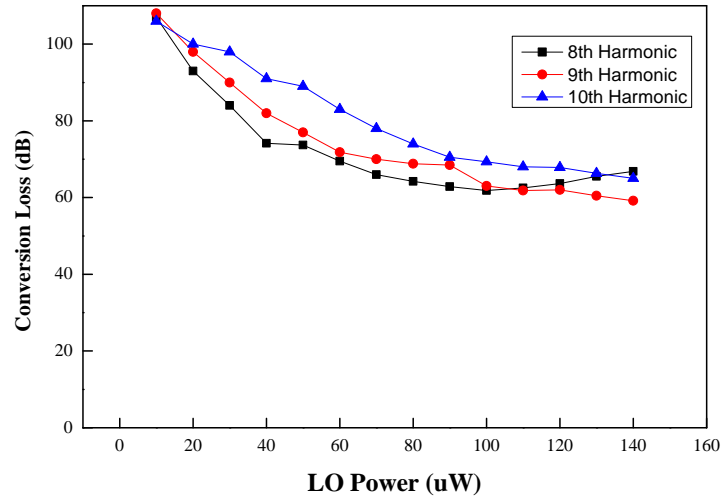


Figure B.7.

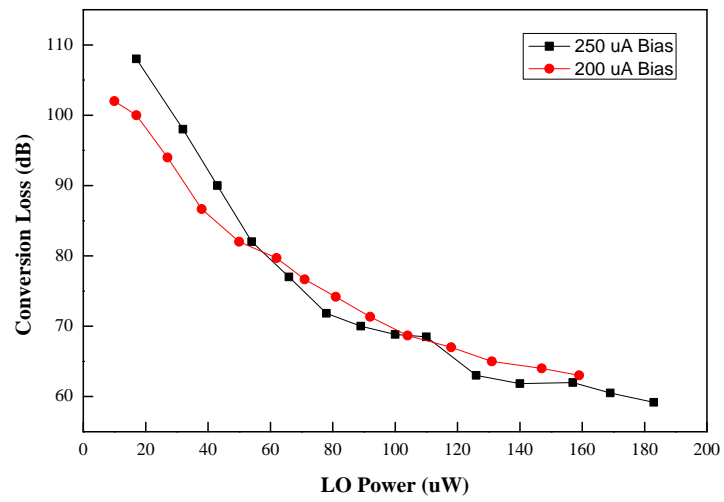


Figure B.8.

C. WM-86 (WR0.34) Harmonic Mixer

Block Design

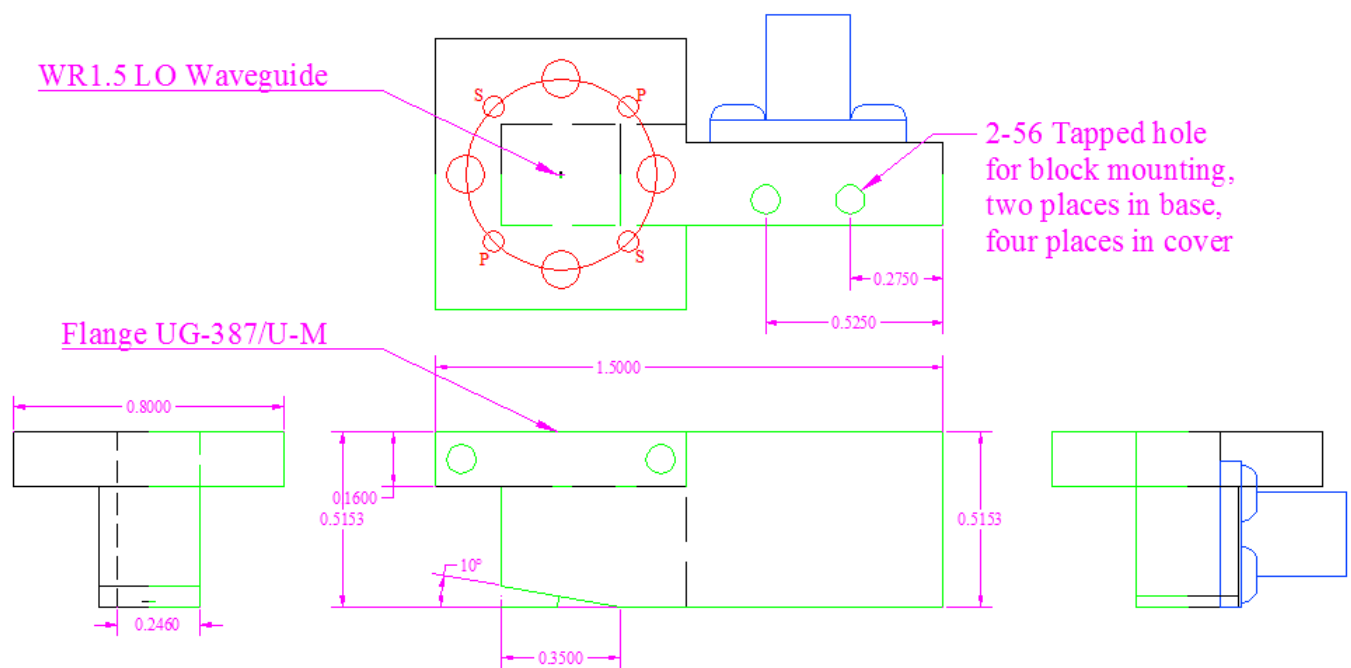


Figure C.1.

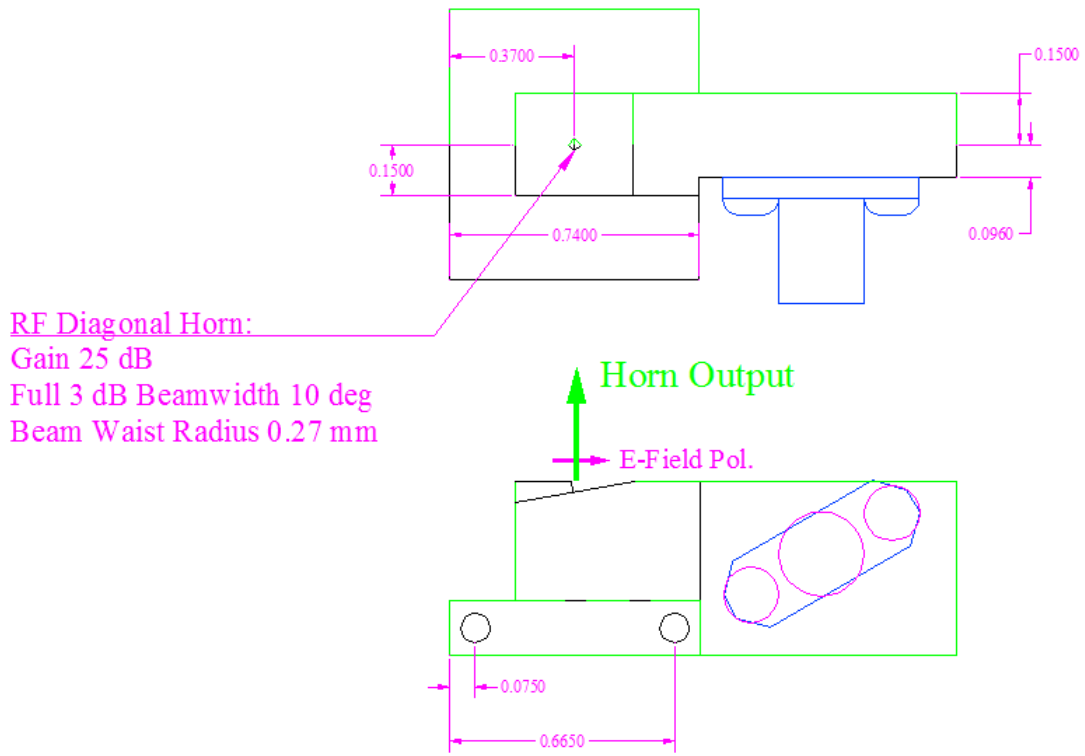


Figure C.2.

D. QCL Mount Design

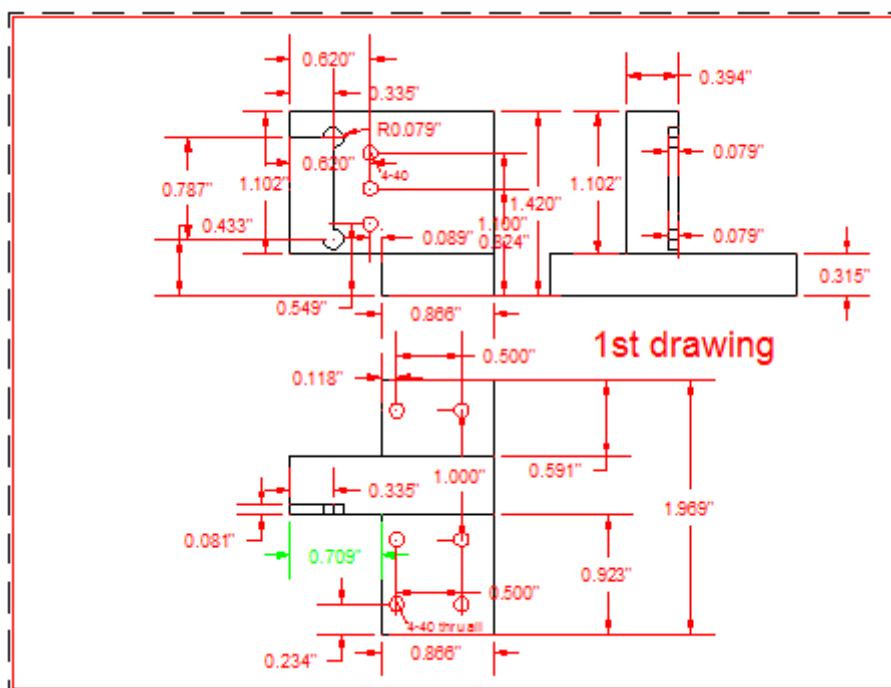


Figure D.1.

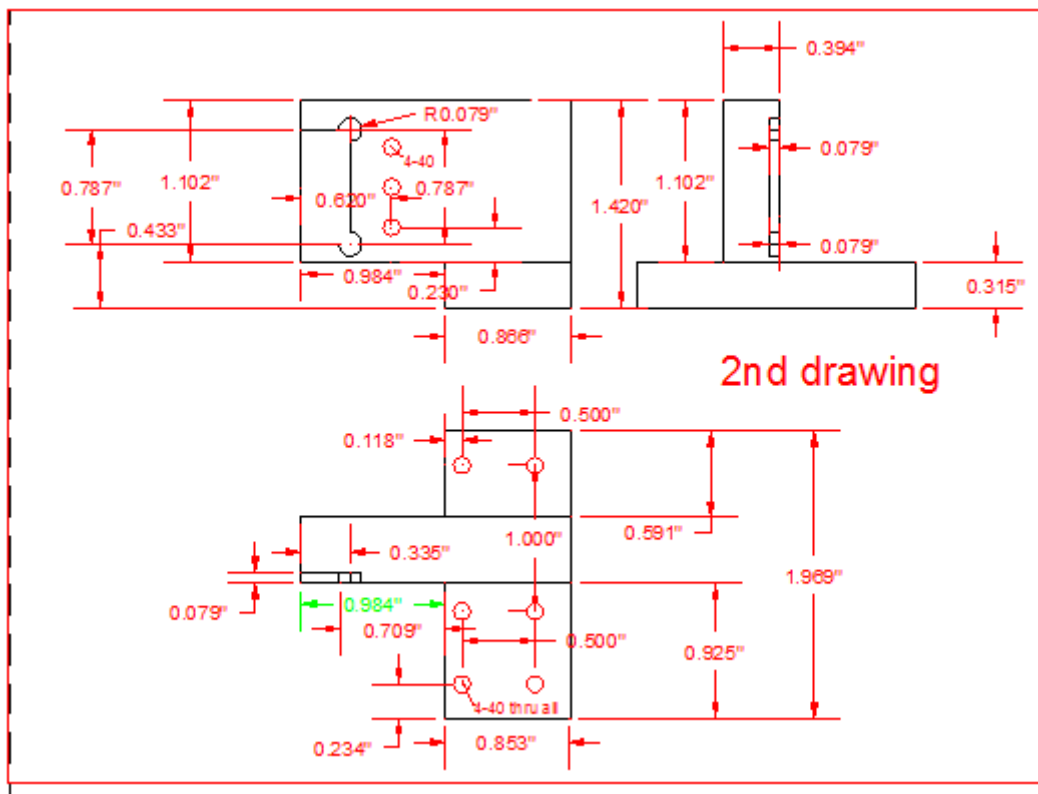


Figure D.2.

Bibliography

- [1] Betz, A. L. and Boreiko, R. T. and Williams, B. S. and Kumar, S. and Hu, Q. and Reno, J. L., “Frequency and phase-lock control of a 3 THz quantum cascade laser,” *Opt. Lett.*, vol. 30, pp. 1837–1839, July 2005.
- [2] Khosropanah, P. and Baryshev, A. and Zhang, W. and Jellema, W. and Hovenier, J. N. and Gao, J. R. and Klapwijk, T. M. and Paveliev, D. G. and Williams, B. S. and Kumar, S. and Hu, Q. and Reno, J. L. and Klein, B. and Hesler, J. L., “Phase locking of a 2.7 THz quantum cascade laser to a microwave reference,” *Opt. Lett.*, vol. 34, pp. 2958–2960, Oct. 2009.
- [3] D. J. Hayton, A. Khudchenko, D. G. Pavelyev, J. N. Hovenier, A. Baryshev, J. R. Gao, T. Y. Kao, Q. Hu, J. L. Reno, and V. Vaks, “Phase locking of a 3.4 thz third-order distributed feedback quantum cascade laser using a room-temperature superlattice harmonic mixer,” *Applied Physics Letters*, vol. 103, p. 051115, 2013.
- [4] Andriy A. Danylov, Alexander R. Light, Jerry Waldman, Neal R. Erickson, Xifeng Qian, and William D. Goodhue, “2.32 thz quantum cascade laser frequencylocked to the harmonic of a microwave synthesizer source,” *Optics Express*, vol. 20, no,25, p. 27914, 2012.
- [5] Hayton, D. J. and Khudchenko, A. and Pavelyev, D. G. and Hovenier, J. N. and Baryshev, A. and Gao, J. R. and Kao, T. Y. and Hu, Q. and Reno, J. L. and Vaks, V., “Phase

- locking of a 3.4 THz third-order distributed feedback quantum cascade laser using a room-temperature superlattice harmonic mixer,” *Applied Physics Letters*, vol. 103, no. 5, p. 051115, 2013.
- [6] A. Y. Tang, *Modelling and Characterisation of Terahertz Planar Schottky Diodes*. Doctoral thesis, Chalmers University of Technology, 2013.
- [7] G. Sun, “The intersubband approach to si-based lasers,” tech. rep., University of Massachusetts Boston, Massachusetts, USA.
- [8] A. A. Tavallae, *Terahertz Quantum-Cascade Transmission-Line Metamaterials*. PhD thesis, UCLA, 2012.
- [9] Gaidis, M.C. and Pickett, H.M. and Siegel, P.H. and Smith, C. D. and Smith, R.P. and Martin, S.C., “A 2.5 THz receiver front-end for spaceborne applications,” in *1998 IEEE Sixth International Conference on Terahertz Electronics Proceedings, 1998. THz Ninety Eight*, pp. 13–17, Sept. 1998.
- [10] Baryshev, A. and Hovenier, J. N. and Adam, A. J L and Kasalynas, I. and Gao, J.R. and Klaassen, T.O. and Williams, B.S. and Kumar, S. and Hu, Q. and Reno, J.L., “Phase locking and spectral linewidth of a two-mode terahertz quantum cascade laser,” *Applied Physics Letters*, vol. 89, pp. 031115–031115–3, July 2006.
- [11] P. Sobis, *Subharmonic Sideband Separating Schottky Diode Mixer for Submillimetre Wave Applications*. PhD thesis, Chalmers University of Technology, 2010.
- [12] Glyavin, M.Yu. and Luchinin, A.G. and Morozkin, M.V., “Development and experimental investigations of high power THz gyrotrons,” in *2013 International Kharkov Symposium on Physics and Engineering of Microwaves, Millimeter and Submillimeter Waves (MSMW)*, pp. 353–355, June 2013.

- [13] G.Chain, “Optical pumped submillimeter laser heterodyne receivers astrophysical observation and recent technological development,” *Proceedings of the IEEE*, vol. 80, no.11, pp. 1788–1799, 1992.
- [14] Maestrini, A. and Mehdi, I. and Siles, J.V. and Ward, J.S. and Lin, R. and Thomas, B. and Lee, Choonsup and Gill, J. and Chattopadhyay, G. and Schlecht, E. and Pearson, J. and Siegel, P, “Design and characterization of a room temperature all-solid-state electronic source tunable from 2.48 to 2.75 THz,” *IEEE Transactions on Terahertz Science and Technology*, vol. 2, pp. 177–185, Mar. 2012.
- [15] H. P. Riser, “Heterodyne for submillimeter and far infrared wavelength from 100um to 500um,” pp. 287–299, Sppt.1986.
- [16] Miao, W. and Zhang, W. and Zhou, K. M. and Li, S. L. and Zhang, K. and Duan, W. Y. and Yao, Q. J. and Shi, S. C, “Phase-locking of a terahertz solid-state source using a superconducting hot-electron bolometer mixer,” *Supercond. Sci. Technol.*, vol. 26, p. 085005, Aug. 2013.
- [17] Khudchenko. A.V, Hayton. D.J, Pavelyev. D.G, Baryshev. A.M, Gao. J.R, Kao. T.Y, Hu. Q, Reno. J.L, Vaks. V.L, “Phase locking a 4.7 thz quantum cascade laser using a superlattice diode as harmonic mixer,” *IEEE Conference Publications*, 2014.
- [18] A.M. Baryshev, P. Khosropanah, W. Zhang, W. Jellema, J.N. Hovenier, J.R. Gao, T.M. Klapwijk, D.G. Paveliev, B.S. William, S. Kumar, Q. Hu, J.L. Reno, B. Klein, J.L. Hesler, “Phase-locking of a 2.7-thz quantum cascade laser to a microwave reference,” *Opt. Lett.*, 2009.
- [19] M. Ravaro, C. Manquest, C. Sirtori, S. Barbieri, G. Santarelli, K. Blary, J.F. Lampin, S. P. Khanna, and E. H. Linfield, “Phase-locking of a 2.5 thz quantum cascade laser to a frequency comb using a gaas photomixer,” *Optics Letters*, vol. 36, no.20, p. 3969, 2011.

-
- [20] Stefano Barbieri, Pierre Gellie, Giorgio Santarelli, Lu Ding, Wilfried Maineult, Carlo Sirtori¹, Raffaele Colombelli, Harvey Beere and David Ritchie, “Phase-locking of a 2.7-thz quantum cascade laser to a mode-locked erbium-doped fibre laser,” *Nature Photonics*, 2010.
- [21] H. Richter, M. Greiner-Bar, K. Rosner, A. Semenov, M. Wienold, L. Schrottke, K. Biermann, H. T. Grahn, and H.-W. Hbbers, “4.7-thz local oscillator for sofia based on a quantum-cascade laser,” *IRMMW-THz*, 2014.
- [22] Sushil Kumar, “Recent progress in terahertz quantum cascade lasers,” *IEEE*, 2011.
- [23] J. Faist, F. Capasso, D. L. Sirtori, A. L. Hutchinson, and A. Y. Cho 1994.
- [24] Christoph Deutsch, Hermann Detz, Tobias Zederbauer, Michael Krall, Martin Brandstetter, Aaron M Andrews, Pavel Klang, Werner Schrenk, Gottfried Strasser, Karl Unterrainer, “InGaAs/GaAsSb/InP terahertz quantum cascade lasers,” *Infrared Milli Terahz Waves*, 2013.
- [25] C. Walther, M. Fischer, G. Scalari, R. Terazzi, N. Hoyler, and J. Faist, “Quantum cascade lasers operating from 1.2 to 1.6 thz,” *Applied Physics Letters*, vol. 91, no. 13, p. 131122, 2007.
- [26] C. Walther, G. Scalari, J. Faist, H. Beere, and D. Ritchie, “Low frequency terahertz quantum cascade laser operating from 1.6 to 1.8 thz,” *Applied Physics Letters*, vol. 89, no. 23, p. 231121, 2006.
- [27] M. Rochat, L. Ajili, H. Willenberg, J. Faist, H. Beere, G. Davies, E. Linfield, and D. Ritchie, “Low threshold terahertz quantum-cascade lasers,” *Applied Physics Letters*, p. 1381, 2002.
- [28] R. Kohler, A. Tredicucci, F. Beltram, H. E. Beere, E. Harvey, E. H. Linfield, A. G. Davies,

- D. A. Ritchie, R. C. Iotti, and F. Rossi, "Terahertz semiconductor-heterostructure laser," *Nature*, vol. 417, no. 6885, pp. 156–159, 2002.
- [29] G. Scalari, L. Ajili, J. Faist, H. Beere, E. Linfield, D. Ritchie, and G. Davies, "Far-infrared ($\lambda = 87 \mu\text{m}$) bound-to-continuum quantum-cascade lasers operating up to 90 K," *Applied Physics Letters*, vol. 82, no. 19, pp. 3165 – 3167, 2003.
- [30] T. Liu¹ and Q. J. Wang, "Fundamental frequency noise and linewidth broadening caused by intrinsic temperature fluctuations in quantum cascade lasers," *Physical Review*, 2011.
- [31] Steed, Robert J. and Ponnampalam, Lalitha and Fice, Martyn J. and Renaud, Cyril C. and Rogers, David C. and Moodie, David G. and Maxwell, Graeme D. and Lealman, Ian F. and Robertson, Michael J. and Pavlovic, Leon and Naglic, Luka and Vidmar, Matjaz and Seeds, Alwyn J, "Hybrid integrated optical phase-lock loops for photonic terahertz sources," *IEEE Journal of Selected Topics in Quantum Electronics*, vol. 17, pp. 210–217, Jan. 2011.
- [32] A. Hajimiri, "Noise in phase-locked loops," in *2001 Southwest Symposium on Mixed-Signal Design*, pp. 1–6, 2001.
- [33] N. Erickson, "Am noise in drivers for frequency multiplied local oscillators," *IEEE on Microwave Theory and Techniques*, 2004.
- [34] W. H. Schottky, "Halbleitertheorie der sperrschicht," *Naturwissenschaften*, vol. 26, pp. 843–843, 1938.
- [35] F. Johansson, D. Whyborn, "Antennas for sum-millimetre wave receivers," *Second International Symposium on Space Terahertz Technology*, p. 63, 1991.
- [36] Tang, A.Y. and Bryllert, T. and Stake, J, "Geometry optimization of THz sub-harmonic

- schottky mixer diodes,” in *2012 37th International Conference on Infrared, Millimeter, and Terahertz Waves (IRMMW-THz)*, pp. 1–2, Sept. 2012.
- [37] Drakinskiy, V.T. and Zhao, H.S. and Sob, P.S., “Terahertz gas schottky diode mixer and multiplier mic based on e-beam technology,” *25th International Conference on Indium Phosphide and Related Materials, Kobe, Japan*, 2013.
- [38] *VDI PM5 Manual*.
- [39] D. M. Pozar, *Microwave engineering 4th ed.* John Wiley and Sons, Inc., 2013.
- [40] H. Xu, *Millimeter and Sub-millimeter Wave Tunerless Planar Varactor Frequency Up-converters*. PhD thesis, University of Virginia, 2005.
- [41] Steven A. Retzloff; Abram Young; and Jeffrey L. Hesler, “A 1.46 THz Schottky Receiver at Cryogenic Temperatures,” *IEEE Conference Publications*, 2014.
- [42] W. Martienssen, *Handbook of Condensed Matter and Materials*. Springer, 2006.
- [43] D. A. Naylor, R. T. Boreiko, and T. A. Clark, “Mylar beam-splitter efficiency in far infrared interferometers, angle of incidence and absorption effects,” *Applied Optics*, 1978.
- [44] B. S. Williams, “Terahertz quantum-cascade lasers,” *Nature Photonics*, 2007.
- [45] L. Schrottke, M. Wienold, R. Sharma, X. Lu, K. Biermann, R. Hey, A. Tahraoui, H. Richter, H. W. Hubers, H.T. Grahn, “Quantum cascade lasers as local oscillators for heterodyne spectrometers in the spectral range around 4.745THz,” *Semiconductor Science and Technology*, 2013.
- [46] P. F. Goldsmith, *Quasioptical Systems*. IEEE press Chapman and Hall Publisher Series on Microwave Technology and RF, 1998.
- [47] *VDI Power Measurement App Note 2007*.

- [48] *N9030A Real-Time Spectrum Analyzer User's & Programmer's Reference.*
- [49] F. M. Gardner, *Phaselock Techniques.* Wiley Interscience, 2005.
- [50] R. E. Best, *Phase Locked Loops: design, simulation and application.* McGraw-Hill, 1999.
- [51] Steven A. Retzloff, Abram Young, and Jeffrey L. Hesler, "A 1.46 thz schottky receiver at cryogenic temperatures," *IRMMW-THz*, 2014.
- [52] Abigail Hedden, Patrick Piitz, C. d'Aubigny, Dathon Golish, Christopher Groppi, Christopher Walker, Benjamin Williams, Qing Hu, and John Reno, "Micromachined spatial filters for quantum cascade lasers," *17th International Symposium on Space Terahertz Technology*, 2006.
- [53] M.I. Amanti, M. Fischer, C. Walther, G. Scalari and J. Faist, "Horn antennas for terahertz quantum cascade lasers," *Laser Science to Photonic Application*, 2007.